JGP Journal of General Physiology

ARTICLE

The Donnan-dominated resting state of skeletal muscle fibers contributes to resilience and longevity in dystrophic fibers

Catherine E. Morris[1,2], Joshua J. Wheeler[3], and Béla Joos[2,3]

Duchenne muscular dystrophy (DMD) is an X-linked dystrophin-minus muscle-wasting disease. Ion homeostasis in skeletal muscle fibers underperforms as DMD progresses. But though DMD renders these excitable cells intolerant of exertion, sodium overloaded, depolarized, and spontaneously contractile, they can survive for several decades. We show computationally that underpinning this longevity is a strikingly frugal, robust Pump-Leak/Donnan (P-L/D) ion homeostatic process. Unlike neurons, which operate with a costly "Pump-Leak–dominated" ion homeostatic steady state, skeletal muscle fibers operate with a low-cost "Donnan-dominated" ion homeostatic steady state that combines a large chloride permeability with an exceptionally small sodium permeability. Simultaneously, this combination keeps fiber excitability low and minimizes pump expenditures. As mechanically active, long-lived multinucleate cells, skeletal muscle fibers have evolved to handle overexertion, sarcolemmal tears, ischemic bouts, etc.; the frugality of their Donnan dominated steady state lets them maintain the outsized pump reserves that make them resilient during these inevitable transient emergencies. Here, P-L/D model variants challenged with DMD-type insult/injury (low pump-strength, overstimulation, leaky Nav and cation channels) show how chronic "nonosmotic" sodium overload (observed in DMD patients) develops. Profoundly severe DMD ion homeostatic insult/injury causes spontaneous firing (and, consequently, unwanted excitation–contraction coupling) that elicits cytotoxic swelling. Therefore, boosting operational pump-strength and/or diminishing sodium and cation channel leaks should help extend DMD fiber longevity.

Introduction

Overview

Skeletal muscle (SM) fibers (SMFs) constitute ∼40% of human body mass (Janssen et al., 2000). The sarcolemma of these mechanical, long-lived, multinucleate cells is fortified by dystrophin, a filamentous entropic-spring-like membrane skeleton protein (Campbell and Kahl, 1989; Ibraghimov-Beskrovnaya et al., 1992; Khairallah et al., 2012; Constantin, 2014; Allen et al., 2016; Le et al., 2018). Dystrophin protects against sarcolemmal tearing and bleb damage; with bleb damage, membrane skeleton/bilayer adhesions detach, resulting in fragility and the decay of cell-mediated bilayer organization (Methfessel et al., 1986; Sheetz et al., 2006; Lundbaek et al., 2010; García-Pelagio et al., 2011; Morris, 2012; Ameziane-Le Hir et al., 2014; Dos Santos Morais et al., 2018; Burden et al., 2018). Via linkages within the massive trans-sarcolemma dystrophin–glycoprotein complex, dystrophin also facilitates physiological signaling (Dowling et al., 2021). Healthy SMF capillary beds require dystrophin-expressing endothelial and smooth muscle cells (Verma et al., 2019; Podkalicka et al., 2019). Dystrophin-expressing thymus-derived cells contribute to inflammatory repair of injured muscle (e.g., Farini et al., 2021). Sporadically, damaged SMFs regenerate by fusion with their stem (satellite) cells, a process reliant on satellite cell dystrophin (Dumont et al., 2015; Filippelli and Chang, 2021).

Individuals with the X-linked muscle-wasting disease Duchenne muscular dystrophy (DMD; Fig. 1 A) have no functional dystrophin. Non-ambulatory by their teens, DMD patients can nevertheless survive until SMFs of the respiratory system become nonviable, i.e., for 3 to 4 decades (Landfeldt et al., 2020). With its gene discovered (Hoffman et al., 1987), dystrophin was localized at the sarcolemma (Zubrzycka-Gaarn et al., 1988), and the dystrophin-minus mouse (*mdx*) was established as a dystrophin-minus mouse model for DMD (Ryder-Cook et al., 1988). DMD remains incurable (Bishop et al., 2018; Datta and

[1]Neuroscience, Ottawa Hospital Research Institute, Ottawa, Canada; [2]Center for Neural Dynamics, University of Ottawa, Ottawa, Canada; [3]Department of Physics, University of Ottawa, Ottawa, Canada.

Correspondence to Béla Joos: bjoos@uottawa.ca.

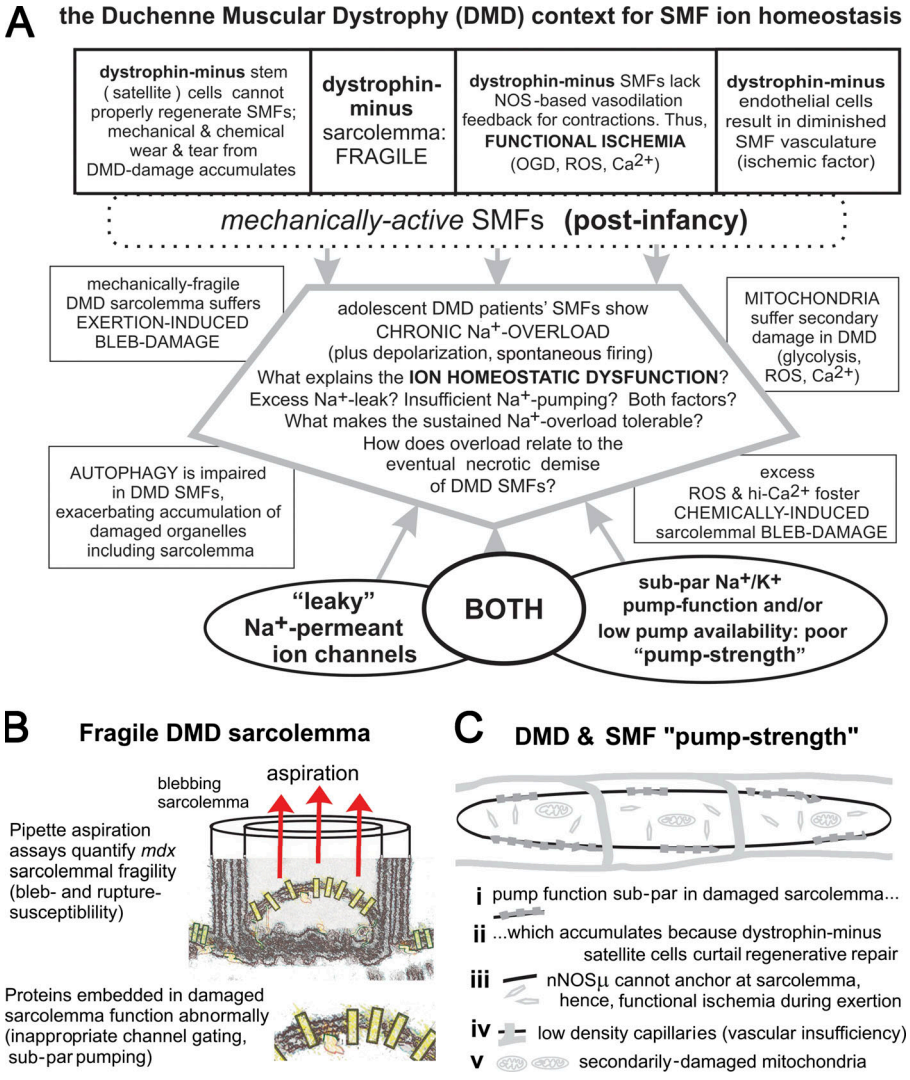

Figure 1. **DMD and impaired SMF ion homeostasis. (A)** After infancy in DMD patients, as muscle loading/exertion increases (Duan et al., 2021), primary and secondary effects (top-line and dispersed boxes, respectively) of the dystrophin-minus condition degrade SMF ion homeostasis (Murphy et al., 2019; Gerhalter et al., 2019; Dabaj et al., 2021). A generic excitable SMF ion homeostasis model is used here to probe how DMD deficits (excess Na^+ leaks and diminished operational pump strength) would alter SMF ion homeostasis. **(B)** DMD sarcolemma suffers chemical damage (as per A, from the ↑ROS and ↑$[Ca^{2+}]_i$; Allen et al., 2016) and mechanical bleb damage (García-Pelagio et al., 2011). Nav1.4 channels are among the many membrane proteins whose activities change in damaged membrane (Morris et al., 2006; Wang et al., 2009; Morris, 2012; Morris and Joos, 2016) due to altered bilayer and disrupted protein-partner interactions. **(C)** As DMD advances, SMF pump reserves (ratio, maximal to steady-state pump activity) diminish due to ↑steady-state Na^+ leaks and ↓operational pump strength (see Operational "pump strength" defined). nNOS, neuronal NO synthase; OGD, oxygen-glucose deprivation.

Ghosh, 2020; Duan et al., 2021). Though chronic Na^+ overload of dystrophic muscles (first documented in 1955) is now noninvasively detectable via ^{23}Na–magnetic resonance imaging (MRI) in young patients (Table 1, items 1, 5, 6, 9, and 10), how SMF ion homeostasis falters in DMD, and if/how this relates to fiber loss, remain unclear.

Ion homeostasis is the autonomous Pump-Leak/Donnan (P-L/D) feedback process (Fig. 2) by which cells, after ionic perturbations, reestablish their "set point" (i.e., steady-state values for membrane potential [V_m] + volume cell model parameter [Vol_{cell}] + [ions]$_i$). Fig. 2 A outlines the "P-L and the D-mediated" feedbacks of ion homeostasis. Different cell types' particular set points are established by evolutionary history. Though concepts depicted in Fig. 2 B are not new, new terms are introduced there to the ion homeostasis lexicon: P-L/D systems, minimal (versus nonminimal) P-L/D steady states, Pump-Leak–dominated steady states, and Donnan-dominated steady states.

The charge difference (CD) approach for P-L/D ion homeostasis modeling is rigorous and powerful (Fraser and Huang, 2004, 2007; Fraser et al., 2011; Cha and Noma, 2012; Hübel et al., 2014; Dijkstra et al., 2016; Kay, 2017; Dmitriev et al., 2019) but has not yet been used to address DMD-afflicted fibers, which, in spite of an encyclopedic list of deficits (e.g., Murphy et al., 2019; Dowling et al., 2021), can nevertheless survive decades. Here, via CD-modeling, we therefore ask not only what is wrong with DMD ion homeostasis but also what is right. Globally, we conclude, what is wrong relates to Pump-Leak malfunctions, while what is right relates to SMFs' ion homeostatic strategy, which, unlike that of neurons, is built around an ultra–energy-efficient and thence physiologically robust Donnan dominated (i.e., based on [big P_{Cl}][small I_{Naleak}]) steady-state. Cytoplasmic Donnan effectors are a source of electro-osmotic free energy; as membrane-impermeant ions, they passively influence the transmembrane distribution of membrane-permeant ions and of H_2O (Fig. 2, A and B). Neurons are high-input–impedance, electrically agile, high-excitability cells with [small P_{Cl}][big I_{Naleak}] steady states; when pumping falters, neurons' [big I_{Naleak}] and resultant small pump reserves quickly eventuate in treacherous Donnan-effector–mediated swelling (= lethal Na^+ + Cl^- + H_2O influxes). SMFs, too, are excitable, but they spend most of their time at their hyperpolarized steady states. SMF resilience against profound physiological insult starts from the collaboration of [big P_{Cl}] with Donnan effectors, a pairing that exploits the no-added-cost free

Table 1. **Chronic Na^+ overload of DMD patient muscles and *mdx* SMFs**

#	Reference	$[Na^+]_i$	Notes
1	Horvath et al., 1955	$[Na^+]_i$ higher (and $[K^+]_i$ lower) in dystrophic than in normal muscle fibers	Horvath et al. (1955) is referenced in Rudman et al. (1972); biopsy, elemental analysis; fibers of 20 patients with unspecified muscular dystrophies.
2	Dunn et al., 1993	Diaphragm, gastrocnemius control: 13.0, 13 *mdx*: 23.5, 24	Two techniques: Na^+ electrode for diaphragm, cyto-volumetrics plus serum and bulk muscle Na^+ values for gastrocnemius. Mice.
3	Hirn et al., 2008	1.4× more $^{22}Na^+$ uptake in *mdx* than in control	$^{22}Na^+$ uptake. Tetrodotoxin reduces uptake in both and makes them identical (see their Fig. 1). Mice.
4	Miles et al., 2011	Control: 11.5 mM; *mdx*: 22.5 mM	Na^+-dye measurements. Mice.
5	Weber et al., 2011, 2012	Total sodium content: volunteers: 25–26 mM; DMD patients: 38 mM	^{23}Na-MRI. First noninvasive observation of chronic Na^+ overload; German DMD patient cohort. Authors wondered if ↑myoplasmic Na^+ might signify cytotoxic osmotic Na^+ loading…but see 10.
6	Lehmann-Horn et al., 2012	Sustained small decrease of cytoplasmic Na^+ (and H_2O) overload (n = 1)	^{23}Na-MRI, pilot study, prolonged off-label eplerenone treatment, one 22-yr-old female DMD patient.
7	Altamirano et al., 2014	Vastus lateralis control: 8 mM; *mdx*: 18 mM	Na^+ electrodes. Shear-stress stimulation of NO pathway reduced *mdx* $[Na^+]_i$ to 10 mM without altering control level (see their Fig. 1 B). Mice.
8	Burr et al., 2014	Control: 5.3 mM; *mdx*: 7.3 mM	Na^+ electrodes (see their Fig. 10). Mice.
9	Glemser et al., 2017	∼20% drop in muscle Na^+ overload (n = 1)	^{23}Na-MRI, pilot study, 6 mo off-label eplerenone treatment, one 7-yr-old male DMD patient (see their Table 1).
10	Gerhalter et al., 2019	Total sodium content: volunteers: 16.5 mM; DMD patients: 26 mM	^{23}Na-MRI, French DMD patient cohort. Na^+ overload regularly observed in the absence of water T_2 increases; this is, therefore, nonosmotic Na^+ loading (see also 9).

energy of Donnan effectors to keep SMFs difficult to excite. Meanwhile, [small I_{Naleak}] ensures hyperpolarized resting potential (V_{rest}) values, slow rundowns when pump strength falters, and the large resilience-conferring pump reserves that ensure SMFs can handle intermittent peak demands.

Operational "pump strength" defined

Ion homeostatic pump strength here is an operational term, given as percentage of normal (100%) maximal pump strength. Pump-strength units are attomol/s (amol/s; 10^{-18} mol/s) ATP consumed or, equivalently, pA of $I_{NaKpump}$ (see Materials and methods). Facilitating intermodel comparisons, for all P-L/D models here, maximal (100%) pump strength = 566 amol/s of ATP consumption (i.e., 54.5 pA of $I_{NaKpump}$ for $I_{maxNaKpump}$) and pump kinetic parameters are identical. A P-L/D system's operational pump strength would, then, depend, in vivo, on (1) the quantity of pump proteins (an expression issue), (2) the functionality of membrane-resident pumps (a "machinery" issue), and (3) the supply issue of ATP availability (i.e., [oxygen-glucose →→→ATP]). Thus (hormonal) up-regulation would give pump strengths >100% whereas (e.g.) tourniquet application, chronic or episodic ischemia, malfunctioning pumps, ouabain, vascular deterioration, etc., would give pump strengths <100%. As DMD progressed, cumulative defects of the dystrophin-minus condition (Fig. 1, A–C) would diminish pump strength, thus defined.

Reduced pump strength and elevated Na^+ leaks in DMD

The mitochondrial damage of DMD is first a pump-strength supply issue, and second, from reactive oxygen species (ROS) and Ca^{2+} damage to pump-bearing sarcolemma, a machinery issue (Whitehead et al., 2010; Timpani et al., 2015; Moore et al., 2020; Dubinin et al., 2020; Ramos et al., 2020; Capitanio et al., 2020). A further supply issue is inadequate DMD vasculature (Dietz et al., 2020). Because of early reports of above-normal Na^+/K^+-adenosine triphosphatase (ATPase) protein levels in *mdx* SMFs (Anderson 1991; Dunn et al., 1995), pump expression was not considered problematic. New work shows otherwise. Kravtsova et al. (2020) find, for $3Na^+/2K^+$ATPase isozymes in *mdx* respiratory (diaphragm) and postural (soleus) muscles, reduced protein (and mRNA) levels, depolarized V_{rest} values, and diminished ouabain depolarization. Moreover, given the sensitivity of Na^+/K^+-ATPases to bilayer lipids (Cornelius et al., 2015; Habeck et al., 2017; Petrov et al., 2017; Hossain and Clarke, 2019; Else, 2020), the pathologically redistributed diaphragm endplate cholesterol Kravtsova et al. (2020) observe likely further diminish pump strength as a machinery issue. Pediatric DMD patients' dyslipidemia worsens with age, while deep remodeling of energy metabolism occurs in DMD SMFs (this includes reduced SMF ATP, a supply issue) and changes in multiple membrane-forming lipids (Anderson, 1991; White et al., 2020; Dabaj et al., 2021). These deficits are consistent with sarcolemmal damage of DMD due to mechanical and oxidative (Ca^{2+}/ROS) stress (Petrof et al., 1993; Dudley et al., 2006; Allen et al., 2016; Murphy et al., 2019).

Acutely, during exertion, healthy SMFs locally bolster their vascular supply: a nitric oxide (NO) synthetase (NOS) linked via dystrophin to the dystrophin–glycoprotein complex activates, producing NO to vasodilate capillaries. In dystrophin-minus fibers, this feedback fails (Sander et al., 2000; Asai et al., 2007). The result is functional ischemia. This is exacerbated by DMD muscles' degenerated vascularization (Dudley et al., 2006; Thomas, 2013; Bosco et al., 2021). Compounding these supply issues, longer-term, oxidative stress (Ca^{2+}, ROS) from functional ischemia causes membrane damage, a machinery issue.

On the Na^+-leak side, perturbed gating in bleb-damaged *mdx* sarcolemma could explain overactive voltage-gated sodium

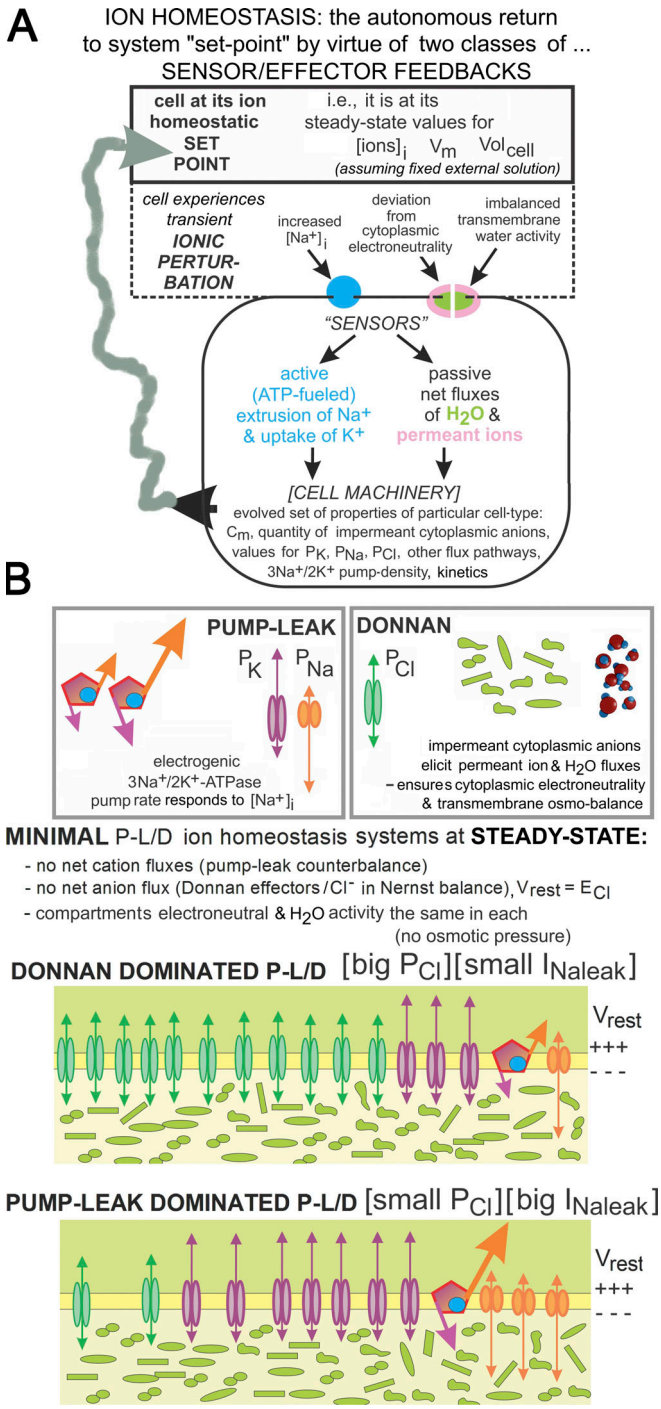

Figure 2. **P-L/D ion homeostatic feedback processes at steady state.** See List of abbreviations. **(A)** Fundamentals. The ion homeostasis process autonomously returns cells to steady state after ionic perturbations. It uses two sensor/effector feedback mechanisms, one active, one passive. Any cell system's ion homeostatic set point is its steady state, uniquely defined by the set of variables: V_m, Vol_{cell}, and $[ion]_{i(ntracellular)}$ (set point is thus a set-set). Deviations from the set are not what is sensed and responded to. An otherwise blind-to-system values ATP-fueled $3Na^+/2K^+$ pump makes a sensor/effector response by extruding Na^+ (and retrieving K^+) faster, thereby hyperpolarizing V_m more strongly whenever $[Na^+]_i$ permeability increases. Simultaneously, the fixed quantity of impermeant cytoplasmic anions, i.e., Donnan effectors, and a P_{anion} (modeled here as P_{Cl}) in a P_{Na}- and P_K-equipped H_2O-permeable membrane, operate as a passive ion homeostatic sensor/effector feedback mechanism, in thrall to thermodynamic/electrostatic constraints. The passive feedbacks, too, operate blind-to-system values, counteracting any osmo-imbalance and any departure from cytoplasmic neutrality. Evolution arbitrates cell-type–appropriate membrane area (C_m), N_{Ai} (the impermeant anion quantity), permeability values P_K, P_{Na}, P_{Cl}, P_{H2O}, pump density, and pump and $[Na^+]_i$ (also, $[K^+]_e$) sensitivity. As Fraser and Huang (2004) explain, a cell's N_{Ai} is the major determinant of its normal size. **(B)** The always-in-force feedback processes of P-L/D ion homeostasis, sensing a perturbation, immediately begin to reestablish steady state (at which point, net fluxes = 0). Depicted here are two minimal P-L/D steady states, meaning steady states achieved using only the minimal collection of components required (assuming a fixed external milieu) for autonomous return. As depicted, the balanced fluxes at top are Donnan dominated and below are Pump-Leak dominated. Each has three ion-selective permeabilities (P_{Na}, P_K, and P_{Cl}), an electrogenic ($3Na^+out/2K^+in$) $[Na^+]_i$-sensitive ATPase pump, a fixed quantity of impermeant cytoplasmic anions (A^-_i; Donnan effectors; −1 = assumed average valence), and a H_2O-permeable membrane area of specified capacitance. ATP ad libitum is assumed. In cells with $P_{Cl} >> P_K >>> P_{Na}$ (SMFs), steady-state fluxes are Donnan dominated. In cells with $P_K >> P_{Na} > P_{Cl}$ (neurons), steady-state fluxes are Pump-Leak dominated. At steady-state, Na^+-extrusion ($I_{NaKpump}$) matches steady-state Na^+ influx (I_{Naleak}). V_{rest} (steady-state V_m) depends on P_K:P_{Na}. In minimal systems at steady state, $V_{rest} = E_{Cl}$. Neurons' Pump-Leak dominated steady state is nonminimal due to constitutively operating K/Cl cotransporters (compare CN-CD against MN-CD; Table 2). When cotransporters activate in SMFs, they too have nonminimal steady states, but the ultra-basic model here for SMF membrane (SM-CD) has a minimal Donnan dominated P-L/D steady state. In healthy SMFs (and SM-CD), channels underlying excitability (AChRs, Nav, and Kv) are not open at steady state.

channel (Nav) 1.4 channels and overactive (unidentified) cation channels (Methfessel et al., 1986; Morris and Horn, 1991; Wan et al., 1999; Morris, 2012, 2018; Morris and Joos, 2016; Hirn et al., 2008; Lansman, 2015).

The capacity for sarcolemmal repair is retained

Stretch injury can leave *mdx* fibers depolarized and inexcitable for days but is not inherently lethal (Anderson, 1991; Call et al., 2013; Pratt et al., 2015; Baumann et al., 2020). In spite of their heightened susceptibility to rupture, microtears, and bleb damage (Menke and Jockusch, 1991, 1995; Petrof et al., 1993; Williams and Bloch, 1999; García-Pelagio et al., 2011; Hernández-Ochoa et al., 2015; Houang et al., 2018; Fig. 1 B), DMD fibers, like healthy SMFs, can repair sarcolemma tears. Ca^{2+}-mediated exocytosis seals the tear; endocytosis then retrieves excess bilayer, though *mdx*-fibers' impaired autophagy impedes subsequent reprocessing (McNeil and Steinhardt, 2003; Corrotte et al., 2013; Andrews et al., 2014; Barthélémy et al., 2018; Stoughton et al., 2018; Call and Nichenko, 2020).

Na^+ overload: Though rapidly lethal in injured neurons, chronically tolerated in DMD SMFs

Na^+ overload of ischemically injured central neurons rapidly elicits treacherous osmotic swelling (Hübel et al., 2014; Dreier et al., 2018). In cortical neurons (CNs), this accelerates lethally when normally cryptic Cl^- channels activate (Rungta et al., 2015). Dijkstra et al. (2016) explained this cerebral ischemia scenario using a neuronal P-L/D ion homeostasis model, here termed CN-CD.

^{23}Na-proton-MRI measurements from leg muscles of preteen boys with DMD show a chronic Na^+ overload that has been

shown to be "nonosmotic," i.e., not accompanied by water uptake (Table 1, items 5, 6, and 10; Weber et al., 2011, 2012; Gerhalter et al., 2019). This presents a seeming conundrum because, like their healthy counterparts, DMD-afflicted SMFs have an exceptionally large resting P_{Cl} (chloride permeability), or "[big P_{Cl}]," ∼80% of which is due to ClC-1 channels (Cozzoli et al., 2014; Pedersen et al., 2016; Jentsch and Pusch 2018). CNs' "[small P_{Cl}]" helps minimize swelling during normal brief Na^+ loads but is inadequate during sustained ischemia-induced Na^+ loading. Then, for well-understood reasons, once the abnormal P_{Cl} component joins in, the neurons succumb even faster to cytotoxic [$Na^+ + Cl^- + H_2O$] (osmotic) influxes or "death-by-Donnan effect." How, then, do [big P_{Cl}] DMD fibers, with their low pump strength, chronically sustain nonosmotic Na^+ overloads? Though P_K values differ nontrivially in neurons and SMF, the explanation does not lie there. Modeling here will show those differences to be constrained by far more critical neuron/SMF differences in P_{Na} and P_{Cl} values.

Neurons, to support their easy-to-excite electrically agile electrophysiological lifestyle, evolved a costly Pump-Leak–dominated ([small P_{Cl}][big I_{Naleak}]) strategy for ion homeostatic steady state. SMFs, cells that spend most of their time at steady state, where they need to remain difficult-to-excite, rely on a different strategy ([big P_{Cl}][small I_{Naleak}]).

A useful P-L/D model for excitable SMFs, one that can resolve the neuron/SMF "P_{Cl} conundrum," should explain healthy SMF ion homeostasis while clarifying how DMD-afflicted, Na^+-overloaded SMFs avoid osmotic swelling. The model used here does so. It shows how SMFs' [big P_{Cl}]/(Donnan effector) collaboration physiologically exploits free energy embodied in impermeant myoplasmic anions to deeply stabilize, for no added cost, their Pump-Leak–determined steady state. This strategy keeps SMF excitability low and extraordinarily safe from osmotic swelling, provided they maintain the [small I_{Naleak}]. Modeling likewise shows how the Donnan dominated (i.e., [big P_{Cl}][small I_{Naleak}]) SMF ion homeostatic steady state would eventually fail, as severe (late-stage) DMD damage rendered I_{Naleak} too big and global SMF pump strength too small.

Comparative CD modeling to address DMD

To probe healthy SMF volume regulation, Fraser and Huang (2004) established the biophysically rigorous CD approach to ion homeostasis modeling (Fraser and Huang, 2007; Kay, 2017; Dmitriev et al., 2019) used here. Unlike earlier approaches, it explicitly incorporates the thermodynamic feedbacks (constraints) imposed by cytoplasmic Donnan effectors (Fig. 2 A). That first Fraser and Huang (2004) P-L/D model (like models here) is 0-D, meaning that flux properties are spatially invariant. It is, however, nonexcitable. A later model addressing action potential (AP) propagation in K^+-accumulating t-tubules adds spatial complexity and excitability (Fraser et al., 2011; see T-tubules in the supplemental text at the end of the PDF), but is unsuited for addressing the resilience of SMF ion homeostasis in the face of DMD.

For that purpose, we use parallel (i.e., comparative) P-L/D modeling. SM-CD is our as-basic-as-possible P-L/D model for a slice of generic excitable SMF; as per Fig. 3 A–C and Table 2 (see List of abbreviations), it parallels the extant model, CN-CD (Dijkstra et al., 2016). SM-CD has SMF-appropriate resting permeabilities and excitability, but matches CN-CD for membrane area, maximal (100%) pump strength, and steady-state volume. Parallel models make intersystem comparisons of (1) steady-state values and (2) post-perturbation trajectories biophysically meaningful. SM-CD has a minimal steady state, but CN-CD (with its neuronally important K/Cl cotransporter) has a nonminimal steady state. In all models, $I_{NaKpump}$ (i.e., hyperpolarizing Na^+ extrusion from $3Na^+out/2K^+in$) is the direct electrophysiological consequence of ion homeostatic ATP consumption. For SM-CD, steady state is Donnan dominated; to quantitatively clarify the benefits of that steady state, an additional parallel model, weak Donnan (WD)–CD is devised: it is a counterfactual SM-CD analog with a Pump-Leak–dominated steady state.

Donnan effectors rehabilitated

It is widely and correctly understood that energetically compromised cells risk death-by-Donnan effect. It is widely underappreciated, however, that Donnan effectors are cell-physiologically indispensable (Fig. 2 A). However, because "Donnan equilibrium" (DE) equals death, Donnan has come to be a dirty word. Thus, the all-important "passive stabilization of E_{Cl} near V_{rest}" in SMFs is alluded to frequently (e.g., Pedersen et al., 2016), but the mechanism by which this is achieved (i.e., by exploiting the osmo-electrical free energy inherent in SMFs' abundant cytoplasmic Donnan effectors) is not. Thus, ion homeostasis gets overlooked as a role for SMFs' ClC-1 channels (Jentsch and Pusch, 2018). Thus, the immense importance for vertebrate evolution of SMFs' robust efficient Donnan dominated ([big P_{Cl}][small I_{Naleak}]) steady state seems to go unnoticed.

Underappreciated, by extension, is the pivotal role of SMFs' unidentified small-valued P_{Na}. This oversight is explicable because V_{rest} is usually calculated with the GHK voltage equation (e.g., Sperelakis, 2012; and see Hille, 2001, Eq. 14.10). There, the smaller the P_{Na}, the less consequential the tiny I_{Naleak} carried by P_{Na}. Using P-L/D equations for SMF steady state, however, shows that small P_{Na} carries not an inconsequentially tiny I_{Naleak} but a powerfully tiny I_{Naleak}. It is powerful because it underlies SMFs' tiny steady-state ATP consumption.

Rehabilitating Donnan effectors' bad reputation as we do here highlights that, for vertebrate bodies (on a body mass basis), low-cost Donnan dominated steady states (as in SMFs) are the norm. High-cost Pump-Leak dominated steady states (as in neurons) are, and always have been (on a body mass basis), the special case (Table S1).

DMD: Fiber demise and fiber survival

DMD fiber necrosis is typically ascribed to Ca^{2+} necrosis (Claflin and Brooks, 2008; Allen et al., 2016; Mareedu et al., 2021), but as emphasized by Burr et al. (2014), who examined *mdx* Ca^{2+} necrosis via reverse operation of Na^+/Ca^{2+} exchangers, underlying that Ca^{2+} necrosis is a preexisting Na^+ overload. Summary comments by Burr and Molkentin (2015) reveal that the provenance of DMD Na^+ overload is poorly understood. They write that "given the known mechanical defects within the dystrophic

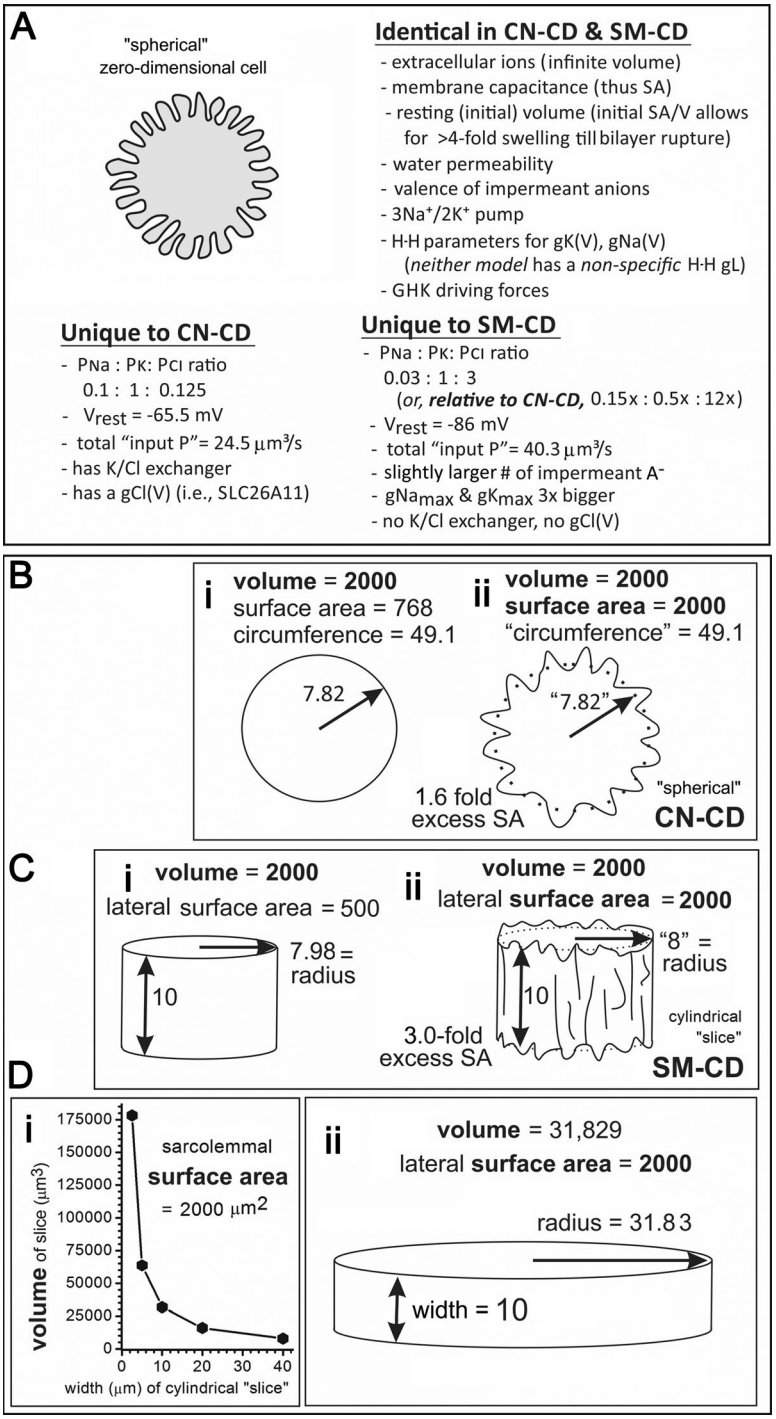

Figure 3. **Model building. (A)** CN-CD→SM-CD. SM-CD was devised by modifying CN-CD (specifics in Materials and methods, Table 2, and List of abbreviations). CN-CD assumes a round cell with excess SA. Though Dijkstra et al. (2016) compute X-sectional area (relevant to confocally imaged neurons in brain slice; Rungta et al., 2015), we recalculate CN-CD for Vol_{cell}. **(B–D)** SA/Vol: from CN-CD via SM-CD to SMFs. When extrapolating from SM-CD to myofibers, SA/Vol will impact P-L/D efficiency and time courses (see text). Thus, two steps, B, i and ii, and C, i and ii, show how one ion homeostatic unit (with its given excess SA) would be disposed for mononuclear CN-CD versus multinuclear SMFs. In SMFs, one SM-CD unit would be one of many for a cylindrical syncytial myofiber. Enclosed versus encircled is not computationally relevant here (P-L/D models here are 0-D, not 3-D), but topology matters for extrapolating to actual myofibers, as in D, i, where, for cylindrical geometry, 2,000 μm^2 of sarcolemma disposed as a ring (no excess SA) would encircle far more Vol_{cell} than 2,000 μm^3 (Vol_{cell} depending on slice width); e.g., the 10-μm slice (D, ii) would enclose ∼32,000 μm^3 of myoplasm (SA/Vol ratio: ∼0.125/μm, compared with 1/μm for C, ii). Linear, area, and volume dimension units here: μm, μm^2, and μm^3, respectively. Schematics not to scale (for reference [using their SA/Vol units], Fraser and Huang (2004) modeled a 75-μm-diameter fiber with SA/Vol_{cell} = 5×10^5 cm^2/liter; the D, ii, slice has SA/Vol_{cell} = 6×10^5 cm^2/liter, and SM-CD [as per C, ii] SA/Vol_{cell} = 25×10^5 cm^2/liter). See also T-tubules in the supplemental text.

plasma membrane…alterations in calcium and sodium levels likely stem…from excessive activation of various channels and exchangers." While this is mechanistically vague, what is clear is their implication that too much Na^+ leak would account for chronic Na^+ overload. Our analysis strongly suggests, however, that for chronic Na^+ overload to result in fiber loss, too little Na^+ pumping (i.e., low pump strength) would be a major factor, while too much Na^+ leaking would be a dangerous exacerbating factor, but not a sole cause.

Specifically, modeling here shows how low pump-strength conditions elicit unwanted Na^+ entry through normal Nav channels. Additionally, DMD fibers can have pathologically leaky Nav and/or cation channels that, under low pump-strength conditions, would contribute to chronic Na^+ overloads. Modeling shows, too, the vastly different thresholds for cytotoxic swelling (elicited by spontaneous firing) in SMFs versus neurons.

For SMFs, the physiological "Na^+-leak channel" (P_{Na}) is not identified, but in neurons, smooth muscle, pancreatic cells, and others, the physiological (ion homeostatic) Na^+-leak channel is a nonselective cation channel (Na leak channel nonselective [NALCN]; Lu et al., 2007; Kang et al., 2020). For decades,

Table 2. **Parameter values for CN-CD and SM-CD models and variants**

		Excitable P-L/D charge difference (CD) model				
	Notes	**CN-CD**	**MN-CD**	**SM-CD**	**WD-CD**	**LA-CD**
Parameter	Nature of model's steady state →→	P-L domin'd st-st nonminimal (neuron)	P-L domin'd st-st / minimal (no co-transporter)	Donnan domin'd st-st / minimal (healthy SMF)	P-L domin'd st-st / minimal (counterfactual)	Donnan domin'd st-st / minimal (DMD-like)
C_m		20 pF	20 pF	20 pF	20 pF	20 pF
SA (from C_m)	(0.01 pF/μm^2)	2,000 μm^2	2,000 μm^2	2,000 μm^2	2,000 μm^2	2,000 μm^2
P_{Na}		2 μm^3/s	2 μm^3/s	0.3 μm^3/s	1.06 μm^3/s	0.3 μm^3/s
P_K		20 μm^3/s	20 μm^3/s	10 μm^3/s	36.7 μm^3/s	10 μm^3/s
P_{Cl}		2.5 μm^3/s	2.5 μm^3/s	30 μm^3/s	2.5 μm^3/s	30 μm^3/s
P_{Na}:P_K:P_{Cl}	P_{ionX} ratios	0.1:1:0.125	0.1:1:0.125	0.03:1:3	0.03:1:0.07	0.03:1:3
Impedance^{-1}	(Summed P_{ionX})	24.5 μm^3/s	22.5 μm^3/s	40.3 μm^3/s	40.3 μm^3/s	40.3 μm^3/s
P_{H2O}		2 μm^3/(s Pa)	2 μm^3/(s Pa)	2 μm^3/(s Pa)	2 μm^3/(s Pa)	2 μm^3/(s Pa)
N_{Ai}		296 fmol	296 fmol	299.2 fmol	299.2 fmol	298.4 fmol
Pump as ATPase	Max ATP/s or 100%	566 amol/s	566 amol/s	566 amol/s	566 amol/s	170 amol/s
$I_{maxNaKpump}$	Max $I_{NaKpump}$	54.5 pA	54.5 pA	54.5 pA	54.5 pA	16.35 pA
Max P_{Nav}	Like H-H g_{max}	800 μm^3/s	800 μm^3/s	2,400 μm^3/s	2,400 m^3/s	2,400 μm^3/s
Max P_{Kv}	Like H-H g_{max}	400 μm^3/s	400 μm^3/s	1,200 μm^3/s	1,200 m^3/s	1,200 μm^3/s
U_{KCl}	(Strength)	1.3 (fmol/s)/(J/Coul)	0	0	0	0
Max P_{Clv}	(Pathological)	19.5 μm^3/s	19.5 μm^3/s	0	0	0
Electrolytes (mM): extracellular [fixed] and intracellular (calculated at steady state)						
$[Sol]_{e,\ i}$	Total solutes	[310] & (310)	[310] & (310)	[310] & (310)	[310] & (310)	[310] & (310)
$[Na^+]_{e,\ i}$	Sodium	[152] & (10)	[152] & (9.8)	[152] & (3.7)	[152] & (6.8)	[152] & (6.5)
$[K^+]_{e,\ i}$	Potassium	[3] & (145)	[3] & (145.2)	[3] & (151.3)	[3] & (148.2)	[3] & (148.5)
$[Cl^-]_{e,\ i}$	Chloride	[135] & (7)	[135] & (12.2)	[135] & (5.4)	[135] & (5.4)	[135] & (5.5)
$[A^-]_{e,\ i}$	Impermeant	[20] & (148)	[20] & (142.8)	[20] & (149.6)	[20] & (149.6)	[20] & (149.5)
Calculated steady-state (resting-state) values of P-L/D systems with above values						
Vol_{cell}	(Volume)	2,000 μm^3	2,072 μm^3	2,000 μm^3	2,000 μm^3	2,000 μm^3
V_m	(V_{rest})	−65.5 mV	−64.3 mV	−86.0 mV	−86.0 mV	−85.6 mV
$[Sol]_i$	$[Solutes]_{cytoplasm}$	310 mM	310 mM	310 mM	310 mM	310 mM
E_{Na}	(Nernst pot'l)	72.6 mV	73.1 mV	99.2 mV	82.9 mV	84.0 mV
E_K	(Nernst pot'l)	−103.6 mV	−103.6 mV	−104.7 mV	−104.2 mV	−104.2 mV
E_{Cl}	(Nernst pot'l)	−79.0 mV	−64.3 mV	−86.0 mV	−86.0 mV	−85.6 mV
I_{Naleak} (st-st)	(Through P_{Na})	−78.2 pA	−77.1 pA	−14.75 pA	−52.1 pA	−14.66 pA
I_{Nav} (st-st)	(Through P_{Nav})	−0.07 pA	−0.14 pA	-2.3×10^{-7} pA	-2.4×10^{-7} pA	-3.3×10^{-7} pA
m	(H-H)	0.013	0.013	0.000	0.000	0.000
h	(H-H)	0.987	0.987	1.000	1.000	1.0000
m^3h	(H-H)	2.2×10^{-6}	2.2×10^{-6}	1.75×10^{-12}	2.0×10^{-12}	2.8×10^{-12}
n	(H-H)	0.003	0.003	0.000	4.8×10^{-5}	5.3×10^{-5}
ATP/s (st-st)	Consumption	270.9 amol/s	267.3 amol/s	51.0 amol/s	180.4 amol/s	50.7 amol/s
Pump reserve	Max ATP/s /consumption	2.1-fold	2.12-fold	11.1-fold	3.1-fold	3.4-fold
Miscellaneous						
$Vol_{cellDonnanEq}$	(Notional)	14,000 μm^3	14,000 μm^3	14,960 μm^3	14,961 μm^3	14, 952 μm^3
$Vol_{cellrupture}$	(Bilayer limit)	8,920 μm^3	8,920 μm^3	8,920 μm^3	8,920 μm^3	8,920 μm^3

CN-CD entries are from Table 1 of Dijkstra et al. (2016). Parameter terms: see List of abbreviations. As per Dijkstra et al. (2016), permeabilities (in μm^3/s) are particular to the invariant membrane area here (2,000 μm^2). Constants: F, Faraday constant, 96,485.333 coulombs/mol; R universal gas constant, 8.31446 J mol^{-1}°K^{-1}; absolute temperature, 310°K; specific membrane capacitance, 0.01 pF/μm^2.

unidentified nonselective *mdx* fiber cation channels (their physiology unknown) have been considered problematic for passing unwanted I_{Ca} (Franco and Lansman, 1990; Yeung et al., 2005; Lansman, 2015; Ward et al., 2018). Whether they account for the SMF P_{Na} is unknown, but as per Yeung et al. (2003) and as per simulations here, such channels, if overactive, would constitute a pathological I_{Naleak}.

DMD SMFs, whose ion homeostatic resilience declines with advancing disease state, experience what is, in effect, a chronic state of emergency. They cope by relying on the extraordinarily robust ion homeostatic strategy evolved by syncytial vertebrate SMFs for handling the inevitable (but for healthy fibers, transient) emergencies of SMF life: membrane tearing, interrupted vascular supply, and bouts of overexertion. Modeling suggests that refurbishing the emergency preparedness of DMD fibers (via improved operational pump strength and decreased Na^+ leak via Nav1.4 and/or cation channels) could extend their already remarkable longevity.

Materials and methods

A P-L/D model for SMFs

The features of SMF ion homeostasis are modeled using SM-CD, a zero-dimensional single compartment limited by a semipermeable membrane in an infinite (fixed concentrations) extracellular volume (Fig. 3 A, Table 2, and List of abbreviations). SM-CD constitutes one P-L/D ion homeostatic unit; multinucleate SMF would comprise hundreds or even thousands of such units (depending on sarcolemma area). A SMF with a smaller SA/Vol ratio than SM-CD would exhibit slower $\Delta[ion]_i$ dynamics (Fig. 3, C and D). SM-CD encloses a fixed quantity of Donnan effectors: A^-, impermeant monovalent anions (as discussed by Fraser and Huang, 2004). The extracellular medium has a fixed A^- concentration. The membrane is permeable to Na^+, K^+, and Cl^- ions, whose extracellular concentrations are fixed. SM-CD has the same physical characteristics as the Dijkstra et al. (2016) neuronal cell, CN-CD (see Table 2): a resting cell volume (Vol_{cell}) of 2,000 μm^3 and a constant total membrane capacitance of the cell model (C_m) corresponding to an SA of 2,000 μm^2. As such, resting state cells are flaccid; lipid bilayers tolerate little lateral expansion, but only if a model cell inflated its membrane to spherical would tension and rupture be relevant (see Table 2). The permeation pathways of SM-CD and CN-CD (given below) include resting leak conductances (i.e., permeation pathways) for I_{Naleak}, I_{Kleak}, I_{Clleak}, and voltage-gated conductances (permeation pathways) for a transient sodium current, I_{Nav}, for delayed rectifier potassium current, I_{Kv}, and CN-CD but not SM-CD has a V_m-dependent chloride current, I_{Clv}, plus an electroneutral cotransporter, J_{KCl}. Driving forces acting on ions are, in all cases, electrodiffusive, as depicted by Goldman–Hodgkin–Katz (GHK) current equations (Hille 2001). The same $3Na^+_{out}/2K^+_{in}$ ATPase pump model used by Dijkstra et al. (2016) as taken by them from Hamada et al. (2003) is used throughout. It produces hyperpolarizing current,

$$I_{Na,pump} = 3I_{NaKpump} = -3/2\ I_{Kpump}, \quad (1)$$

in response to the intracellular $[Na^+]$ (as per Fig. 4 A).

Since animal cells do not sustain osmotic pressures, intra/extracellular (osmolyte) inequalities elicit a H_2O flow until osmotic balance is restored; this results in Vol_{cell} changes at rates limited by the slower net flux component, at any time, of the two ions ($[Na^+ + Cl^-]$) whose joint net entry underlies osmotic Na^+ loading.

Choice of leak permeabilities

Whereas CN-CD is precisely the Dijkstra et al. (2016) model, the SM-CD leak permeability ratio $P_{Na}:P_K:P_{Cl}$ is broadly consistent with Fraser and Huang (2004); for more detail, see Setting V_{rest} in SM-CD and other CD models below.

GHK driving forces

Currents through open channels (permeability pathways), ion-specific or not, are modeled with the GHK formulation (Hille, 2001; see Fig. 4 C). For ionX = Na^+, K^+, or Cl^-, the GHK current is given by

$$I_{GHK}(X, P_{ionX}, V_m) = P_{ionX}(z_{ionX}F)\ \times$$
$$\frac{z_{ionX}FV_m}{RT}\ \frac{[ionX]_i - [ionX]_e exp\left(-\frac{z_{ionX}FV_m}{RT}\right)}{1 - exp\left(-\frac{z_{ionX}FV_m}{RT}\right)}, \quad (2)$$

where P_{ionX} is the permeability, z_{ionX} is the valence, $F = eN_{Avog}$ is the Faraday constant (e is the electronic charge [1.6×10^{-19}Coul] and N_{Avog} is the Avogadro number), and $[ionX]_i$ and $[ionX]_e$ are the intra- and extracellular concentrations of ionX, respectively.

Resting or leak currents

Leak permeability mechanisms use the GHK formulation

$$I_{ionX} = I_{GHK}(ionX, P_{ionX}, V_m), \quad (3)$$

where ionX is Na^+, K^+, or Cl^-. Leak permeability (P_X) values were adjusted for model variants used here (Table 2) in the context of appropriate setting of V_{rest}.

Cation channel currents

For nonselective cation channels, we use a $P_K:P_{Na}$ ratio of 1.11:1 and the formulation

$$I_{catleak}(t) = I_{GHK}(Na^+, P_{Na,catleak}, V_m) + I_{GHK}(K^+, P_{K,catleak}, V_m). \quad (4)$$

In the present models, cation channel leaks do not contribute to healthy steady states; they are either transient stimulatory currents through SMF-endplate–type acetylcholine receptor (AChR) channels (Hille 2001), or pathological leaks (hence "leaky" cation channels).

Voltage-gated Na^+ current

$$I_{Nav} = m^3hI_{GHK}(Na^+,\ P_{Nav},\ V_m) \quad (5)$$

P_{Nav} is the maximal membrane permeability to Na^+ through a V-gated channel (operating in a Hodgkin-Huxley [H-H] fashion). m is the H-H Na^+ channel activation/deactivation gating variable, and h is the H-H Na^+ channel inactivation/recovery gating variable. The current's driving force also follows the GHK form of Eq. 1.

List of abbreviations

A^-_i, impermeant intracellular anion (= Donnan effector)
AChR, acetylcholine receptor (i.e., SMFs' nicotinic cation-selective channel)
amol/s, attomoles/second (10^{-18} mole/second)
AP, action potential ($V_m(t)$)
ATP, adenosine triphosphate
C_m, total membrane capacitance of the cell model
CD, Charge Difference (all models are thus designated: CN-CD, MN-CD, SM-CD, LA-CD, WD-CD)
CN-CD, Cortical Neuron-CD (MODEL; the "parent" model; see Table 2)
DE, Donnan equilibrium
DMD, Duchenne muscular dystrophy
E_{ionX}, Nernst potential for named ion
EPSC, excitatory post-synaptic current (for SMFs, the endplate current)
GHK, Goldman–Hodgkin–Katz (electrodiffusive fluxes; open channel I/V relations)
H-H, Hodgkin-Huxley (for V-gated channels: non-dimensional parameters, *m,h,n*)
I_{ionX}, currents through channels permeant to ionX (or, if gated, then I_{Nav}, I_{Kv})
$I_{NaKpump}$, $I_{Na,pump}$, $I_{K,pump}$, $I_{maxNaKpump}$ (below, see $3Na^+/2K^+$-ATPase & max)
Kv, voltage-gated potassium channel (or delayed rectifier)
LA-CD, Low ATPase-CD (MODEL; a low pump-strength SM-CD variant; see Table 2)
max, 100% levels for pump: maximal ATP-consumption (amol/s) or $I_{maxNaKpump}$
mdx, dystrophin-minus mouse
MN-CD, Minimal Neuron-CD (MODEL; CN-CD without co-transporter; see Table 2)
MRI, magnetic resonance imaging
$3Na^+/2K^+$-ATPase, "the pump"; as an electrogenic ATP-consuming enzyme, it generates... unidirectional ((efflux) $I_{Na,pump}$ + (influx) $I_{K,pump}$) = hyperpolarizing $I_{NaKpump}$
N_{Ai} , the quantity (attomoles) of cytoplasmic impermeant anions
Nav, voltage-gated sodium channel
Nav-CLS, coupled left-shift (of Nav channel gating)
$P_{catleak}$, permeability of cation-selective channel
P_{Cl}, P_{Na}, P_K, permeabilities of always-open ("background," "resting," "leak" channels selective for Cl^-, Na^+, K^+ (thus, P_{Na}:P_K:P_{Cl} -- relative values in a specified membrane)
P_{H2O}, membrane water permeability
$P_{Nav\ (or\ Kv\ or\ Clv)}$, for V-gated channels permeability equivalents to g_{max}
P-L/D, Pump-Leak/Donnan
ROS, reactive oxygen species
SA, surface area (directly proportional to model parameter C_m)
SM-CD, Skeletal Muscle-CD (MODEL; see Table 2)
SMF, skeletal muscle fiber
U_{KCl}, K/Cl cotransporter – maximal flux capacity
V_m, V_{rest}, membrane potential, resting (steady-state) potential
Vol, volume (Vol_{cell} is the corresponding cell model parameter)
WD-CD, Weak Donnan-CD (MODEL; an SM-CD analog, see Table 2)

Delayed rectifier K^+ current

$$I_{Kv} = n^2 I_{GHK}(K^+,\ P_{Kv},\ V_m) \tag{6}$$

P_{Kv} is the maximal membrane permeability of K^+ through a V-gated channel (delayed rectifier voltage-gated potassium channel [Kv], operating in a H-H fashion); n is the delayed rectifier K^+ channel activation/deactivation gate variable.

Voltage-dependent gating

The nondimensional gating parameters m, h, and n evolve in time according to

$$dq/dt = \alpha_q(V_m)(1-q) - \beta_q(V_m)q, \tag{7}$$

where q is m, n, or h, as defined above, and the voltage dependent $\alpha_q(V_m)$ and $\beta_q(V_m)$ refer, for m and n, to gate activation and deactivation, and for h, to inactivation and recovery from inactivation. Table 3 gives the voltage dependences for the relevant rate constants.

Voltage-dependent Cl^- current

The SLC26A11 ion exchanger–based voltage-dependent Cl^- conductance (Rungta et al., 2015) is as described by Dijkstra et al. (2016):

$$I_{Clv} = \frac{I_{GHK}(Cl^-, P_{Clv}, V_m)}{1 + \exp\left(-\frac{V_m + 10\ mV}{10\ mV}\right)}. \tag{8}$$

Except in CN-CD and minimal neuron (MN)–CD, this pathological CN-specific conductance is set at zero.

K/Cl cotransporter

This cotransporter (strength K/Cl cotransporter–maximal flux capacity [U_{KCl}]) is present in CN-CD (SM lacks it; Pedersen et al., 2016) where (as per Dijkstra et al., 2016, except for an error in the log term of their Eq. 6) it is given by

$$J_{KCl} = U_{KCl}\frac{RT}{F} ln\left(\frac{[K^+]_i[Cl^-]_i}{[K^+]_e[Cl^-]_e}\right). \tag{9}$$

$3Na^+/2K^+$ ATPase pump current

The electrogenic $3Na^+$(out)/$2K^+$(in)-ATPase modeled here (as in Dijkstra et al., 2016; and as plotted in Fig. 4 A) is given as

$$\frac{I_{NaKpump}([Na^+]_i)}{I_{maxNaKpump}} = \frac{0.62}{1 + \left(\frac{6.7\ mM}{[Na^+]_i}\right)} + \frac{0.38}{1 + \left(\frac{67.6\ mM}{[Na^+]_i}\right)^3}, \tag{10}$$

where

$$\begin{aligned} I_{NaKpump} &= I_{Na,pump} + I_{K,pump} \text{ or} \\ I_{NaKpump} &= 1/3\left(I_{Na,pump}\right) = -1/2\left(I_{K,pump}\right). \end{aligned} \tag{11}$$

Thus, $I_{NaKpump}$ signifies a net hyperpolarizing current ($3Na^+$ outflow partially balanced by $2K^+$ inflow). This formulation is appropriate for models that assume an invariant extracellular medium. It depicts the pump's two intracellular Na^+-binding sites (with ~10-fold different affinities) but has no term for the extracellular K^+-binding site. Here, maximal pump strength ($I_{maxNaKpump}$) is varied in various computations (e.g., it is set to zero to depict anoxia or ouabain, diminished toward zero to depict lower percent pump strengths, and multiplied for up-regulation).

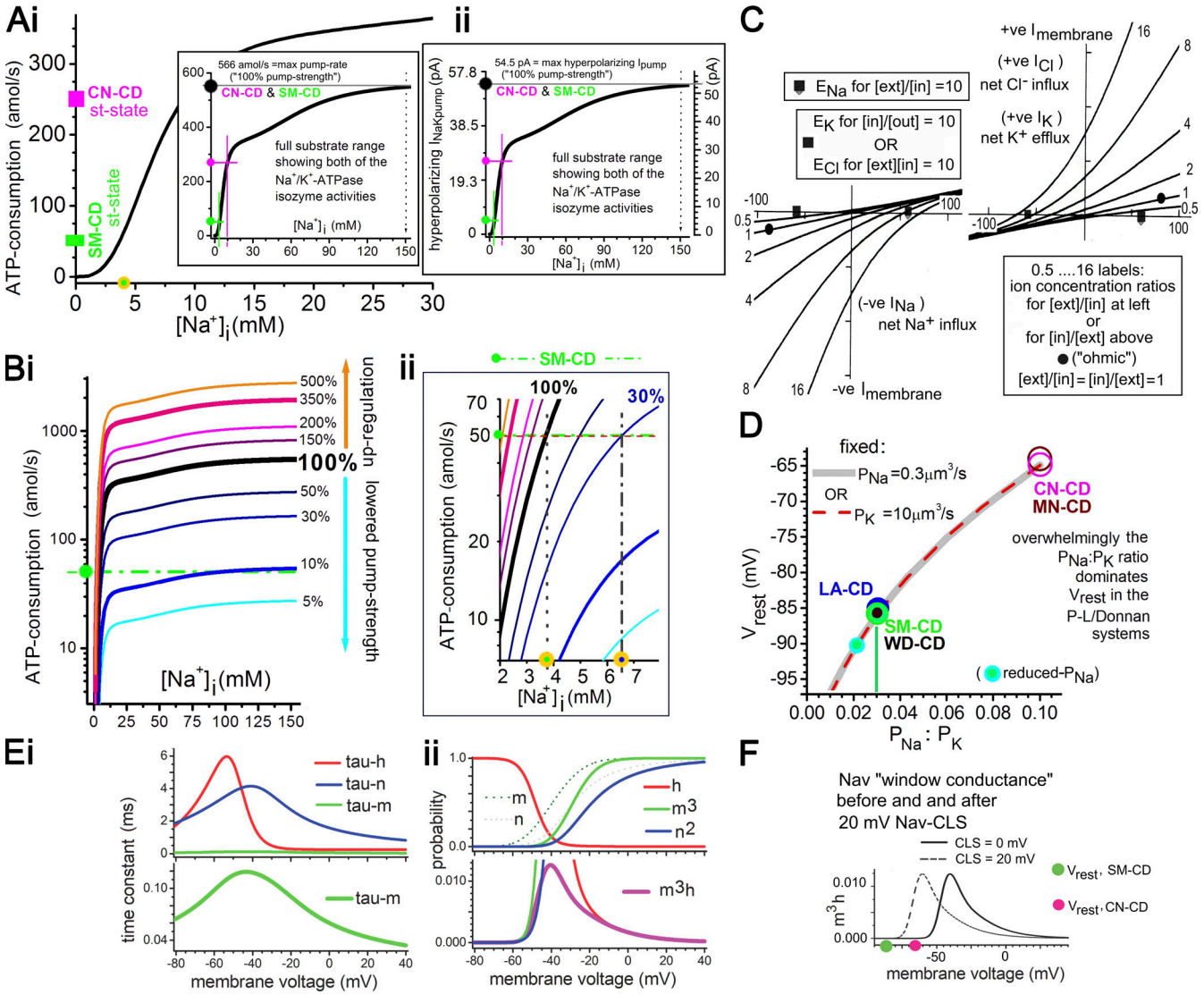

Figure 4. **The pump, GHK fluxes, excitability, Vrest(PNa:PK), Nav-CLS. (A)** i and ii, $3Na^+/2K^+$ATPase. The P-L/D models here have pumps described by Eq. 10, copied from CN-CD (Dijkstra et al., 2016, who took them from Hamada et al., 2003); at saturating $[Na^+]_i$, for 100% pump strength (the normal or standard condition), ATP consumption is maximally 566 amol/s = 54.5 pA of $I_{NaKpump}$ (see black dots). For SM-CD (green) and CN-CD (pink), the inset box pair shows the one-to-one correspondence of {steady-state [st-state] ATP consumption ($[Na^+]_i$)} and {$I_{NaKpump}$ ($[Na^+]_i$)}. Double-color dot (A, i, main plot): steady-state $[Na^+]_i$ for SM-CD. In the P-L/D models here, the external milieu is fixed, so pump sensitivity to $[K^+]_e$ does not affect pump rates. **(B i)** Different pump strengths: up-scaled and down-scaled 100% curves from A, as labeled (note logarithmic y axis). Horizontal green dot-dash line: SM-CD ATP consumption (as in A). **(B ii)** expanded lower left B, i, shows that (for near-identical ATP-consumption) SM-CD and LA-CD maintain very different $[Na^+]_i$. **(C)** Electrodiffusion I-V plots (see GHK electrodiffusion flux Eq. 2 [Hille, 2001; Eq. 14.5) for the noted [ext]/[in] ratios for Na^+ and [in]/[ext] ratios K^+ and Cl^- (y axis amperes are not specified since permeability values are not specified). Nernst potentials for 10-fold gradients (assuming room temperature) are shown. **(D)** V_{rest} in SM-CD with P_{Na}:P_K varied as shown. V_{rest} for P-L/D systems here (SM-CD, WD-CD, LA-CD, CN-CD, and MN-CD [100% pump strength]), their diverse P_{Cl} and E_{Cl} values notwithstanding, depends overwhelmingly on P_{Na}:P_K as shown. Blue dot: SM-CD with P_{Na} reduced to 0.22 $\mu m^3/s$. **(E)** For the Table 3 parameter values used here for excitable P-L/D models, voltage dependence of H-H variables tau-*m,h,n* and *m,m*^{3}*,h,m*^{3}*h,n,n*^{2}. Excitable P-L/D models use leak permeabilities (P_{Cl}, P_K, and P_{Na}) in lieu of H-H g_{Leak}, and the driving forces are electrodiffusive. **(F)** In bleb-damaged membrane, Nav channel activity exhibits irreversible hyperpolarizing shifts that scale with damage intensity (Wang et al., 2009; Boucher et al., 2012; Morris and Joos, 2016; Joos et al., 2017). In H-H terms, the damage makes both fast activation (m^3) and fast inactivation (h) shift leftward by the same amount (CLS). Illustrated: before and after imposing 20 mV of Nav-CLS on the computational Nav channels. Encroachment on V_{rest} of the window conductance (expressed nondimensionally as $m^3h(V_m)$) differs greatly for CN-CD versus SM-CD. -ve, negative; +ve, positive.

ATP consumption and hyperpolarizing $I_{NaKpump}$

ATP consumption by the $3Na^+/2K^+$ ATPase pump in all the CD models is given as

$$ATP/s = I_{NaKpump}/F. \quad (12)$$

In other words, an $I_{NaKpump}$ of 1 pA is equivalent to an ATP consumption of 10.38 amol/s.

Cell volume

Cellular swelling (or shrinking) is driven by an influx (or efflux) of water at rates that depend on the transmembrane osmotic gradient. The rate of change of cell volume, Vol_{cell}, due to water flux is given by

$$dVol_{cell}/dt = J_{H2O} = P_{H2O}\Delta Osm, \quad (13)$$

Table 3. **Voltage-dependent rates for H-H gating variables[a] (functions plotted in Fig. 4 E)**

Term	Expression	Description
$\alpha_m(V_m)$	$0.32(V_m + 52\ mV)/\left[1 - exp\left(-\frac{V_m + 52\ mV}{4\ mV}\right)\right]\frac{kHz}{mV}$	Activation rate, voltage-gated Na^+ channels (Nav)
$\beta_m(V_m)$	$0.28(V_m + 25\ mV)/exp\left(-\frac{V_m + 25\ mV}{5\ mV}\right)\frac{kHz}{mV}$	Deactivation rate, voltage-gated Na^+ channels (Nav)
$\alpha_h(V_m)$	$0.128exp\left(-\frac{V_m + 53\ mV}{18\ mV}\right)kHz$	Inactivation rate, voltage-gated Na^+ channels (Nav)
$\beta_h(V_m)$	$4/\left[1 + exp\left(-\frac{V_m + 30\ mV}{5\ mV}\right)\right]kHz$	Recovery from inactivation rate, voltage-gated Na^+ channels (Nav)
$\alpha_n(V_m)$	$0.016(V_m + 35\ mV)/\left[1 - exp\left(-\frac{V_m + 35\ mV}{5\ mV}\right)\right]\frac{kHz}{mV}$	Activation rate, delayed rectifier K^+ channels (Kv)
$\beta_n(V_m)$	$0.25exp\left(-\frac{V_m + 50\ mV}{40\ mV}\right)kHz$	Deactivation rate, delayed rectifier K^+ channels (Kv)

[a]Based on Kager et al. (2000), but as used in Dijkstra et al. (2016) with a typographical error corrected.

where the osmotic gradient, $\Delta Osm = RT([Sol]_i - [Sol]_e)$, and $[Sol]_i$ and $[Sol]_e$ denote total concentrations of intra- and extracellular solutes, and P_{H2O} is the effective membrane water permeability. This equilibration is typically (including in modeling here) assumed to be nearly instantaneous relative to the ion flows (Fraser and Huang, 2004; Dijkstra et al., 2016; Kay, 2017; though see also Dmitriev et al., 2019) so that osmotic ion fluxes, not H_2O fluxes, are what limit the rate of osmotic swelling or shrinkage.

Nernst potentials

The equilibrium potential (Nernst potential) for each ion is

$$E_{ionX} = (RT/z_{ionX}F)\log([ionX]_e/[ionX]_i), \quad (14)$$

where ionX is Na^+, K^+, or Cl^- ions, and z_{ionX} is the valence of each ion.

CD and membrane potential

Because CD models keep track of the absolute number of ions flowing across the cell membrane (of capacitance C_m), no differential equation is needed for V_m. Instead, an accounting equation is used, made simple because the extracellular space is kept neutral:

$$V_m = FC_m^{-1}(N_{Na,i}(t) + N_{K,i}(t) - N_{Cl,i}(t) - N_{Ai,i}) = FC_m^{-1}(dN_{Na}(t) + dN_K(t) - dN_{Cl}(t) - dN_{Ai}), \quad (15)$$

where $dN_{ionX} = N_{ionX,j}(t) - N_{ionX,i0}$ is the difference in the number of ions of species ionX, between its present value $N_{ionX,j}$ and a reference value $N_{ionX,i0}$. The reference values are those yielding $V_m = 0$ mV, which is equivalent to a neutral intracellular space $N_{Na,i0} + N_{K,i0} - N_{Cl,i0} - N_{Ai0} = 0$. Because the quantity (attomol) of cytoplasmic impermeant anions (N_{Ai}) is constant, note that $dN_{Ai} = 0$ in Eq. 15. Number differences, dN_{ionX}, are easier to work with than total numbers of ions N_{ionX} (or than concentrations). For typical cell C_m values, voltages in the mV range correspond to net intracellular CDs (measured as a number of singly charged ions) of the order of amol (10^{-18} mol). For instance, when V_m varies in the range [−100 mV, 100 mV] this corresponds to a change in net singly charged ions of [−20.7, +20.7] amol. With our Vol_{cell} = 2,000 μm³, this yields tiny concentration changes [−0.01, 0.01] mM. For solutions whose concentrations are in the 1–100 mM range, there could be four or five orders of magnitude difference between steady-state values and the changes (in the 0.0001–0.01 mM range). Computations based on absolute concentrations, therefore, tend to be unstable. For this reason, in this study, calculations are based on changes in ion numbers (in amol units).

Number of intracellular ions

CD models account for the change in intracellular ions at any given moment (Fraser and Huang, 2004, 2007; Dijkstra et al., 2016), via the following simple relationships of the respective currents:

$$dN_{Na}/dt = -F^{-1}(I_{Nav} + I_{Naleak} + 3I_{NaKpump}), \quad (16)$$
$$dN_K/dt = -F^{-1}(I_{Kv} + I_{Kleak} - 2I_{NaKpump}) - J_{KCl}, \quad (17)$$
$$dN_{Cl}/dt = F^{-1}(I_{Clv} + I_{Clleak}) - J_{KCl}. \quad (18)$$

Setting V_{rest} in SM-CD and other CD models

An excitable cell's V_{rest} (i.e., steady-state V_m) is typically more accessible (experimentally) than any cytoplasmic [ion] or Vol_{cell}. A consensus V_{rest} value is thus used for anchoring SM-CD; we chose V_{rest} = −86 mV. Other parameter determinants were then established iteratively as follows: first, a number is chosen for impermeant anions, N_{Ai}, consistent with the system's total cation concentration (given the extracellular solution). Starting with CN-CD the value, we fine-tuned to meet our (self-imposed) requirement that SM-CD and CN-CD have the same resting Vol_{cell}. Thus, note in Table 2 the slightly different N_{Ai} for CN-CD and SM-CD (likewise, low ATPase [LA]-CD and SM-CD) and identical steady-state Vol_{cell}.

At steady state, Na^+ and K^+ leak currents (for a system with a given pump strength), must precisely balance. In other words, V_m converges (along with ion concentrations and Vol_{cell}) on steady state (=V_{rest}) when

passive Na^+ influx + active Na^+ extrusion = zero

and

passive K^+ efflux + active K^+ uptake = zero.

For a $3Na^+/2K^+$ ATPase, this steady-state requirement is met when

$$-I_{Naleak} = I_{Na,pump} = -3/2(I_{K,pump}) = -3/2(-I_{Kleak}). \quad (19)$$

For P-L/D systems of a given pump strength, V_{rest} varies monotonically with P_{Na}:P_K (Fig. 4 D); low ratios yield hyperpolarized V_{rest} values, high ratios, depolarized ones. V_{rest} = −86 mV for SM-CD (and WD-CD) requires P_{Na}:P_K = 0.03:1. Absolute values for P_{Na} and P_K, and for P_{Cl} (Table 2), were guided by the P_{Na}:P_K:P_{Cl} ratio (0.02:1:3) reported for amphibian SM (Fraser and Huang 2004) and our choice to give SM-CM the same area (C_m) as CN-CD.

As per Eq. 16, a pump stoichiometry other than $3Na^+$out/$2K^+$in would, all else being equal, alter V_{rest}. Pump stoichiometry is invariant here, but see Dmitriev et al. (2019).

Excitability and safety factor for SM-CD

For SM-CD to be hyperpolarized and appropriately excitable (i.e., relatively inexcitable), its input impedance had to be (1) notably less than for CN-CD and (2) predominantly P_{Cl}-based (Pedersen et al., 2016). With resting P values set, the need to trigger spikes near −60 mV (Fu et al., 2011) with a reasonable-sized safety factor (Ruff 2011) had to be met. To achieve safety factor ∼1.5, Nav and Kv densities in SM-CD were set at 3× the CN-CD level (a larger P_{Cl} would have required even greater V-gated channel densities). Thus, absolute P_{Cl}, P_{Na}, and P_K values of SM-CD are biologically appropriate, but leave room for physiological modulation (to, say, alter V_{rest} via ΔP_{Na} or ΔP_K, or to modulate excitability by ΔP_{Cl}).

Table 2 shows that m^3h is vanishingly small at V_{rest} in SM-CD; for CN-CD it adds an extremely small Nav channel contribution to the operational value of P_{Na} that negligibly affects V_{rest}.

Cytoplasmic Donnan effectors

Once V_{rest} is set via P_{Na} and P_K, the intracellular anion concentrations are determined uniquely for the resting state. If Cl^- transport is purely passive (i.e., no involvement of secondary transport) as in SM-CD, then $E_{Cl} = V_{rest}$, and therefore,

$$[Cl^-]_i = [Cl^-]_e exp\left(\frac{FV_{rest}}{RT}\right). \quad (20)$$

The value of $[A^-]_i$ then follows from the voltage and osmotic balance requirements.

The voltage requirement yields

$$[Na^+]_i + [K^+]_i - [Cl^-]_i - [A^-]_i = -\Delta conc, \quad (21)$$

where Δconc is the tiny excess concentration of anions associated with V_{rest} and equal to [intracellular anions] − [intracellular cations]

$$\Delta conc = -V_{rest}C_m/\ FVol_{cell}. \quad (22)$$

For V_{rest} = −86 mV, Δconc = 0.00886 mM. The osmotic equilibrium condition is

$$[Na^+]_i + [K^+]_i + [Cl^-]_i + [A^-]_i = [S]_i = [S]_e, \quad (23)$$

where $[S]_i$ and $[S]_e$ are defined below Eq. 13. Eqs. 21 and 23 yield

$$[A^-]_i = ([S]_i + \Delta conc)/2 - [Cl^-]_i. \quad (24)$$

A P-L/D model-cell's design for steady state imposes its $[A^-]_i$. Therefore, the choice of N_{Ai} determines the cell volume $Vol_{cell} = N_{Ai}/[A^-]_i$. As mentioned above, SM-CD's N_{Ai} was set to give a resting Vol_{cell} = 2,000 μm³. Here, the quantity of impermeant anions N_{Ai} is invariant, but for many in vivo circumstances, it would vary, and Vol_{cell} would vary accordingly in such cases.

Instantaneous perturbations

Experimental solution changes (e.g., as in brain slice experiments) typically require finite "wash-in/wash-out" times. Dijkstra et al. (2016) mimicked such solution changes (affecting pump rates and channel gating, etc.), but here, doing so would have unnecessarily obscured mechanistic underpinnings of responses. Thus, pump-off (anoxia) and pump-on (restoration of pump strength) changes and channel gating changes (Nav and cation channels open probabilities) are applied instantaneously.

Maximum cell volume before lysis

Both CN-CD and SM-CD have C_m = 20 pF and steady-state Vol_{cell} = 2,000 μm³. If 0.01 F/m² (= 0.01 pF/μm²) is the specific capacitance of the bilayer, membrane area is 20/0.01 = 2,000 μm². With $4\pi R^3/3$ the volume of a spherical cell and $4\pi R^2$ its surface area (SA), maximum Vol_{cell} as the cell swells (to spherical) would be = $4/3\pi(2{,}000/4\pi)^{3/2}$ = 8,410.4 μm³. Given a 4% bilayer elasticity strain limit (yielding membrane area = 2,080 μm²), rupture would occur at 8,920 μm³. Thus, in bifurcation plots, the notional DE values indicated for reference are unachievable by these models. Note too that present models depict neither SA regulation nor membrane tension homeostasis (see Morris, 2018).

Excitatory post-synaptic current (EPSC) via AChR channels

SM-CD APs are initiated by macroscopic EPSC through AChRs, which are nonselective cation channels that pass Na^+ and K^+ as per the GHK formalism. Our EPSC time course mimics a g(t) reported by Wang et al. (2004). As per Hille (2001), P_K:P_{Na} for I_{EPSC} = 1.11:1. The function g(t) has a maximum of 1, and $P_{Na,EPSC}$ yields a 1.5-fold safety factor (i.e., an amplitude adjusted to 1.5× the threshold required to elicit an AP in SM-CD).

The end-plate current is

$$I_{EPSC}(t) = g(t)\ [I_{GHK}(Na^+,\ P_{Na,EPSC},\ V_m)] + [I_{GHK}(K^+,\ P_{K,EPSC},\ V_m)]. \quad (25)$$

Nav–coupled left-shift (CLS) depiction of bleb damage to Nav-bearing membrane

The extent (in mV) of Nav-CLS as depicted in Fig. 1 D increases with bleb-damage intensity (Wang et al., 2009; Boucher et al., 2012; Morris et al., 2012a, 2012b; Joos et al., 2017). Cell survival seems improbable with 100% of Nav-bearing membrane damaged so arbitrarily. We model damage to 30% of the Nav population (i.e., affected channels [AC] = 0.3); imposed damage intensity is thus Nav-CLS(0.3) mV. Voltage dependences of rate constants α_q (V) and β_q (V) for *m* and *h* are the same as in Eq. 7, but shifted in the hyperpolarizing direction by left shift (LS; in mV). Therefore, for the affected Nav channels (AC), *m* and *h* evolve according to

$$dq/dt = \alpha_q(V_m + LS)(1 - q) - \beta_q(V_m + LS), \quad (26)$$

where *q* is either *m* or *h*.

Computational methods

Calculations involved solving sets of first order differential equations. These were done using Python with the ordinary differential equation solver *odeint*.

Online supplemental material

Fig. S1 is a high-resolution look at P-L/D processes as they move away, then back to steady state, during the several minutes it takes to redress the ion perturbations associated with a single synaptically triggered AP. Note the question and answer section in the supplemental text; it pertains to Fig. S1. Fig. S2 shows anoxic rundown (V_m(t) only) for SM-CD at variable time resolutions; anoxic rundown trajectories for CN-CD (V_m, $[ion]_i$, Vol_{cell}); anoxic rundown for WD-CD (V_m and ATP consumption); an example of the consequences of altering pump Michaelis–Menten constants (dose–responses and steady-state $[Na^+]_i$ computed for SM-CD in each case); and for the ischemic V_m(t) rundown of Fig. 6, the concurrent $[Na^+]_i$(t). Fig. S3 shows multiparameter bifurcation plots for SM-CD, including the spontaneous V_m(t) trajectory from the pathological steady-state continuum back to the continuum of physiological steady states. Table S1 emphasizes that, while in humans, the large disparity between the tissue mass of brains and SM is well-recognized, in the common ancestors of contemporary vertebrates, this disparity would have been substantially greater, making costly neuronal ion homeostasis in those early vertebrates relatively unproblematic, while placing a premium, even then, on the evolution of efficient and robust SM ion homeostasis. Supplemental text at the end of the PDF includes sections entitled P-L/D modeling of myotonia congenita: SMFs with a [small P_{Cl}][small I_{Naleak}] steady state, and P-L/D modeling of SM injury, tourniquets, compartment syndrome.

Results

P-L/D systems at steady state

Fig. 3 A and Table 2 show how SM-CD, a generic P-L/D model for excitable SMF membrane, parallels CN-CD (see Materials and methods). SM-CD uses the minimal set of flux elements (Fig. 2) needed for autonomous return to ion homeostatic steady state after an ionic perturbation. CN-CD incorporates a K/Cl cotransporter and thus has a nonminimal P-L/D steady state (poisoning the K/Cl cotransporter reveals its impact; in Table 2, compare steady-state values for CN-CD versus MN-CD). Including SMFs' many cotransporters (see Fraser and Huang, 2004; Usher-Smith et al., 2009) in generic SM-CD would have been unhelpful (nevertheless, the CN-CD/MN-CD exercise is a simple how to). Because the extracellular milieu is fixed, pump sensitivity to $[Na^+]_i$ (see Materials and methods; Fig. 4, A and B; Eq. 10) but not to $[K^+]_{ext}$ is invoked.

At ion homeostatic steady state, by definition, passive entry and active extrusion of Na^+ and of K^+ precisely balance. In all models, $P_K >> P_{Na}$, and electrodiffusion driving forces (see Fig. 4 C) are almost always greater on Na^+ than on K^+. As detailed in Materials and methods and shown in Fig. 4 D, the P_K:P_{Na} ratio sets V_{rest} in conjunction with pumping that always operates electrogenically ($3Na^+out/2K^+in$). Consequently, both the passive and active fluxes of K^+ are constrained by the passive and (hyperpolarizing) active fluxes of Na^+. Accordingly, when steady state is perturbed, I_{Naleak} (not I_{Kleak}) is rate limiting for flux trajectories, so throughout, Na^+ fluxes are emphasized while the attendant K^+ fluxes, though plotted, are mentioned less frequently.

In neuronal CN-CD, with P_K the major permeability and resting I_{Naleak} large (78.2/14.75 = 5.3× that of SM-CD; Table 2, steady-state section), there is a Pump-Leak–dominated steady state, meaning that the balanced fluxes mostly use P_K, P_{Na}, and the Na^+/K^+ pump. For SM-CD, with P_{Cl} the major permeability and resting I_{Naleak} very small, steady-state fluxes are mostly permeant anions (only Cl^- is modeled) via P_{Cl} whose influx/efflux is balanced by anionic Donnan effectors. SM-CD has a Donnan dominated steady-state. Before making further intermodel comparisons and subjecting them to DMD-like deficits, SM-CD's broad "SMF credibility" is assessed via a physiological stress test.

Stress testing SM-CD

The Fig. 5 A AP stress test mimics a procedure for isolated rat soleus muscle, except that SM-CD is stimulated not electrotonically but by a train of EPSCs (through cation channels; see Materials and methods). As APs fire, $[Na^+]_i$ rises, $[K^+]_i$ falls, and ATP consumption abruptly increases. This is the P-L/D system's $[Na^+]_i$-sensitive P-L active feedback in operation. Simultaneously, small increases in $[Cl^-]_i$ and Vol_{cell} reflect the Donnan effector–mediated passive feedbacks (Fig. S1 details the EPSC and AP fluxes).

During, between, and after APs, permeability and driving forces for K^+ and Na^+ almost match. With the constraint for compartment electroneutrality thus almost met, the small excess Na^+ influx is addressed by Cl^-+ H_2O influxes. Immediately after APs stop (AChR cation channels, Nav, and Kv all closed), only elements of SM-CD's minimal P-L/D system remain in play. V_m hyperpolarization reflects the ↑$[Na^+]_i$, as pumping ↓$[Na^+]_i$ to 3.7 mM, V_m converges to V_{rest} ($I_{Naleak} = -I_{NaKpump}$).

During the autonomous return to steady state, $[Na^+]_i$ and $[K^+]_i$ change monotonically, but $[Cl^-]_i$ and Vol_{cell} oscillate. The quantity N_{Ai} (attomol of cytoplasmic Donnan effectors) is fixed; consequently, $[A^-]_i$ falls and rises inversely with Vol_{cell} and $[Cl^-]_i$ (not shown). During the AP train, $[Cl^-]_i$ increases slightly with each AP's small excess Na^+ influx and consequent electroneutralizing Cl^- influx, a double entry constituting a cyto-osmolyte excess. With H_2O activity higher externally than internally, an osmo-balancing influx of H_2O occurs. Thus, for minimal SM-CD, $[Cl^-]_i$ changes (~4 mM increase when APs stop) are precisely mirrored by Vol_{cell} changes (~2.5% increase; ΔVol_{cell} <50 μm³; because P_{H2O} is very large, no time lag is evident). Were the system to swell to notional DE (Table 2), Vol_{cell} (initially 2,000 μm³) would be ~14,000 μm³ (↑700%). This provides a "thermodynamic size gauge" of how effectively, during 1,200 EPSC-triggered APs, Donnan dominated SM-CD forestalls osmotic swelling. With [I_{Naleak}] so small, [big P_{Cl}] does not render SM-CD vulnerable to osmotic Na^+ loading. In SM-CD, the driving force on Cl^- approaches 0 as the system converges on V_{rest} (a minimal P-L/D steady-state feature).

At 120 Hz, ion homeostasis does not quite fully restore steady state before the next AP, so parameter changes mount. When firing stops, reshrinkage begins immediately, undershooting before Vol_{cell} reconverges on steady state. This $[Cl^-]_i$(t), Vol_{cell}(t), $[A^-]_i$(t) oscillation, or "Donnan bounce," is the slowest aspect of ion homeostatic restoration. Normal excitability would seldom be as demanding as the stress test; the speedy system rebound

(only slightly more prolonged after 1,200 APs than after 1 AP (as per Fig. S1) is consistent with a hefty pump-reserve capacity for handling additional E_{Na}-depleting tasks.

To handle multiple gradient-dissipating tasks (e.g., APs, E_{Na}-dependent secondary transport, restoring gradients after microtear repair), ion homeostatic systems need a reserve, i.e., pump strength in excess of the steady-state requirement. Pump reserve is the thus the ratio (maximal ATP consumption)/(steady-state ATP consumption); or, in electrophysiological terms, pump reserve is (maximal $I_{NaKpump}$)/(steady-state $I_{NaKpump}$ [= −steady-state I_{Naleak}]). The SM-CD pump reserve is 11.1-fold (see Table 2); for various rat muscles, pump reserves in the range 7–22-fold are reported (Clausen, 2015).

In DMD, pump reserve would decrease as pump strength fell and/or as Na^+ leaks increased. Though maximal (100%) pump strength is identical in healthy CN-CD and healthy SM-CD, the [big I_{Naleak}] of CN-CD leaves it with a mere 2.1-fold pump reserve. No one parameter expresses how pump strength relates to a system's global physiological resilience, but SMFs' large pump reserves augur well.

For the same stress test but with pump reserve doubled (pump strength up-regulated to 200%), Fig. 5 B plots ATP consumption; peak ATP consumption is greater and recovery is faster (see legend regarding the recovery in rat soleus with a similar pump reserve) and (not shown) steady-state $[Na^+]_i$ would drop to 2.7 mM (from 3.7 mM). The steady-state ATP consumption increase is trivial (compare Fig. 5, A and B, baselines: the ATP consumption increase in Fig. 5 B is almost undetectable). This feature (the ability to increase pump reserve with almost no increased steady-state expenditure) is crucial for physiological resilience. But to respond to transient physiological Na^+ loading, mechanisms other than boosted pump strength are invoked; during episodes of intense firing, SMFs have a rapid-acting (seconds) "excitation-activation feed-forward" process that results in sustained post–AP-train $[Na^+]_i$ undershoots (Nielsen and Clausen, 1997). While pump up-regulation (as per Fig. 5 B) operates in the direction needed, it would be too slow. The data by Nielsen and Clausen (1997) point to more expeditious mechanisms involving altered transport characteristics. For instance, if excitation-activation feed-forward signaling were to act by (arbitrarily) halving the SM-CD pump's Na^+-binding Michaelis–Menten constants, a $[Na^+]_i$ undershoot (3.7→1.9 mM) would result (see Fig. S2 E). For perspective, pump strength up-regulation to 1,000% ($I_{maxNaKpump}$ to 545 pA; maximal ATP consumption to 5,660 amol/s) reduces steady-state $[Na^+]_i$ to 1.7 mM. While increased quantities of functional pump protein (thence bigger pump reserves) serve overall resilience well, fast-acting (and presumably temporary) pump kinetic adjustments serve physiological agility.

In summary, SM-CD, though radically simple, handles an excitability stress test in a manner qualitatively similar to rodent fibers. This general verisimilitude justifies using and modifying SM-CD to learn how altered or added features reflect the DMD situation.

Syncytial SMF morphology boosts ion homeostatic robustness

Steady state P-L/D values depend on membrane SA. Time courses depend on SA/Vol (represented here as C_m/Vol_{cell}). All

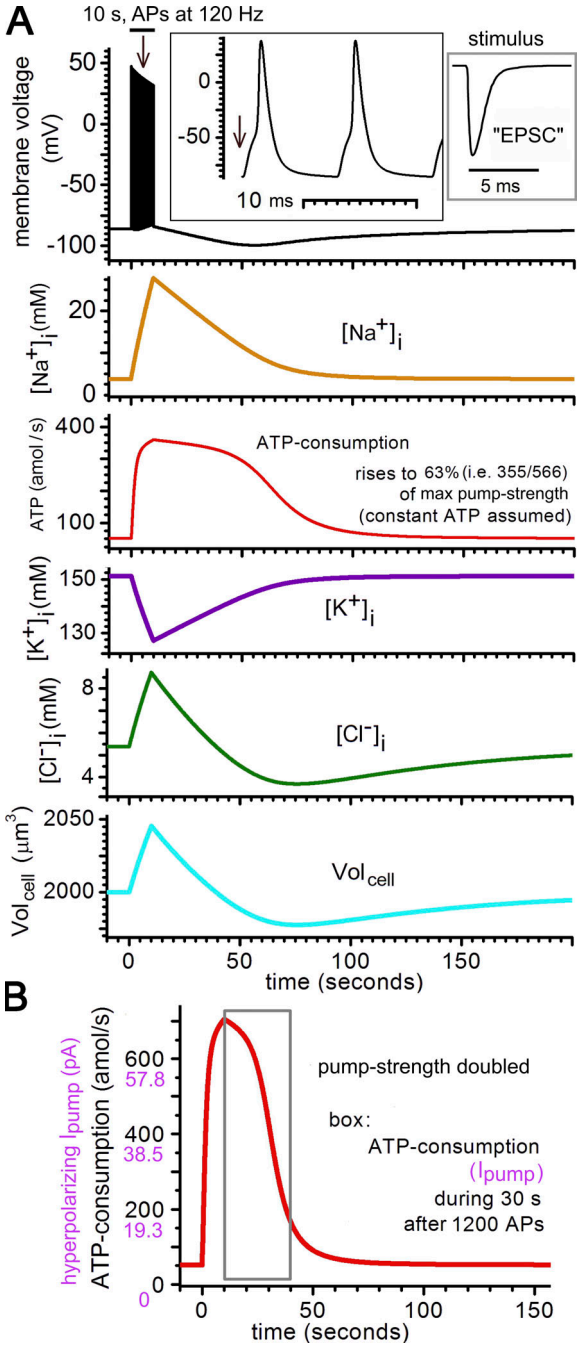

Figure 5. **Stress testing SM-CD. (A)** In SM-CD, V_m, $[Na^+]_i$, ATP-consumption, $[K^+]_i$, $[Cl^-]_i$, and Vol_{cell} trajectories before, during, and after 1,200 EPSC-stimulated APs; this mimics a rat muscle experiment (Nielsen and Clausen, 1997) summarized by Clausen (2015) as: "In isolated rat soleus…after 10 sec of stimulation at 120 Hz, the net Na^+ reextrusion measured in the subsequent 30 sec of rest reaches a 22-fold increase in Na^+, K^+ pump activity corresponding to 97% of the theoretical maximum rate of active Na^+, K^+ pumping measured and calculated on the basis of total content of ^{3}H-ouabain binding sites." During AP train, SM-CD swells by <2.5%; more extreme SMF swelling might engage SMFs' caveolar tension-buffer (see Sinha et al., 2011; Morris, 2018). This feature is not modeled here. **(B)** Y axis double-labeling in B serves as a reminder of the one-to-one correspondence between ATP-consumption and hyperpolarizing $I_{NaKpump}$ (Fig. 4 A). Here, pump reserve is increased (from 11.1-fold, A) to 22.2-fold (closer to rat soleus; boxed area references Clausen's (2015) summary.

models here have SA = 2,000 μm² enclosing steady-state Vol_{cell} 2,000 μm³ (Table 2; and Fig. 3, A and B). However, to relate SM-CD to particular myofibers, syncytial morphology (Fig. 3, C and D) would matter. In an SMF, each 2,000 μm² unit would encircle (not enclose) a myoplasmic volume. One fiber would comprise hundreds to thousands of contiguous 2,000 μm² SM-CD ion homeostatic units, with cylindrical slice width varying with fiber radius (Fig. 3 D, i). Steady state would be 10× more efficient in a myofiber with SA/Vol 0.1 that of SM-CD. During rundown, that myofiber's gradients would benefit from slower passive dissipation than SM-CD, but once dissipated, active recovery would also be slower than in SM-CD.

Steady-state costs: CN-CD versus Donnan dominated SM-CD versus Pump-Leak–dominated WD-CD

The P_{Na}:P_K ratio of SM-CD puts its V_{rest} >20 mV more negative than the reference model, CN-CD. In spite of the bigger driving force on Na^+, SM-CD's extremely small P_{Na} makes its [small I_{Naleak}] and thence its steady-state ATP consumption 5.3× smaller. Since all models have the same maximal (100%) pump strengths, SM-CD's pump reserve, too, is 5.3× that of CN-CD (Table 2). SM-CD pump reserve would coincide with CN-CD's meager normal (2.1-fold) value when SM-CD pump strength fell to a mere 18%. Thus, even without factoring in syncytial morphology (a feature of SMFs, and not of neurons), the 5.3× differential bespeaks the extraordinary frugality and robustness of the ion homeostatic strategy adopted by SMFs relative to that of central neurons.

SM-CD/CN-CD comparisons are physio/pathophysiologically informative. They do not, however, provide a direct readout of how much of SM-CD's robustness is attributable to its Donnan dominated steady state. For this we devised a counterfactual (Pump-Leak dominated) SM-CD analog, WD-CD. WD-CD, like SM-CD, is a minimal P-L/D system. Its maximal pump strength, P_{Na}:P_K ratio, V_{rest}, and low input impedance are all identical to SM-CD's (Table 2). Having set the WD-CD P_{Cl} equal to CN-CD's, we matched SM-CD's low input impedance via large-valued P_K and P_{Na} (in Table 2, see absolute permeabilities and P_{Na}:P_K:P_{Cl}). WD-CD has [small P_{Cl}][big I_{Naleak}] steady state that consumes ATP at 180 amol/s (versus 51 amol/s for SM-CD). This drops WD-CD's pump reserve to 3.1-fold (SM-CD: 11.1-fold). While WD-CD can handle the stress test, it is continually consuming (180/51) 3.5× more ATP than SM-CD, and after stress test, it takes more than two times longer than SM-CD to restore steady state (Fig. S2 D versus Fig. 5 A). For energetic efficiency, and by extension, for resilience during emergencies, SM-CD far outmatches its electrically equivalent analog, WD-CD.

Provenance of DMD fiber Na^+ overload: Insufficient pumping? Too much leaking?

The provenance of chronic DMD fiber Na^+ overload is unclear. To address this via SM-CD, we therefore ask the following: could chronic (i.e., steady state) overloads arise solely from (1) too little Na^+ pumping (low pump strength) or from (2) too much Na^+ leaking (leaky channels in damaged sarcolemma), or (3) do both contribute? As a principal cause of chronic DMD Na^+ overload (i.e., with pump strength at 100% and Na^+-permeant channels all functioning normally), hyperactive secondary transporters are not plausible and are not addressed here.

The magnitude of P_{Na} in DMD fibers is unknown since SMF P_{Na} is not identified. But *mdx* fibers have leaky nonselective cation channels (identified and unidentified; Carlson and Officer 1996; Lansman, 2015) and leaky Nav1.4 channels (Hirn et al., 2008). SMF pump proteins are well studied (e.g., Clausen, 2013, 2015; Hakimjavadi et al., 2018; Kravtsova et al., 2020), but for this generic comparison of SMF versus neuronal ion homeostatic strategies, we kept the same simple pump model as in CN-CD.

Kravtsova et al. (2020) report diminished pump-protein efficacy in *mdx* fibers, and several studies addressing Na^+-overload point to diminished operational pump strength. Modulators that depress pumping (a machinery issue) increase *mdx* fiber Na^+ overload (Table 1, item 4; Miles et al., 2011), and stimulating NO pathways (a supply issue related to functional ischemia) almost fully abolishes Na^+ overload (Altamirano et al., 2014; Table 1, item 7). After reporting chronically elevated Na^+ in DMD patients' muscle (Table 1, item 5), Lehmann-Horn et al. (2012) noted unexpectedly improved muscle function in a dystrophic patient treated (to alleviate tissue edema) with eplerenone. Probing the mechanism via a rat diaphragm DMD model (Breitenbach et al., 2016), they found that eplerenone upregulates Na^+/K^+-ATPase (via α-subunit Tyr10 dephosphorylation), causing an ouabain-sensitive fiber repolarization.

To exemplify an advanced-DMD (i.e., after infancy; Fig. 1 A) SM-CD variant, we use LA-CD (Table 2): it is SM-CD with pump strength at 30% and N_{Ai} decreased slightly so Vol_{cell} = 2,000 μm³. Further, we systematically characterize SM-CD's P-L/D characteristics across pump strengths (SM-CD steady states as pump strength varies, below).

Pump reserve in DMD-like LA-CD is 3.4-fold (better than 2.1-fold in healthy CN-CD, substantially less than the 11.1-fold of healthy SM-CD), but V_{rest} and ATP consumption for LA-CD and SM-CD are almost the same. LA-CD's 6.5 mM $[Na^+]_i$ is inside the healthy range for mouse fibers according to some studies (see Table 1). So would LA-CD really represent an ailing DMD-like fiber? Yes. $[Na^+]_i$ values for mice are extremely variable, but if, say, an *mdx* mouse fiber was using an E_{Na}-depleting Na^+ transporter (e.g., Iwata et al., 2007), 6.5 mM could easily become 7.3 mM, which Burr et al. (2014) (Table 1, item 8) report as chronically Na^+ overloaded for *mdx* fibers. Moreover, even without knowing that healthy rodent SMFs maintain pump reserves in the 7–22-fold range (versus LA-CD's 3.4-fold), LA-CD is a substandard P-L/D system vis-à-vis steady-state energetics: whereas SM-CD consumes ATP at 51 amol/s to achieve $[Na^+]_i$ = 3.7 mM, LA-CD consumes ATP at 50.7 amol/s to achieve only 6.5 mM (see Materials and methods; Fig. 4 B, ii). LA-CD's minimally lower ATP consumption is clearly no bargain. Compared with SM-CD, LA-CD would be classified as chronically Na^+ overloaded, due solely to too little pumping. How nonlinear aspects of Na^+ fluxes (too little pumping and too much leaking) contribute here will emerge further in the systematic pump-strength analysis (below).

Ischemic rundown to spontaneous firing

DMD fibers suffer exertion-induced bouts of functional ischemia (Thomas, 2013). A downstep to 0% pump strength would mimic

anoxic or ouabain-poisoned rundown. As if severe ischemia suddenly reduced the ATP supply, Fig. 6 follows $V_m(t)$ in SM-CD after a pump-strength downstep from 100% to 7.9% (maximally 44.7 amol/s ATP consumption, or 4.3 pA of $I_{NaKpump}$; trial and error show that 8% suffices but 7.9% is marginally less what SM-CD requires to maintain a steady state). In this trajectory, the system seems to restabilize near −65 mV but in fact continues depolarizing for hours at an exquisitely slow rate (barring any current noise, a syncytial fiber would depolarize even more slowly). Then, spontaneously, it fires APs. Why? Because at that V_m, I_{Naleak} (through P_{Na} + Nav channels; in Fig. 4 E, see $m^3h(V_m)$) exceeds the maximal Na^+ extrusion achievable at 7.9% pump strength (4.3 pA). When firing ceases (after ∼30 s), the system slowly converges on a profoundly depolarized, pathological V_{rest}. As the inset plot shows, with even deeper ischemic downsteps, rundown to spontaneous firing speeds up, taking 22.7 min for 100%→0% pump strength (Fig. 6 plots only $V_m(t)$, but $[Na^+]_i(t)$ is in Fig. S2 F).

Fig. 6 could mimic application of tourniquets (MacDonald et al., 2021) and compartment syndrome (Tatman et al., 2020). Depending on the severity of vascular constriction in compartment syndrome, ischemic and anoxic fibers' rundown to firing threshold would vary enormously, consistent with reports, in compartment syndrome, of the unpredictable timing of lethal threshold events (Johnstone and Ball, 2019). In DMD, compartment syndrome is thought to contribute to limb contracture (Siegel, 1992; Dooley and Chiasson, 2014). Extremely slow ischemic rundown buys time, fostering survival in connection with bouts of functional ischemia.

Anoxic rundown to spontaneous firing

In Fig. 6, pump feedback continually fights the passive cation (Na^+ and K^+ leaks (though too weakly) while, concurrently, Donnan effector–mediated feedbacks operate at full force. In anoxic rundowns (i.e., 100%→0% pump strength at t = 0; Fig. 7), only the passive processes remain operative. Fig. 7 A, i, shows the SM-CD trajectories during anoxic rundown; spontaneous firing starts at 22.7 min. This $V_m(t)$ is expanded in Fig. S2 A and compared there (Fig. S2 B) against the $V_m(t)$ for CN-CD, where spontaneous firing starts at ∼100 ms. Because Dijkstra et al. (2016) mimic a brain-slice experiment's slow wash-in of the pump-poison ouabain, their rundown is slow. Step changes, as used here, render the biophysics more transparent (e.g., $I_{NaKpump}$-off for SM-CD causes a ∼Δ2 mV RC-type depolarization).

During prefiring rundown in SM-CD, Na^+ influx (small P_{Na}, large initial driving force) and K^+ efflux (large P_K, small initial driving force) nearly match. But a small excess (net) Na^+ influx engenders small net influxes of Cl^- and H_2O (ΔVol_{cell} reflects a net H_2O flux); electro-neutrality and osmo-balance are thus maintained (see expanded prefiring Cl^- and Vol_{cell} trajectories, Fig. 7 A, ii).

SM-CD's biggest leak, P_{Cl}, does not set the pace for rundown toward DE. If, at t = 0, P_{Na} and P_K were blocked along with the pump, the cytoplasmic Donnan effectors would hold SM-CD at $V_m = E_{Cl} = -86$ mV. Upon reopening of P_{Na} and P_K, rundown would commence; the system's smallest leak ([small I_{Naleak}]) with its large driving force would set the rate for ion gradient dissipation. Note that SM-CD depolarizes from −75 mV to −65 mV in ∼12 min, reasonably close to the rundown rate of ouabain-poisoned rat soleus SMFs (10 mV/10 min; Clausen and Flatman, 1977), whose rundown is consistent with a somewhat larger operational P_{Na} and with those fibers' more depolarized V_{rest}. Fig. 7 B, i, shows how sensitively SM-CD responds to a ΔP_{Na}; there a 27% $\downarrow P_{Na}$ (0.3→0.22 μm³/s) hyperpolarizes V_{rest} (−86→−90 mV), reduces steady-state ATP consumption (51→39 amol/s), and prolongs prefiring anoxic rundown (22.7→34.0 min).

With spontaneous firing, system permeabilities change vastly; intermittently open Nav and Kv channels support very large Na^+ influxes and K^+ effluxes. Cl^- influx through SM-CD's [big P_{Cl}] increases substantially to neutralize the now very large excess Na^+ influx. With that [Na^+ + Cl^-] comes osmo-balancing H_2O; spontaneous firing at 0% pump strength causes gross inflation, i.e., worst case scenario cytotoxic swelling.

Does P_{Cl} influence prefiring rundown speed? Negligibly in SM-CD, because always, the electro-diffusion driving force acting on Cl^- is near zero. Thus, for 0.1× P_{Cl}, 1.0× P_{Cl}, and 10× P_{Cl}, spontaneous firing starts at 20.7, 22.7, and 23.8 min, respectively (not shown). Throughout prefiring rundown, SM-CD's [big P_{Cl}] supports large Cl^- effluxes and (marginally larger) influxes, but while net Na^+ influx stays small, net Cl^- influx stays equally small. The 7.9% pump-strength rundown of Fig. 6 is so slow because, there, pumping almost (but not quite) counters that small net leak. An implication is that though $\uparrow P_{Cl}$ strongly inhibits endplate-triggered APs under energy-depleted conditions (Bækgaard Nielsen et al., 2017; Leermakers et al., 2020), it would not help forestall spontaneous firing in fibers whose pump strength was too low to sustain a steady state. Under those same conditions, however, a $\downarrow P_{Na}$ (as per Fig. 7 B, i) would both diminish endplate excitability (via V_{rest} hyperpolarization) and forestall spontaneous firing (slower rundown).

For SMFs in low pump-strength scenarios like Fig. 6 and Fig. 7 A, excitation–contraction coupling triggered as spontaneous firing started could result in fiber-destroying contractures (due release of $[Ca^{2+}]_i$; Claflin and Brooks, 2008). Though ion homeostatic failure would have brought on fiber demise, it might be characterized as Ca^{2+} necrosis.

Ion homeostatic recovery and spontaneous firing

The pathophysiological virtue of very slow rundown is evident in Fig. 7 A, iii: if pump strength is restored to 100% at any pre-time firing, the system can return to steady state. Just before firing starts, with $[Na^+]_i$ at 20× its steady-state level, the resumed $[Na^+]_i$-sensitive Na^+-extrusion ($I_{NaKpump}$) causes V_m to hyperpolarize until the system reconverges to steady-state $[Na^+]_i$ and V_{rest}. If pumping is restored during spontaneous firing, the system can still return to steady state, but in situ, prospects for such recovery would be moot if anoxic-condition contractures (triggered by the spontaneous APs) had destroyed the fiber (Claflin and Brooks, 2008).

A pathological P-L/D steady state: Nav window conductance

If pump strength is restored even 100 ms after spontaneous firing stops (Fig. 7 A, iii, bottom), the system shows new behavior. Unable to return to healthy V_{rest}, SM-CD instead converges on a depolarized ATP-devouring steady state of degraded

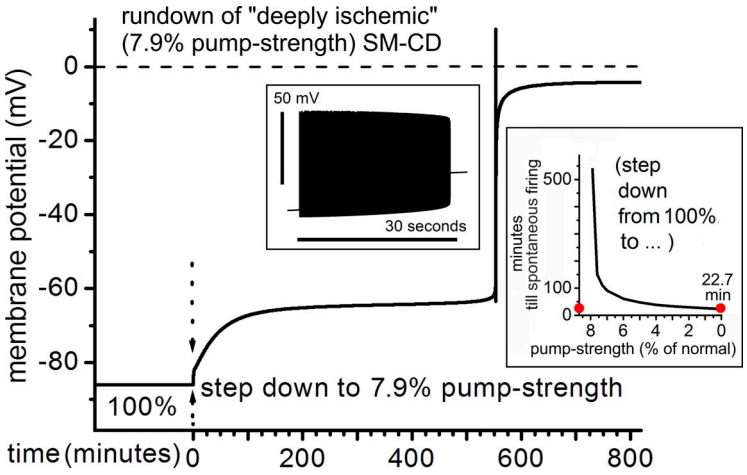

Figure 6. **Ischemic rundown of SM-CD.** $V_m(t)$ trajectory on stepping SM-CD pump strength from 100% to 7.9%, so that marginally, $I_{NaKpump}/I_{Naleak}$ <1. This mimics a tourniquet-application or compartment-syndrome situation (Johnstone and Ball, 2019). Rundown to spontaneous firing takes almost 10 h (a boxed inset expands the AP burst). After firing, SM-CD, still at 7.9% pump strength, slowly restabilizes (computationally) in a degraded pathological steady state. In situ, AP-triggered contractures would likely have destroyed a myofiber (Fig. S2 F is the concurrent $[Na^+]_i$ trajectory). Inset graph: For ischemic transitions to even lower pump strengths, rundown times converge on SM-CD's anoxic rundown time (100%→0%; 22.7 min, as per Fig. 7 A).

ion gradients and a pathological V_{rest} (−22 mV). Hyperpolarizing $I_{NaKpump}$, though maximally stimulated by the extreme $[Na^+]_i$, cannot surmount the depolarizing I_{Naleak}. The problem: operational P_{Na} has acquired a new component (i.e., one not in force at SM-CD's healthy steady state). In the pathologically restabilized system, Nav channel window conductance contributes to I_{Naleak} (for $m^3h(V_m)$ at −22 mV, see Fig. 4 E). The system is in depolarizing block (not shown). To return from this pathological steady state to a physiological steady state would require that maximal $I_{NaKpump}$ up-regulate enough that hyperpolarizing $I_{NaKpump}$ would exceed the depolarizing I_{Nav}-augmented I_{Naleak} (≥339% pump strength is needed; Fig. S3 D, i and ii). For CNs, Dijkstra et al. (2016) propose such recovery scenarios; whether comparable scenarios relate to SMF ischemia-reperfusion injury is outside our scope (Dudley et al., 2006; Schmucker et al., 2015; Li et al., 2020).

The DMD-like low pump-strength SM-CD variant (LA-CD) can handle rundown and recovery

Chronically low–pump-strength (30%) LA-CD has the same P_{Na} as SM-CD. Though LA-CD is mildly Na^+ overloaded, its small P_{Na} (thence [small I_{Naleak}]) keeps anoxic rundown (Fig. 7 C, i) almost as slow as for SM-CD; it fires spontaneously at 22.0 min (22.7 for SM-CD), passing currents essentially indistinguishable from SM-CD (shown for LA-CD only; Fig. 7 C, ii). LA-CD's pump reserve (3.4-fold) suffices to restore the system at any point during rundown and until spontaneous firing stops (Fig. 7 C, iii), but recovery is slower than for SM-CD.

Donnan-driven swelling: Small P_{Na} versus small P_{Cl}

A priori, if a P-L/D system's only flux mechanisms are those operative at steady state, temporary loss of pump strength is always fixable (ignoring perils, in situ, from extreme cell inflation). Thus, systems with V-gated channels zeroed recover after prolonged, deeply depolarizing anoxia, as shown (Fig. 7 D) for SM*-CD (SM-CD with V-gated channels eliminated). After 105 min of anoxia, V_m has depolarized to −20 mV. Then, ∼5 min after restoration of 100% pump strength, V_m = −86 mV; SM*-CD recovers fully (albeit more slowly) with restoration to any value ≥8% pump strength (not shown).

For all parameters, Fig. 8 compares rundown trajectories for SM*-CD and CN*-CD (CN-CD without V-gated channels). Note how SM*-CD, which has [big P_{Cl}] and small P_{Na}, exerts a more powerful brake against Donnan effector–induced swelling than CN*-CD, which has [small P_{Cl}] and large P_{Na}. The [big P_{Cl}]/(Donnan effector) collaboration used by SMFs lets them be electrically leaky yet metabolically tight.

Fig. 8 suggests that during prolonged quiescent periods (as different as hibernation or post-injury tissue remodeling; Jackson, 2002; Baumann et al., 2020), SMFs could optimize prospects for eventual ion homeostatic recovery by preemptively zeroing Nav1.4 channels (e.g., by promoting slow-inactivated [Webb et al., 2009] or other nonpermeant states [Kiss et al., 2014]; likewise for ↓P_{Na} and ↓P_K [Donohoe et al., 2000]).

SM-CD steady states as pump strength varies

Generic neuron models (Hübel et al., 2014) including CN-CD (Dijkstra et al., 2016) show that ion homeostatic steady states change nonlinearly as pump strength falls. Spontaneously, at discrete points (thresholds) in parameter space, CN-CD destabilizes and exhibits bistability. These characteristics are also evident in SM-CD. P-L/D bistability is unrelated to whether a system's steady state is dominated by (actively balanced) cation fluxes or (passively balanced) anion fluxes; bistable ion homeostasis is a (computational) trait of P-L/D systems with embedded voltage-gated channels.

SM-CD has two nonlinear Na^+ flux mechanisms: $I_{NaKpump}([Na^+]_i)$ and $I_{Nav}(V_m)$. How, in principle, their interplay renders SM-CD computationally bistable is shown with the steady-state V_m (pump strength) bifurcation plot in Fig. 9 A (the complete set of SM-CD bifurcation plots, plus the $V_m(t)$ recovery trajectory at 339% pump strength, is in Fig. S3). The solid black line is the continuum of physiological steady states. Spanning the same pump-strength range, the solid blue line is a continuum of pathological steady states. "Bistable" signifies that, across part of the pump-strength range, these two continua overlap. On each continuum, an unstable threshold (bifurcation point) occurs: X and # at pump strengths 7.9% and 339%, respectively. For CN-CD, analogous instabilities (X and #) occur at pump strengths 65% and 181%, respectively (Dijkstra et al., 2016).

For SM-CD, the expectation (in situ) of lethal contracture at X (7.9% pump strength) makes the upper continuum moot. SM-CD is stepped from 100% to 7.9% pump strength in Fig. 6, but if

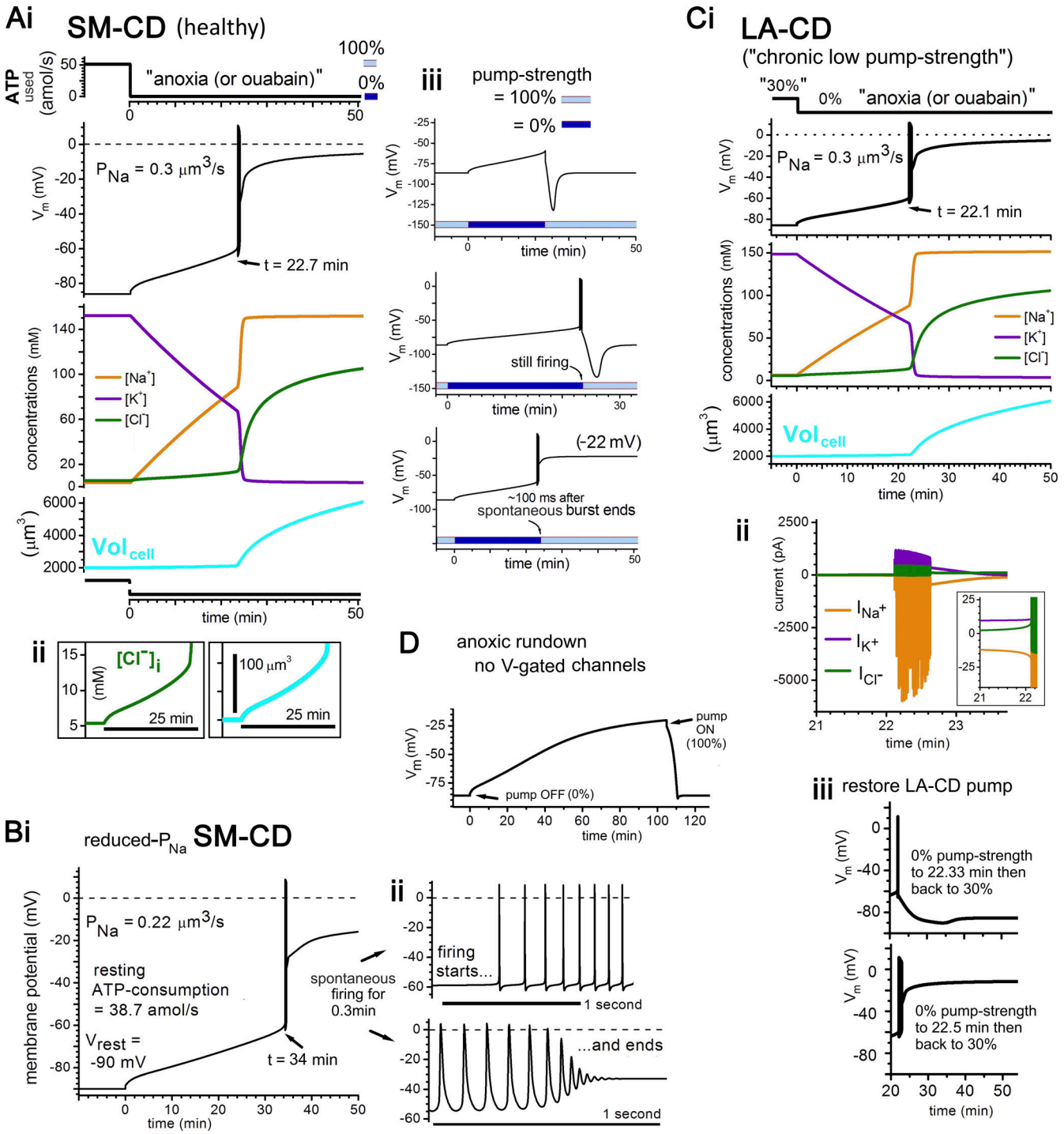

Figure 7. **Anoxic rundown and recovery. (A, i–iii)** SM-CD, anoxic (0% pump strength) rundown trajectories, as labeled, and the consequences (as monitored by $V_m(t)$) of restoring pump function. **(B)** $V_m(t)$ during anoxic rundown of SM-CD with its P_{Na} reduced enough to yield V_{rest} = 90 mV. **(C i)** LA-CD, anoxic rundown trajectories, as labeled. **(C ii)** Ion currents during the minutes just before, during, and after spontaneous firing (onset expanded vertically in inset box). **(C iii)** Effects (as monitored by $V_m(t)$) of restoring pump function. **(D)** $V_m(t)$ for SM*-CD (inexcitable SM-CD) before, during, and after anoxic rundown (excerpt from Fig. 8).

SM-CD was stepped (say) 8% pump strength→X (7.9%), spontaneous firing and (in situ) contracture would follow almost immediately.

Assuming the pathological steady-state continuum to be inaccessible in situ, Fig. 9 B plots only physiological steady states, and only for the range most relevant to DMD (encircled in Fig. 9 A), i.e., from 100% → through the saddle-node (X) to 0% pump strength. SM-CD, 30% pump strength, plotted here is almost the same as LA-CD.

LA-CD is the tolerably robust low pump-strength (30%) system (e.g., Fig. 7 C) whose elevated steady-state $[Na^+]_i$ already indicated that, in principle, too little pumping alone could

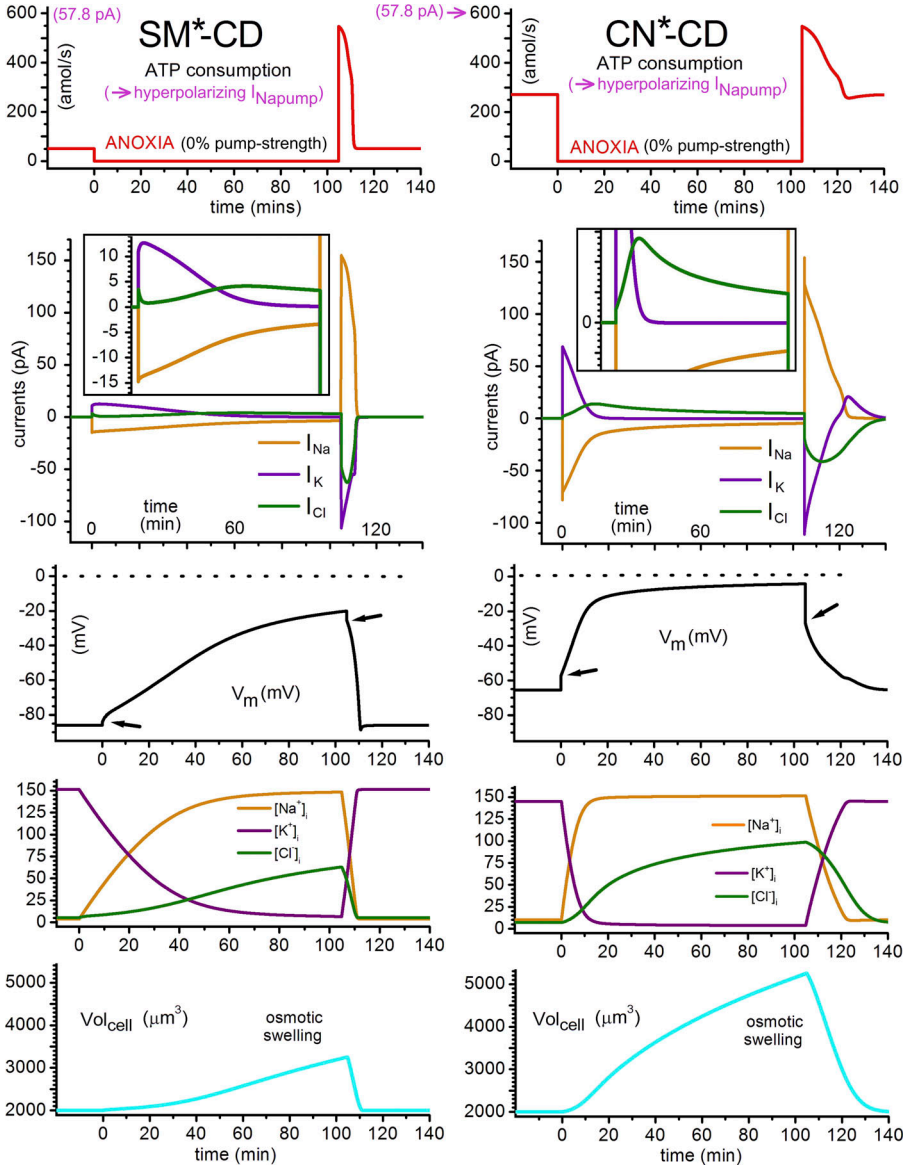

Figure 8. **Anoxic rundown of inexcitable (*) SM-CD and CN-CD.** SM*-CD and CN*-CD are SM-CD and CN-CD with all V-gated channels zeroed (gNav, gKv, and the gCl(V) of CN-CD). CN*-CD, like CN-CD, has a nonminimal steady state since its K/Cl cotransporter remains operative. SM*-CD is a minimal P-L/D system. V_m panel arrows indicate ΔV_m at $I_{NaKpump}$-off and $I_{NaKpump}$-on (depolarizing and hyperpolarizing, respectively). $I_{NaKpump}$-off depolarizes SM*-CD by <2 mV and CN*-CD by ∼8 mV (in excitable CN-CD, the ΔV_m from $I_{NaKpump}$-off elicits spontaneous APs; see Fig. S2 B). SM*-CD rundown is like Fig. 2 of Fraser and Huang (2004) (inexcitable amphibian SMF, V_{rest} = −90 mV). CN*-CD swells 140% in 20 min. SM*-CD swells 140% in 76 min. At 105 min ($I_{NaKpump}$-on), the ↑$[Na^+]_i$ maximally stimulates pumps (54.5 pA) in CN*-CD. After 15.5 h (not shown) of anoxic rundown, SM*-CD shows the Na^+-gradient dissipation present in CN*-CD at 105 min. After 272 min of rundown, both models recover (not shown). If recovery is initiated with both systems at any given V_m, the larger P_{Na} of CN*-CD makes its recovery slower (not shown).

underlie a small chronic Na^+ overload. The Fig. 9 B $[Na^+]_i$ plot shows that as pump strength drops below that 30%, extreme chronic Na^+-overload values develop, approaching 88 mM before system destabilization at the saddle node (7.9% pump strength, X). At pump strengths from ∼20% to 15% down through 8%, SM-CD would unquestionably be considered chronically Na^+ overloaded.

Insofar as pump strengths ≤30% mimic advanced disease-state DMD fibers, chronic Na^+ overload of DMD/*mdx* fibers could result solely from too little Na^+ pumping with the proviso that, in that situation, unwanted Nav channel window conductance increases operational P_{Na} in the low pump-strength danger zone leading to X. That pathological ↑P_{Na}, we emphasize, is attributable to normally functioning Nav channels. Nav channels overactive in the damaged sarcolemma of DMD fibers will be addressed below.

Functional ischemia: Moving in and out of the danger zone

In DMD, transient functional ischemia could take chronically low pump-strength fibers (say, at 30%) perilously rightward toward X, as depicted in Fig. 9 C. Equally important, however, is what this plot conveys regarding prospects for recovery as fibers approach X: 8% pump strength is still on the physiological continuum, so any intervention, no matter how small, that elevates operational pump strength >8% will contribute to fiber survival by moving the system leftward. This seems self-evident/unremarkable until consideration is given to CN-CD, whose saddle node (X) is at 65% pump strength. If CN-CD pump strength falls <65%, recovery is only possible if pump strength can be boosted to ≥181% (yielding the ↑hyperpolarizing $I_{NaKpump}$ needed to take CN-CD to its #, the unstable recovery threshold on its pathological continuum; Dijkstra et al., 2016; or pink X, # in Fig. S3). For DMD-afflicted SMFs, Fig. 9 C suggests that provided pump strength is ≥8%, even procedures as minor as massage treatments and vibration that improves bloodflow could, and evidently do (Saxena et al., 2013; Carroll et al., 2020), improve DMD fiber viability.

Extracellular Donnan effectors are invariant in SM-CD, but at very small pump reserve (the danger zone), their concentration would affect steady state (Mehta et al., 2008). Because Coles

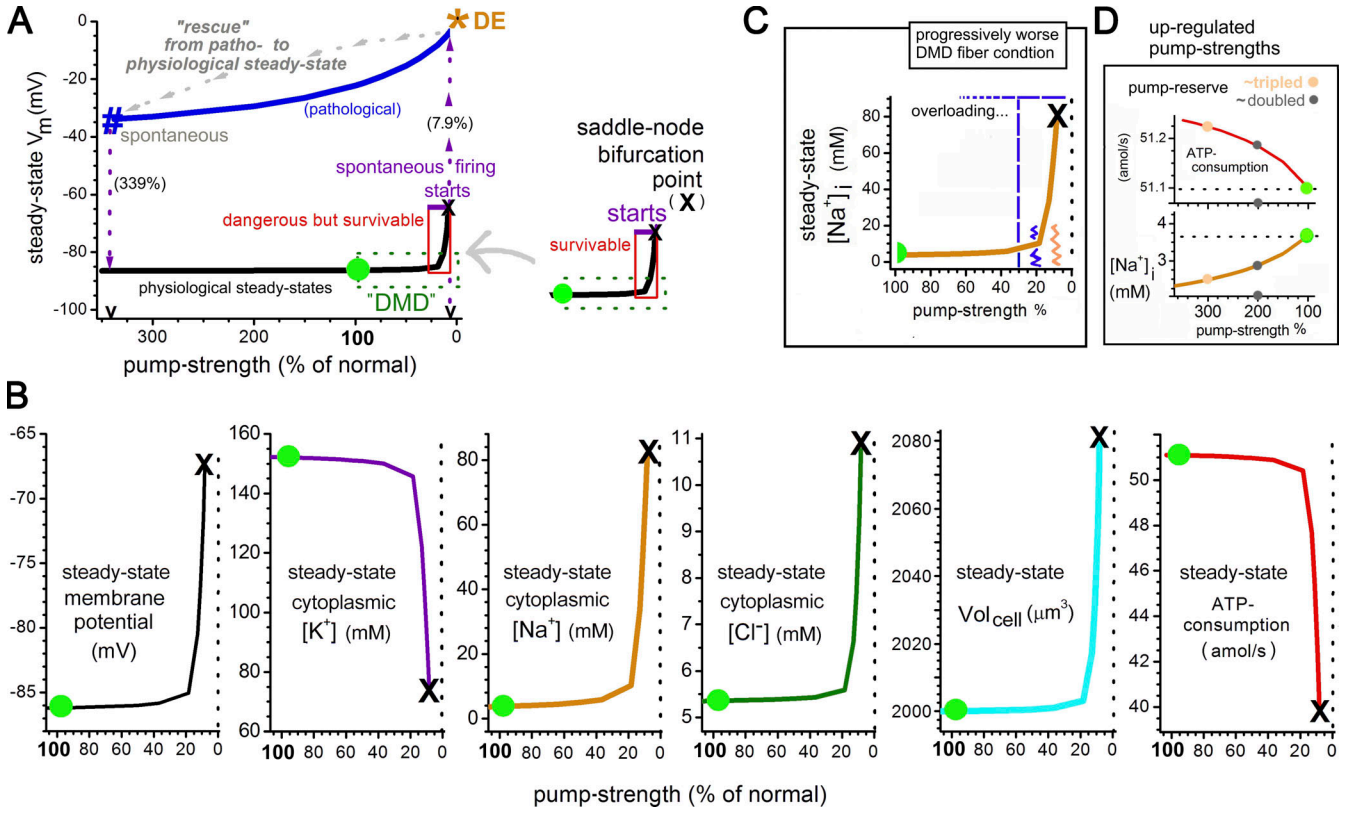

Figure 9. **SM-CD steady-state bifurcation plots. (A)** The SM-CD bifurcation plot for steady-state V_m (pump strength); stable values form physiological (black line) or pathological (blue line) continua (for the full set of SM-CD bifurcation plots, see Fig. S3). Green dot: normal steady state for SM-CD (V_{rest} in A). DE is the notional DE point. Unstable values (thresholds): # and the saddle node (X) (7.9% pump strength for SM-CD). In excitable P-L/D systems, instabilities (at # and at X) result in spontaneous APs (as seen for 100%→7.9% in Fig. 6; note that if the system was chronically at low pump strength (e.g., 8%), then dropped to 7.9%, firing would start soon thereafter). If the system attained the pathological continuum, rescue would be possible only by increasing hyperpolarizing $I_{NaKpump}$ to # (pump strength 339%; Fig. S3 D, ii, gives the trajectory). Though A illustrates the inherent computational bistability of SM-CD as an excitable P-L/D system (like CN-CD; Dijkstra et al., 2016), AP-triggered contracture would preclude SMF survival beyond (X) (see Claflin and Brooks 2008). For DMD fibers, the relevant bifurcation analysis sector is therefore that circled; starting from 100%, it takes in the deeply compromised danger zone (boxed region) and the saddle node (X). **(B)** For pump-strengths of 100% and down, the physiological steady-state continuum for SM-CD parameters, as labeled. **(C)** Steady-state $[Na^+]_i$ (pump strength) indicating how an episode of functional ischemia could take the system into the danger zone. **(D)** Up-regulated physiological continua for $[Na^+]_i$ and ATP consumption (note the extremely expanded y axes); in SM-CD, 200% pump strength corresponds to 22.2-fold pump reserve.

et al. (2019) report protease release of extracellular matrix proteins in exercised *mdx* fibers, extracellular Donnan effector influences (particularly in connection with ischemia-related ΔpH; Hagberg, 1985) could be worth revisiting.

Nonosmotic Na^+ loading, even in the danger zone

Fig. 9 B shows SM-CD as robust above ∼40% pump strength (pump reserve there: 4.4-fold) and deteriorating steeply below ∼20%, the danger zone where ATP consumption (=hyperpolarizing $I_{NaKpump}$) falls sharply as $[Na^+]_i$ rises steeply. V_m-related nonlinearities create a vicious positive feedback via two novel flux-mechanism features (i.e., features negligible or not applicable in the 100% to ∼40% pump-strength range): (1) Na^+ saturation of $[Na^+]_i$-sensitive hyperpolarizing Na^+ extrusion (see Materials and methods; Fig. 4 A; see approach to ∼90 mM $[Na^+]_i$), and (2) undesirable recruitment of Nav channels to operational P_{Na}. $[Na^+]_i$ rises steeply as reduced hyperpolarizing $I_{NapKump}$ fails to counteract the Nav-augmented depolarizing I_{Naleak}. These altered steady-state features pull SM-CD ever closer to defeat: i.e., spontaneous firing and cytotoxic swelling at X.

Nevertheless, right through the danger zone (until X), Na^+ loading and K^+ depletion remain well-matched. Thus, Cl^- influx and thus H_2O influx stay small (note the y axis values for steady-state $[Na^+]_i$, $[K^+]_i$, and $[Cl^-]_i$). Not shown, from 100%→X, impermeant cytoplasmic anions dilute slightly ($[A^-]_i$: 149.6 mM→143.1 mM). Even at the saddle node (X), where $[Na^+]_i$ = 88 mM, steady-state $[Na^+ + Cl^-]$ loading is so minor that osmo-balancing H_2O entry has swollen SM-CD by only ∼4.5% (2,000 μm^3→ ∼2,090 μm^3).

Thus, [big P_{Cl}]-endowed SM-CD can sustain enormous low pump-strength–induced Na^+ overloads with inconsequential water uptake. Weber et al. (2012), following the first use of ^{23}Na-MRI with DMD patients, stressed the chronic nature of the overload, but could not assess if it signified cytotoxic swelling. More recently, using ^{23}Na-proton-MRI, Gerhalter et al. (2019) showed that DMD patients' chronic Na^+ overload can occur in the absence of water T_2 alterations, consistent with SM-CD modeling here.

Membrane damage: Too much Na^+ leak in DMD

For SMFs, P_K >> P_{Na}, specifically (as modeled in SM-CD and LA-CD), P_K:P_{Na} is 1:0.03. If, in SMFs, nonselective cation channels

with P_K:P_{Na} = 1:1 were to activate to an extent that doubled resting P_{Na} (0.3 μm³/s→0.6 μm³/s; a 100% increase), total P_K would increase just 3%, making this cation channel leak principally a Na^+ leak. Both the hormonally regulated NALCN of various excitable cells (Lu et al., 2007; Cochet-Bissuel et al., 2014; Lutas et al., 2016; Philippart and Khaliq, 2018; Reinl et al., 2018) and the AChR channels of SMFs are nonselective cation channels serving as physiological Na^+ leaks. To date, no SMF isoform of NALCN has been detected, but SMFs express various cation channels (Metzger et al., 2020), any of which, if overactive, would augment operational P_{Na}. Unidentified overactive mechanosensitive cation channels in *mdx* fibers are a proposed therapeutic target for GsMtx4-based peptides (Franco and Lansman, 1990; Gnanasambandam et al., 2017; Ward et al., 2018). Like inappropriately active *mdx* AChR-cation channels (Carlson and Officer 1996), they are considered dangerous as Ca^{2+}-entry paths (Yeung et al., 2005; Lansman, 2015; Ward et al., 2018), but if so, unavoidably, they would also be pathological Na^+-leak channels (McBride et al., 2000; Yeung et al., 2003).

AChRs are identified, abundant, reportedly leaky in *mdx* (Carlson and Officer 1996), mechanosensitive and inhibitable by GsMtx4 (Pan et al., 2012), and known to exhibit spontaneous activity (Jackson et al., 1990), whose frequency could increase in damaged junctional *mdx* sarcolemma (Barrantes et al., 2010; Baenziger et al., 2017; Pratt et al., 2015; Kravtsova et al., 2020). We model leaky cation channels, therefore, using the SMF AChR channel P_K:P_{Na} ratio (1.11:1; Hille, 2001) but refer simply to leaky cation channels.

SMFs' largest physiological Na^+ influxes are via Nav1.4 channels bound via syntrophin to dystrophin (Gee et al., 1998; Fu et al., 2011). In *mdx*, sarcolemmal Nav1.4 density is subnormal, but gating appears normal (Mathes et al., 1991; Ribaux et al., 2001; Hirn et al., 2008). Hirn et al. (2008) show that in the 3 d after mechanically traumatic fiber isolation, 3 nM tetrodotoxin protects *mdx* fibers from Na^+ loading and die off. In the bleb-damaged sarcolemma of DMD fibers (Fig. 1 B), Nav1.4 channels could exhibit left-shifted window conductance (Nav-CLS; Boucher et al., 2012; see Materials and methods; Fig. 4 F).

The next sections address these two classes of sarcolemma damage–mediated Na^+ leaks: first Nav-CLS, then overactive cation channels.

Nav-CLS: Treacherous but not a sole cause of chronic Na^+ overload

For CN-CD and for SM-CD subjected to increasing Nav-CLS (at pump strength = 100%), Fig. 10 depicts system excitability (normal, hypersensitive, spontaneous; red line, top) and the systems' steady-state P-L/D values. The term affected channels 0.3 (AC = 0.3) means that damage-induced Nav-CLS affects 3/10th of the Nav channel bearing membrane (see Materials and methods); as per Wang et al. (2009), more intense bleb-type damage→↑CLS (in mV).

In CN-CD, V_{rest} (−65.5 mV) is close to firing threshold. Hypersensitivity (sloped line, top) is the only marked Nav-CLS pathology in CN-CD until, at Nav-CLS[0.3] = 9 mV, the shifted window conductance triggers spontaneous firing (not shown). By Nav-CLS[0.3] = 10 mV, spontaneous AP Na^+ influx is overwhelming; CN-CD is cytotoxically swollen (off scale for the plots).

Though SM-CD Nav density is 3× higher, its hyperpolarized V_{rest} (−86 mV) protects against Nav-CLS[0.3]. SM-CD too exhibits ever-increasing hypersensitivity (top) as Nav-CLS intensity increases, but at, say, 10 mV, the Nav-CLS[0.3] has no other impact. At 20 mV, V_{rest} is depolarized almost imperceptibly. Beyond 23 mV, this steepens sharply. See Fig. 10 legend for details.

The SM-CD Nav-CLS damage range between zero Na^+ loading and the onset of highly problematic sustained spontaneous firing (see $[Na^+]_i$ panel, Fig. 10 B, i) is exquisitely narrow. Thus, Nav-CLS alone (i.e., in a full pump-strength system) could not explain chronic Na^+ overload in DMD fibers.

Damage-induced hypersensitivity of Fig. 10 B, i (top), would promote unwanted spontaneous APs. This could be why the single-fiber electromyographic recordings of advanced-stage DMD patients (whose fibers would certainly not be at full pump strength) show "bizarre repetitive discharge bursts" (Trontelj and Stålberg, 1983; see also Yu et al., 2012). Nav-CLS would foster, too, the in situ erratic spontaneous firing and contractility reported for DMD patients (Ishpekova et al., 1999; Emeryk-Szajewska and Kopeć, 2008; Nojszewska et al., 2017); electromyography of *mdx* muscle shows abnormal spontaneous potentials and complex repetitive discharges like those of boys with DMD (Carter et al., 1992; Han et al., 2006).

Depolarization and Na^+ loading due to leaky cation channels

Stretch injury to healthy (McBride et al., 2000) and *mdx* fibers causes sustained depolarization (Baumann et al., 2020). Channels rendered hypermechanosensitive by membrane damage (e.g., Wan et al., 1999) might intermittently activate in *mdx* fibers (Lansman 2015), or normally quiescent cation channels might activate chronically in damaged sarcolemma. Fig. 11 shows what damage-induced chronic activation of sarcolemmal cation channels would contribute to such situations. In SM-CD and LA-CD (and counterfactual WD-CD), normally quiescent cation channels are activated. Systems converge on their membrane-damaged steady states by ∼20 min off trajectories (after 20 min) mimic step-application of a cation channel–specific inhibitor.

Leak amplitude for the P_K:P_{Na} = 1.11:1 cation channel is established by making its P_{Na} = 0.3 μm³/s. For SM-CD and LA-CD, this doubles operational P_{Na}. WD-CD's larger resting P_K and P_{Na} values diminish the cation leak's relative impact. ATP consumption rises almost identically in each system, but for already high-cost Pump-Leak dominated WD-CD, the rise is ∼22%, while for Donnan dominated SM-CD and LA-CD, this cation leak nearly doubles the cost of steady state.

SM-CD depolarizes by 10 mV (V_{rest}, green square); pathophysiologically, 10 mV is consequential (↑system excitability), but the attendant <1 mM Na^+ loading (green asterisk) would hardly register. Low–pump-strength LA-CD depolarizes by 12 mV, and its $[Na^+]_i$ (∼12 mM) is measurably >3.7 mM (the healthy control value for a [LA-CD/leaky] versus [SM-CD/no leak] comparison). The elevated [LA-CD/leaky] Na^+ influx is countered by almost-equal K^+ loss; accordingly, net [Na^+ + Cl^- + H_2O] uptake (= osmotic Na^+ loading) would give a mere 2% cellular

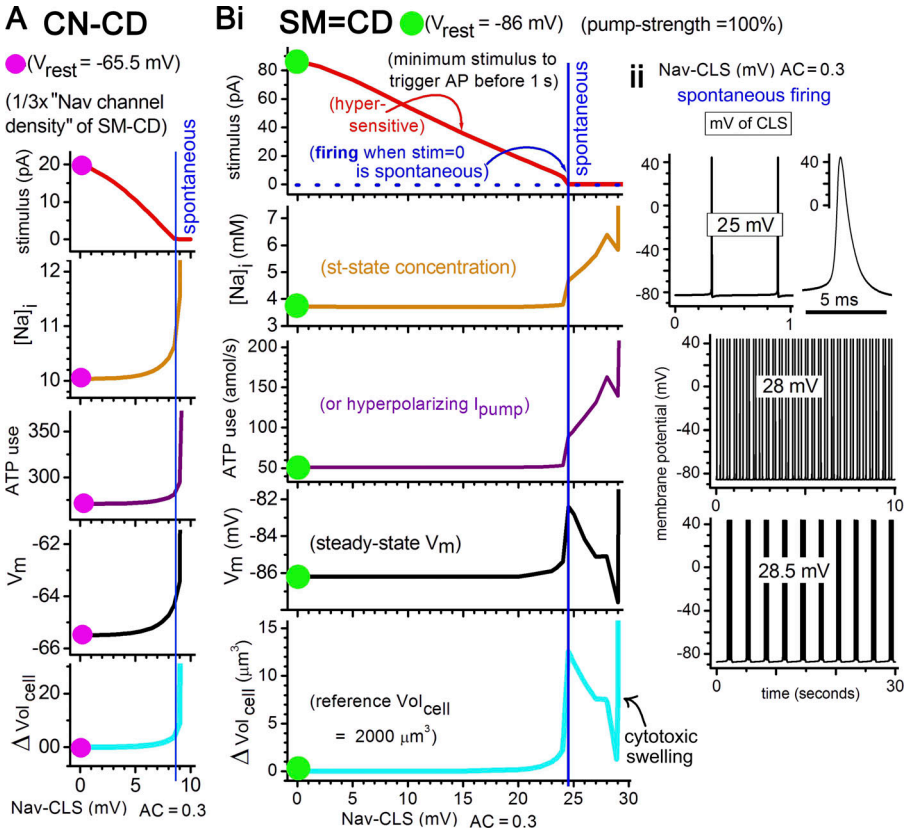

Figure 10. **Membrane-damage induced Nav-CLS in CN-CD and SM-CD. (A)** CN-CD, as labeled, pump strength at 100%. **(B, i and ii)** SM-CD, as labeled, pump strength at 100%. stim, stimulus. Until the onset of spontaneous firing, plots are for steady-state (st-state) values. Beyond vertical blue lines, there is spontaneous firing (beginning at Nav-CLS[0.3] = 24.5 mV for SM-CD) with plots values time averaged (integrated for ≥100 s). Computations beyond Nav-CLS[0.3] = 20 mV were done at x axis values (in mV) 21, 22, 23, 23.5, 24.5, 25, 26, 27, 28, 29, 29.5, and 30. ii illustrates, for SM-CD, low-frequency firing (e.g., <2 Hz, Nav-CLS[0.3] = 25 mV) through to burst firing (e.g., Nav-CLS[0.3] = 28.5 mV). Sustained firing at 28 mV elevates $[Na^+]_i$ only to ∼6 mM. The V_m plot's most hyperpolarized point (for Nav-CLS[0.3] = 29 mV) occurs where spontaneous AP bursts fire from a baseline hyperpolarized by the Na^+-stimulated $I_{NaKpump}$. Across the range 25.0–29 mV, the Nav-CLS[0.3] damage acts as a (pathological) Nav-based pacemaker conductance in a cell that should be quiescent. Then precipitously beyond Nav-CLS[0.3] = 29 mV, the damage-induced I_{Nav} would be lethal with the onset of cytotoxic swelling (i.e., $[Na^+ + Cl^- + H_2O]$ loading). Beyond 29 mV, hyperpolarizing $I_{NaKpump}$ (100% pump strength notwithstanding) is insufficient to redress the depolarizing I_{Naleak} carried by the pathological operational P_{Na} (i.e., normal P_{Na} + left-shifted Nav channels) plus I_{Nav} from the spontaneous APs.

edema (above the [SM-CD/no leak] control). A [LA-CD/leaky] scenario could, therefore, explain depolarized Na^+-overloaded *mdx* fibers (see Table 1, items 2, 3, 4, 7, and 8) and would be consistent with DMD patients' chronic nonosmotic $[Na^+]_i$ overload.

Its elevated ATP consumption (arrow; 90 amol/s) notwithstanding, depolarized [SM-CD/leaky] still has a robust 6.6-fold pump reserve (= 566 amol/s / 90 amol/s). [LA-CD/leaky], however, has only a 1.9-fold pump reserve (= 30% × 566 amol/s/90 amol/s). While undesirable, 1.9 puts [LA-CD/leaky] in league (regarding vulnerability and robustness) with healthy CNs (pump reserve = 2.1-fold for CN-CD). In advanced DMD, where functional ischemia could initiate ischemic rundowns, leaky cation channels would speed rundown (↑I_{Naleak}) and compromise recovery (↑I_{Naleak}→↓pump reserve).

In summary, in a 100% pump-strength system, leaky cation channels, though strongly depolarizing, augment $[Na^+]_i$ too little to be a plausible standalone explanation for DMD fibers' chronic Na^+ overload. In conjunction with low SMF pump strength, however, they would contribute to chronic nonosmotic Na^+ overloads and amplify the loss of ion homeostatic robustness.

Low pump strength + repetitive stimulation + two damage-related Na^+ leaks

Like rat soleus fibers, SM-CD briskly returns to steady state after firing 1,200 APs (Fig. 5); Fig. 12 A shows LA-CD handling this same stress test, albeit with a slower recovery. [LA-CD/leaky] (as per Fig. 11) also manages the stress test (not shown), as does [LA-CD/(Nav-CLS[0.3] = 10 mV)] (not shown). But, as Fig. 12 B, i, shows, the multiply damaged (i.e., [LA-CD/leaky/(Nav-CLS[0.3] = 10 mV)]) stress-tested Donnan dominated P-L/D system is overwhelmed. Having stabilized at a depolarized V_{rest} (−74 mV), it seems to handle the 1,200 APs, but at 10 s, when stimulation stops (expanded, Fig. 12 B, ii), the $V_m(t)$ trajectory reveals that all is not well. It does not return to steady state. For ∼60 s, APs (∼20 Hz) of diminishing amplitude fire spontaneously: then the system converges on a pathological depolarized steady state that (not shown) is swollen and gradient depleted. From the limited perspective of $V_m(t)$, it is unclear when, during the stress test, a lethal threshold was crossed. In this lethal bistability scenario, to know when threshold crossing occurred would require simultaneous monitoring of (A) $I_{NaKpump}$ and (B) total depolarizing I_{Naleak}. Lethal threshold crossing occurs when B > A.

Na^+ overload and DMD ion homeostatic jeopardy

^{23}Na-proton-MRI (Gerhalter et al., 2017, 2019) will increasingly be used to noninvasively monitor DMD patients. Representing worsening DMD severity, Fig. 13 A thus plots SM-CD Na^+ loads corresponding to diminishing pump strength and accumulating (damage-induced) Nav-CLS. The y axis indicates the lowest pump strength able to prevent spontaneous firing at Nav-CLS [0.3] intensity on the x axis. Fig. 13 B extracts values from Fig. 13 A to graphically emphasize tolerable and intolerable $[Na^+]_i$ zones. Coordinates corresponding to a quiescent V_m (no spontaneous firing, so no contracture and no cytotoxic swelling) are deemed safe. Beyond that, coordinates are deemed lethal. The

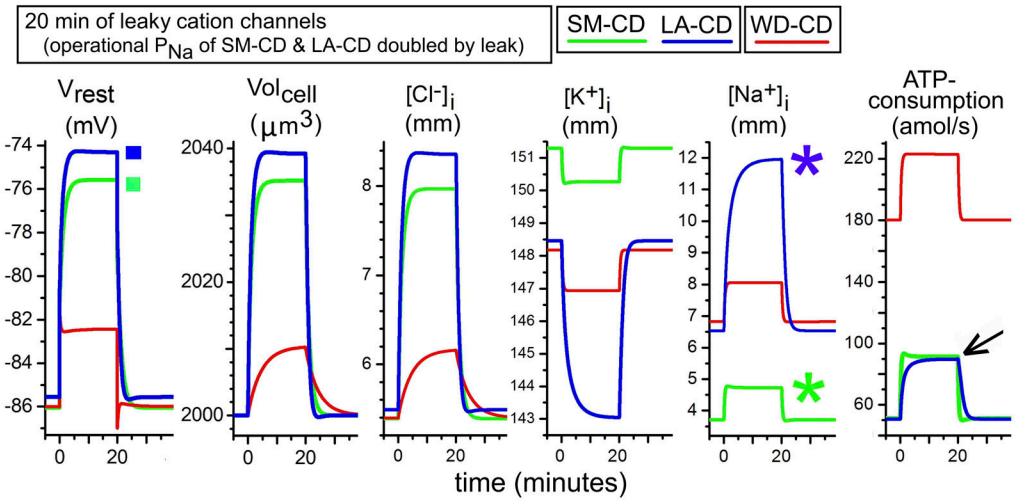

Figure 11. **Leaky cation channels.** For three minimal P-L/D models (Donnan dominated SM-CD and LA-CD, as well as counterfactual Pump-Leak dominated WD-CD), P-L/D trajectories after a step-activation, then 20 min later, a step-deactivation of cation channels. In all models, $V_{rest} = E_{Cl}$, and V_{rest} is close to E_K but far from E_{Na}. Fast depolarizing/hyperpolarizing V_m excursions thus mostly reflect the instantaneous onset/offset of an inward I_{Naleak}. Slower changes reflect ion homeostasis, i.e., active (see ATP consumption, which is directly proportional to $I_{NaKpump}$, which at steady state, = $-I_{NaleakTOTAL}$) and concurrent passive feedbacks (see Cl^- and Vol_{cell}) as the P-L/D systems converge to new steady states. $Vol_{cell}(t)$ changes at the speed of the rate-limiting osmotic flux component; in WD-CD, [small P_{Cl}] makes swelling slower than in the two [big P_{Cl}] models, SM-CD and LA-CD. WD-CD is neuron-like in that its [small P_{Cl}] serves as an osmotic damper for transient Na^+ influxes (whose full metabolic cost must, however, be paid). In LA-CD, lower pump strength slows the attainment of the new steady state (compare $[K^+]_i$ and $[Na^+]_i$ trajectories for SM-CD and LA-CD). Discernible in various trajectories are small single oscillations; these are Donnan bounce manifestations (constrained by $[A^-]_i(t)$). To estimate concurrent Ca^{2+} influx through nonselective cation channels like those modeled here, see Fucile (2004).

Vol_{cell} plot (inset in Fig. 13 A) shows safe zone swelling to be negligible. Fig. 13 C is a sketched (no further computations) reminder that leaky cation channels will diminish the safe $[Na^+]_i$ zone, pulling it nearer the origin (green dot).

An overall message: for damaged SMFs, there is no one canonical safe $[Na^+]_i$-load value. As per Fig. 13 A, for SM-CD pump strengths approaching the saddle-node value (Fig. 9), high $[Na^+]_i$ can be sustained, but only if there is no damage–Na^+ leak. At the other extreme (near 100% pump strength), profound membrane-damage Na^+ leak is tolerated with almost no Na^+ loading, but any pump-strength reduction would bring on lethal spontaneous APs. Between these extremes, chronic $[Na^+]_i$ overloads beneath the descending Na^+ line, though undesirable, are tenable. Quiescent fibers close to the safe boundary would have little resilience: transient physiological demands on the P-L/D system (AP trains, use of secondary transporters, a bout of functional ischemia) could push them into the lethal zone.

DMD-patient muscle $[Na^+]_i$ values assessed by ^{23}Na-MRI would combine individual fibers with coordinates throughout the safe zone. Safe-zone fibers well to the right would be mildly $[Na^+]_i$ loaded but hyperexcitable and thus vulnerable to unwanted (and lethal) excitation–contraction coupling (Claflin and Brooks, 2008). At left (Fig. 13 B), in heavily $[Na^+]_i$-loaded safe-zone fibers, vulnerability to Ca^{2+} necrosis via reverse operation of Na^+/Ca^{2+} exchangers (as per Burr et al., 2014) would be an ever-present danger. Ca^{2+} necrosis and ion homeostatic failure are not mutually exclusive explanations for DMD fiber demise.

Discussion

To address the impaired ion homeostasis of Duchenne MD, a generic ion homeostasis model for excitable SMFs, SM-CD, was devised, then tested under normal and DMD-like conditions. For SMFs, myonuclear domain size is the average cyto-volume transcriptionally served by one nucleus in the syncytium. SM-CD does not represent the syncytial SMF; it is one ion homeostatic unit that, disposed as many contiguous slices, would represent a syncytial SMF. Back-calculating from mice (e.g., Mantilla et al., 2008), SM-CDs' 2,000 μm³ would roughly correspond to one myonuclear domain volume. Cell biologically, this is reasonable because SM-CDs' 2,000 μm³ matches CN-CDs' one neuronuclear domain.

SM-CD and CN-CD are excitable P-L/D systems. SMFs' and neurons' distinctive ion homeostatic P-L/D strategies have been evolutionarily tuned to their distinctive electrophysiological lifestyles: mostly quiescent, low excitability, and resilient during severe ion homeostatic emergencies (syncytial SMFs) and electrically agile, electrically versatile, highly excitable (neurons). SMFs' low-impedance Donnan-dominated steady state is robust and inexpensive. Neurons' high impedance Pump-Leak–dominated steady state is vulnerable and expensive. In ancestral (like modern) vertebrates, SM occupied the largest fractional tissue mass (Mink et al., 1981; Rolfe and Brown, 1997; Helfman et al., 2009; Johnston et al., 2011; Casane and Laurenti, 2013; Dutel et al., 2019; see Table S1); a low-cost steady state for this massive tissue is self-evidently advantageous. Neurons' executive functions are indispensable for the whole organism; that, plus their small fractional body mass (<0.2% in ancestral vertebrates, ~2% in humans), has, self-evidently, rendered their precariously costly ion homeostasis acceptable.

DMD ion homeostasis is simulated here as reduced pump strength and/or inappropriately active Na^+-permeant ion channels. Ca^{2+} necrosis, considered the usual proximate cause

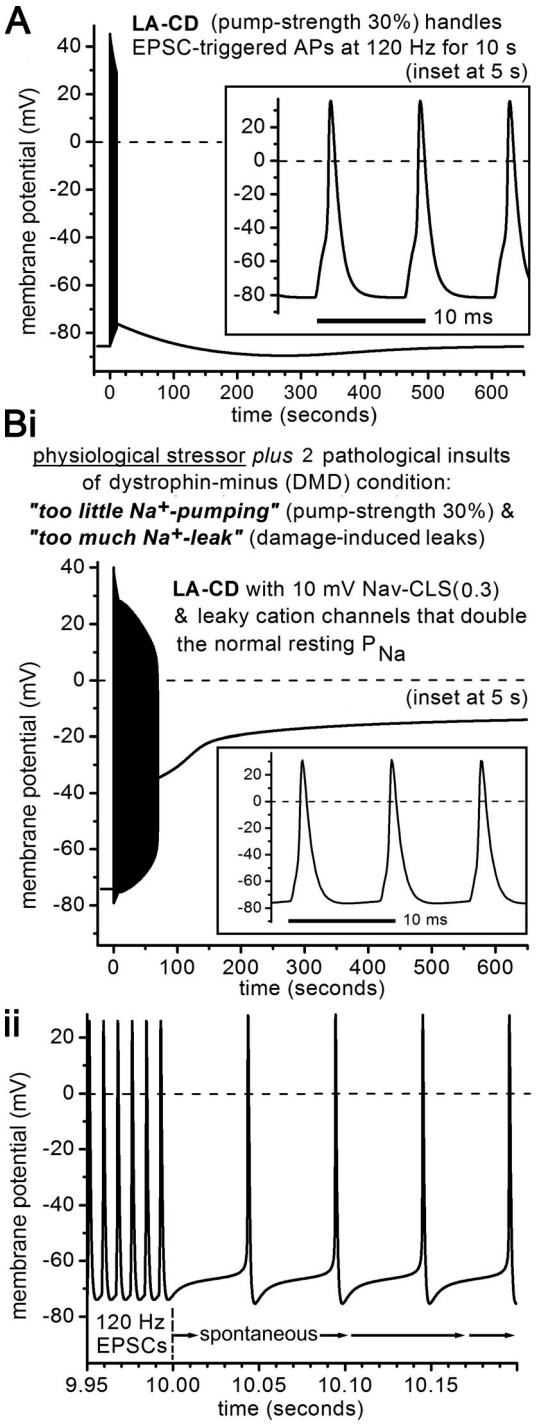

Figure 12. **Stress-testing low–pump-strength LA-CD without/with leaky channels. (A)** $V_m(t)$ for LA-CD before/during/after the stress test of Fig. 5. **(B i)** $V_m(t)$ for LA-CD with bleb damage (i.e., Na^+ leaks through both Nav and cation channels, as described in the text) before/during/after the same stress test. **(B ii)** expanded $V_m(t)$ traces as the stress test ends at 10 s, to show the transition from stimulated (120 Hz) to spontaneous APs (after about a minute $V_m(t)$ becomes quiescent and depolarizes to the damaged system's pathological steady state).

for fiber loss in DMD, is indirectly addressed. Beyond DMD, pathological situations modeled here are relevant to healthy SMFs that experience traumatic/exercise injury, including situations arising as compartment syndrome.

Prospects

DMD molecular-therapy preclinical and clinical trials are in progress (Verhaart and Aartsma-Rus, 2019; Meng et al., 2020; Datta and Ghosh, 2020; Chemello et al., 2020; Wagner et al., 2021; Duan et al., 2021), and noninvasive monitoring of aspects of muscle ion homeostasis is increasingly feasible (e.g., Dahlmann et al., 2016; Mankodi et al., 2017; Forbes et al., 2020; Pennati et al., 2020; Zhang et al., 2020; Dietz et al., 2020; Sherlock et al., 2021). The generic theoretical framework outlined here for excitable SMF ion homeostasis should prove helpful in those contexts. DMD fibers' operational pump strength (as modeled here) depends on the diverse factors mentioned in Fig. 1 C, some of which are therapeutic targets. As pump strength diminished and as fibers accumulated sarcolemma damage in DMD, our analysis indicates that Nav1.4 channels and leaky (Na^+-permeant)–cation channels would be therapeutic targets.

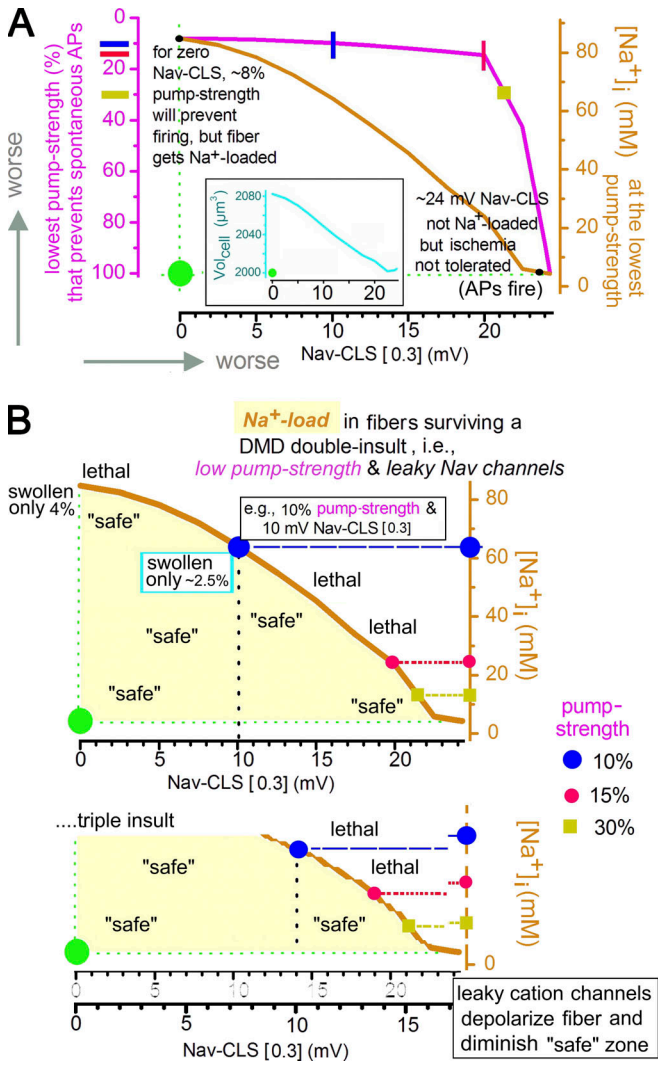

Figure 13. **Safe Na^+ overloads and DMD.** As explained in the text, SM-CD steady-state values under the plotted conditions. **(A)** The master plot (calculated at 2.5 mV x axis intervals up to 22.5 mV Nav-CLS[0.3], then at 24 mV and 24.3 mV. **(B)** Derived from A, and C is sketched from B (no additional computations) as labeled, to visually illustrate the point made in the box.

Generic SMF ion homeostatic theory as captured by SM-CD (as is) should help frame discussion of (for example) fiber-type–specific single-fiber "snap-freeze" proteomics (Deshmukh et al., 2021), studies of fiber-type– and exertion-regimen–specific ClC-1 immunocytochemistry (Thomassen et al., 2018), and so on. For quantitative use in connection with data obtained, for example, by simultaneous monitoring of multiple SMF ions (Heiny et al., 2019; DiFranco et al., 2019), SM-CD needs to be up-graded (e.g., SMF appropriate V-gated channel kinetics and SMF-specific pumps; for the DMD context, this would extend to the different kinetic to diaphragm and postural muscle pump isoforms; Kravtsova et al., 2020; also see supplemental text).

Fig. 14, left, summarizes the "as-is machinery" of SM-CD, and at right, suggests what a next-stage generic SMF model could incorporate. The following section itemizes what as-is SM-CD reveals about how SMF ion homeostasis copes as well as it does under DMD conditions, and also how it would eventually fail.

DMD-related SMF ion homeostasis as seen via the [big P_{Cl}] [small I_{Naleak}] model, SM-CD

Chronic low–pump strength

Chronic low–pump strength is tolerated because [small I_{Naleak}] → a small requirement for ATP-generated $I_{NaKpump}$ at steady state. Thus, even at chronically low pump strengths (say, 30% LA-CD; Table 2), enough pump reserve can remain to handle moderate ionic perturbations (Fig. 7 C, iii; Fig. 11; and Fig. 12 A).

DMD functional ischemia

Transiently, DMD functional ischemia could take already low pump-strength fibers deep into the danger zone (Fig. 9 C). Longer term, the attendant membrane damage could ↑I_{Naleak} and ↓pump strength. A bout of functional ischemia to below a fiber's saddle node would initiate ischemic rundown; the weaker the pump strength and the larger the I_{Naleak}, the faster the rundown (Fig. 6 C, inset plot). However, if that bout ended before spontaneous firing commenced (Fig. 7 C, iii), even pump strength–boosting factors as minor as massage for circulatory improvement (Carroll et al., 2020) will contribute measurably to DMD fiber survival (Fig. 9 C).

Even at ultra-low pump strength, Na^+ loading is mostly nonosmotic

Fig. 9 shows how, even at the saddle node (X), with [Na^+] loading massive, with [small I_{Naleak}] there contaminated by Nav window current, operational I_{Naleak} has remained small enough that Vol_{cell} has increased only a few percent. Hammon et al. (2015) show that during anaerobic exercise, healthy SMFs exhibit a water-independent (i.e., nonosmotic) ↑$[Na^+]_i$; this seems broadly congruent with anoxic and rundown/recovery behavior for SM-CD and LA-CD (Fig. 7).

As per ^{23}Na-proton-MRI, chronic SMF Na^+ overload is nonosmotic

In SM-CD, $P_{Cl} >> P_K >>> P_{Na}$ with $V_{rest} = E_{Cl}$. I_{Naleak} is so small that during stress testing and rundowns, electro-osmo-balance is maintained with very little [$Na^+ + Cl^- + H_2O$] entry. In such situations, if spontaneous firing began (Fig. 6; and Fig. 7 A, i), the concurrence, for actual fibers, of contracture with osmotic Na^+ loading would presumably destroy them. Such fibers would therefore not contribute to whole-muscle ^{23}Na-proton-MRI signals (see Fig. 13). If SMFs' V-gated channels were fully inactivated, osmotic Na^+ loading could develop safely (see, e.g., Fig. 8 [SM*-CD] at ∼50 min: with E_{Na} ∼0 mV (maximal Na^+ loading), swelling is only (2,400/2,000) 1.2-fold (for reference, after exhaustive exercise, 1.2-fold is the upper limit for fiber swelling [Sjøgaard et al., 1985, recounted by Fraser and Huang, 2004]). H_2O loading lags Na^+ loading there, [big P_{Cl}] and very big [P_{H2O}] notwithstanding. Why? Because SM*-CD is a minimal P-L/D system, so E_{Cl} tracks V_m (keeping the driving force on Cl^- small; see I_{Cl}, Fig. 8). Unlike nonosmotic chronic Na^+ overload in DMD, overactive Na-K-2Cl co-transport would produce osmotic Na^+ loading (Fig. 14 E).

Chronic depolarization without swelling

At very low pump strengths, there is insufficient hyperpolarizing $I_{NaKpump}$ to maintain normal V_{rest} (e.g., see V_m for 20% pump strength; Fig. 9 B), so (in the danger zone below ∼20% pump strength) depolarization →↑chronic Nav subthreshold activity. Danger zone depolarization and reduced ATP consumption therefore coincide, making long-term fiber viability in the danger zone improbable. More likely, chronically depolarized DMD fibers have leaky cation channels plus more mildly reduced pump strength, like LA-CD in Fig. 11, whose depolarized state recruits some subthreshold Nav activity along with the leaky cation channels. Such fibers would be Na^+ loaded but barely swollen. If, additionally, there was Nav-CLS damage (Figs. 10 and 13), higher pump strengths would be required for a fiber to remain safe.

Erratic spontaneous contractility

Erratic spontaneous contractility is explicable if damaged DMD sarcolemma was hypersensitized by Nav-CLS (Fig. 10 B, i, top) and if fibers were chronically depolarized as per Chronic depolarization without swelling. Transient cation channel leaks could then trigger spontaneous AP bursts (i.e., not attributed to end plate input). Though unwanted contractile events are undesirable, brief episodes as just described would be manageable, ion homeostatically, for chronically low pump-strength fibers still tolerably far from a saddle node (X).

Low tolerance for sustained exertion

During exertion, fiber ATP is needed for both contractile and ion homeostatic processes. DMD's functional ischemia occurs for lack of the healthy fiber vasodilation that keeps operational pump strength safely high during exertion (Fig. 9 C).

SMF circadian rhythms could imperil already-compromised DMD respiratory muscles

DMD patients minimize daytime muscle exertion, but nights too are problematic. During rapid eye movement sleep, respiratory profiles are acutely compromised (Nozoe et al., 2015; Hartman et al., 2020; MacKintosh et al., 2020). Muscle tissue sleep rhythms diminish SMF glucose availability and oxidative capacity (Harfmann et al., 2015; van Moorsel et al., 2016; Ehlen et al., 2017); the reduced pump strength could take DMD diaphragm and thoracic fibers to their lethal saddle nodes (Fig. 9 C).

Safe Na^+ overload: What can be deemed safe varies with the mix of deficits

Due to DMD membrane damage, Nav channels may have Nav-CLS of unknown intensity. Thus, no one Na^+-overload level can

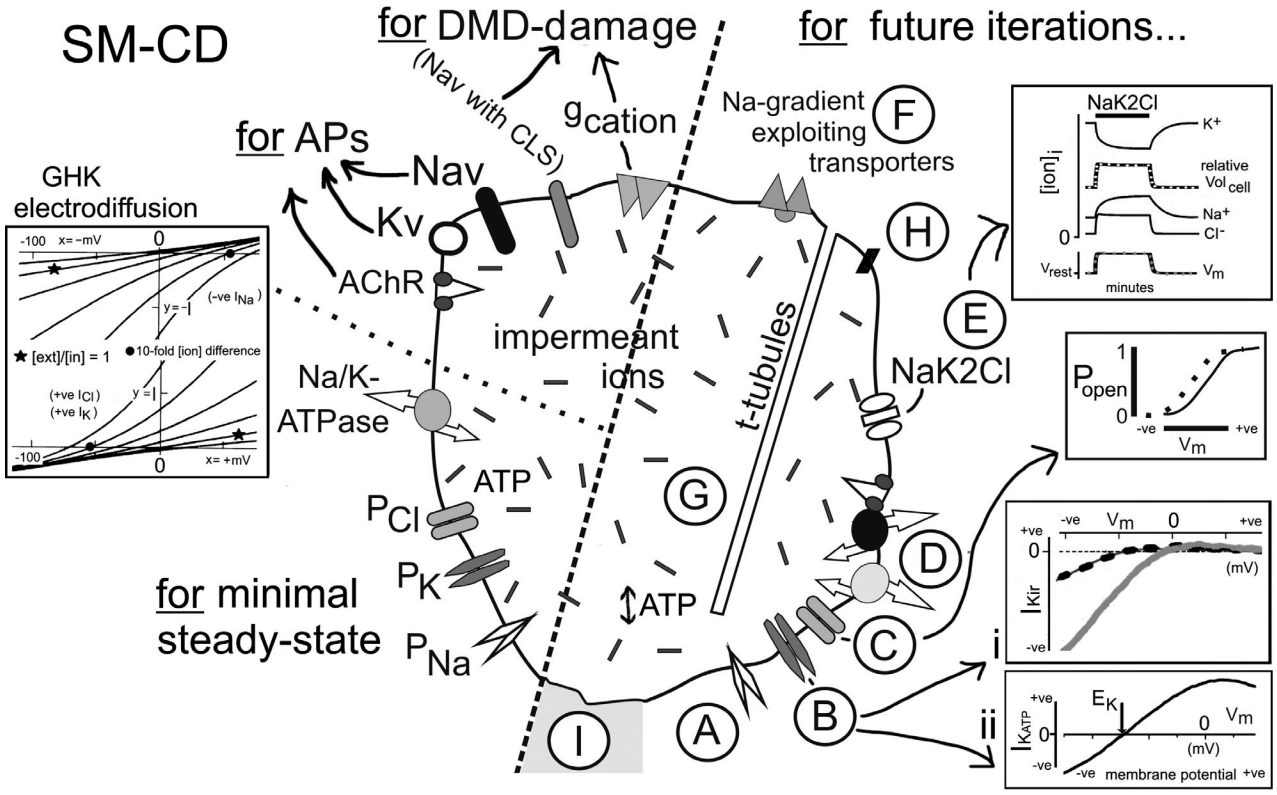

Figure 14. **SM-CD as is and next-stage SM-CD.** Left: SM-CD as is plus conductance (i.e., permeability) modifications for the DMD situation (Nav-CLS and the leaky cation channels). DMD problems that diminish operational pump strength (Fig. 1 C) are modeled simply via ↓maximal pump strength (Fig. 4 B, i). Right (amplified in the supplemental text): Features to consider for future SM-CD iterations. Not indicated pictorially: in lieu of generic (H-H) voltage-gated channels, Nav1.4 and SMF-appropriate Kv channel kinetics could be substituted. **(A)** P_{Na}: of unknown molecular identity; healthy SMFs presumably coregulate P_{Na} relative to P_K to set V_{rest} (Fig 4 D). How such regulation occurs cannot be investigated until P_{Na} is identified. **(B)** P_K: two boxes depict generic I-V relations for inwardly rectifying K currents. B i shows strongly inwardly rectifying $I_K(V)$ for two different $[K^+]_e$:$[K^+]_i$ ratios (illustrating that inward I_K increases and its zero-current potential depolarizes as $[K^+]_e$ increases); for an SMF example, see DiFranco et al. (2015). B ii depicts a weakly inwardly rectifying I_K; for examples, see Bollensdorff et al., 2004 and Scott et al., 2016. **(C)** P_{Cl}: mostly due to ClC-1, a channel expressed exclusively in SMFs. CIC-1 has a weakly voltage-dependent open probability and undergoes a hyperpolarizing shift upon energy depletion (Leermakers et al. 2020). **(D)** $3Na^+/2K^+$-ATPase pumps: in future generic iterations of SM-CD, Eq. 10 variables should be made typical of well-characterized α-isozyme profiles for fast or for slow fibers, and could be further tuned to reflect particular developmental, disease, or work-regimen conditions (Kravtsova et al., 2016; Kravtsova et al., 2020; Deshmukh et al., 2021). Add ons to the appropriately reparameterized Eq. 10 could be used to approximate aspects of feed-forward signaling (e.g., AChR→α2-isoform; Heiny et al., 2010). **(E)** Depiction of how activating a Na-K-2Cl cotransporter would depolarize and swell SMFs due to electroneutral dissipation of Na^+ and K^+ gradients plus Cl^- uptake; the responses depicted are consistent with computations by Fraser and Huang (2004). A pathologically overactive Na-K-2Cl would foster osmotic Na^+ overloads, not the chronic nonosmotic Na^+ overloads reported for DMD (Gerhalter et al., 2019). **(F)** SMFs can intermittently call on multiple other E_{Na}-depleting cotransporters (Usher-Smith et al., 2009). **(G)** T-tubules (the focus of P-L/D modeling by Fraser et al. [2011] and by Sim and Fraser [2014]). **(H)** Cation channels (Metzger et al. [2020] includes a brief review for SMFs). As discussed here, SMF P_{Na} might be a cation channel (see, too, Yeung et al., 2003). **(I)** A finite extracellular volume (to model K^+ loading that affects pumping kinetics, inward rectifier fluxes, and for some cotransporters, including pH regulators). A pump equation with the requisite additional parameters would be needed here.

reliably be designated safe (Fig. 13). The paucity of human SMF data (plus its disparity with respect to mouse data; Table 1) make it hard to assess the $[Na^+]_i$ values of Fig. 13, as does the fact that SM-CD pump kinetics are not those of human (or mouse) SMF pumps (Fig. 14). Anecdotally, Dahlmann et al. (2016) used ^{23}Na-MRI to monitor a young athlete's muscle injury and recovery (control – the noninjured contralateral); this showed at 0, 2, and 8 wk ($[Na^+]_i$ in mM), control/injured, 18/44, 19/38, and 19/22, respectively. By comparison (as per Table 1), control/DMD readings are ($[Na^+]_i$ in mM) 25/38 (Weber et al., 2011) and 16/26 (Gerhalter et al., 2019). The global point of Fig. 13 is that nonlinear interplays among pump strength, V_{rest}, Nav window current, and damage-induced ↑P_{Na} (from Nav-CLS and leaky cation channels) diminish safe Na^+-overload levels nonlinearly. The down-sloping Na^+ line (Fig. 13, B and C) implies that while, say, 80 mM would be safe if the sole DMD deficit is low pump strength, 30 mM could be lethal if there was also, say, ∼20 mV of Nav-CLS[0.3]. If, during tissue remodeling of damaged depolarized SMFs, Nav channels were to chronically slow inactivate (Webb et al., 2009), safety would increase (Fig. 8).

Ca^{2+} necrosis: An elusive consequence of failed ion homeostasis

Here, for low pump-strength systems, Ca^{2+} necrosis can be taken as implied by the onset of spontaneous firing (→Ca^{2+}-mediated excitation–contraction coupling; in ATP-depleted fibers, contraction would be irreversible). Rundowns (Figs. 6 and 7) elicit such firing. Physiological E_{Na} depletion from AP trains (Fig. 12 B)

or, say, an intense bout of cotransporter activity (see Fig. 14 E) could take DMD fibers already coping with insult/injury to a saddle-node threshold (thence to Ca^{2+} necrosis). Conditions for fiber demise are thus diverse. Moreover, though the criterion for the onset of lethal spontaneous firing is simple, hyperpolarizing $I_{NaKpump}$ < depolarizing $I_{Naleak(total)}$, knowing that a threshold has been crossed can be elusive. Even computationally, with multiple nonlinear factors affecting Na^+ fluxes (as per Safe Na^+ overload), recognizing threshold crossing is tricky in the time domain. Depending on the initial conditions before injured SM-CD encountering an unstable threshold (in parameter space), irreversible crossing could happen within milliseconds or might take hours. Consider Fig. 6 (a tourniquet, say, applied at t = 0 to a healthy fiber): this system is now destabilized, but an observer monitoring $V_m(t)$ between, say, 300–320 min would likely report a seriously depolarized but stable V_{rest}. Consider Fig. 12 B: during the stress test, though $V_m(t)$ seems unproblematic, during those 1,200 Aps, the system destabilizes. Recordings that report on SMF $[Ca^{2+}]_i(t)$ are typically visually striking, and they are more easily accomplished recordings of $[Na^+]_i(t)$ or even $V_m(t)$. Instances of fiber loss reported as Ca^{2+} necrosis could therefore reflect ion homeostatic failure. Advances in cell physiological instrumentation could enhance P-L/D investigations of SMFs in the DMD context: it is now possible, with a four-electrode method (Heiny et al., 2019), to follow multi-ion dynamics and transport processes under voltage or current clamp, even monitoring $[Cl^-]_i$ accurately (DiFranco et al., 2019).

Therapeutics and optimizing the P-L/D process in DMD SMFs

Diminishing DMD fiber loss by bolstering SMFs' ion homeostasis robustness (i.e., moving as close as possible to the green dots of Figs. 9, 10, and 13) would require (1) optimizing operational pump strength by countering the factors listed in Fig. 1 C, and (2) minimizing Na^+ leaks. Examples for (1) are up-regulating pumps and/or modifying their kinetics (Breitenbach et al., 2016; Glemser et al., 2017; Raman et al., 2017), ↑vascular sufficiency (e.g., angiogenesis; Verma et al., 2019; Podkalicka et al., 2019), dietary supplementation that increases vascular density (Banfi et al., 2018), ↑vasodilation (e.g., NO reagents; Rebolledo et al., 2016; Patel et al., 2018), and massage (Saxena et al., 2013; Carroll et al., 2020). Insofar as stressors (e.g., during ischemic preconditioning; Rongen et al., 2002) cause myofibers to preemptively up-regulate their pump strength (↑pump reserve), encouraging this (Glemser et al., 2017) could help prevent threshold catastrophes. Examples for (2) are suppression of the danger zone's treacherous subthreshold Nav1.4 current, e.g., via ranolazine and/or anticonvulsant agents that enhance Nav1.4 slow inactivation in SMFs (Lorusso et al., 2019; Skov et al., 2017), neither of which is (yet) in use for DMD. Long-available pharmacological tools could establish whether leaky AChR channels (Carlson and Officer 1996; Pan et al., 2012) contribute to DMD fiber depolarization/Na^+ loading.

Sarcolemmal damage causes Na^+ loading via Na^+-permeant (tetrodotoxin-insensitive) channels (Yeung et al., 2003) thought to be the overactive (and adventitiously mechanosensitive) cation channels of *mdx* fibers (Yeung et al., 2005; Ward et al., 2018). The scenario resembles LA-CD/leaky (Fig. 11). In healthy SMFs, does that cation channel do for SMFs what NALCNs do for neurons and smooth muscle (Lutas et al., 2016; Philippart and Khaliq, 2018)? In other words, is it SMFs' physiological P_{Na}? Perhaps the membrane-active compounds coming into use for DMD patients (Houang et al., 2018; Sreetama et al., 2018; Conklin et al., 2018) will stabilize a leaky SMF P_{Na}, but with SMF P_{Na} unidentified, this would be difficult to test. SMF's small-valued P_{Na} has been overlooked but, as emphasized here, its smallness makes it powerful, not trivial. That smallness is an energetically pivotal feature of the human body's largest tissue. Like the process underway for its neuronal counterpart (NALCN, e.g., Kang et al., 2020) molecular identification and structural characterization of SMF P_{Na} would open routes to rational development of inhibitors and modulators.

Acknowledgments

Jeanne M. Nerbonne served as editor.

We acknowledge financial support from Natural Sciences and Engineering Council (Canada; grant RGPIN-06835-2018 to B. Joos) and support from the Ottawa Hospital Research Institute (to C.E. Morris).

The authors declare no competing financial interests.

Author contributions: C.E. Morris: conceptualization, model validation, figure preparation, and manuscript writing and revising; B Joos: conceptualization, model development, coding, optimizing, and validating the charge difference approach computational models, implementing the models and curating the outputs, writing Materials and methods, and manuscript editing; and J.J. Wheeler: contributing to coding and data presentation.

Submitted: 17 March 2021
Accepted: 30 September 2021

References

Allen, D.G., N.P. Whitehead, and S.C. Froehner. 2016. Absence of dystrophin disrupts skeletal muscle signaling: Roles of Ca^{2+}, reactive oxygen species, and nitric oxide in the development of muscular dystrophy. *Physiol. Rev.* 96:253–305. https://doi.org/10.1152/physrev.00007.2015

Altamirano, F., C.F. Perez, M. Liu, J. Widrick, E.R. Barton, P.D. Allen, J.A. Adams, and J.R. Lopez. 2014. Whole body periodic acceleration is an effective therapy to ameliorate muscular dystrophy in *mdx* mice. *PLoS One.* 9:e106590. https://doi.org/10.1371/journal.pone.0106590

Ameziane-Le Hir, S., C. Raguénès-Nicol, G. Paboeuf, A. Nicolas, E. Le Rumeur, and V. Vié. 2014. Cholesterol favors the anchorage of human dystrophin repeats 16 to 21 in membrane at physiological surface pressure. *Biochim. Biophys. Acta.* 1838:1266–1273. https://doi.org/10.1016/j.bbamem.2014.01.010

Anderson, J.E. 1991. Myotube phospholipid synthesis and sarcolemmal ATPase activity in dystrophic (*mdx*) mouse muscle. *Biochem. Cell Biol.* 69:835–841. https://doi.org/10.1139/o91-124

Andrews, N.W., P.E. Almeida, and M. Corrotte. 2014. Damage control: cellular mechanisms of plasma membrane repair. *Trends Cell Biol.* 24:734–742. https://doi.org/10.1016/j.tcb.2014.07.008

Asai, A., N. Sahani, M. Kaneki, Y. Ouchi, J.A. Martyn, and S.E. Yasuhara. 2007. Primary role of functional ischemia, quantitative evidence for the two-hit mechanism, and phosphodiesterase-5 inhibitor therapy in mouse muscular dystrophy. *PLoS One.* 2:e806. https://doi.org/10.1371/journal.pone.0000806

Bækgaard Nielsen, O., F.V. de Paoli, A. Riisager, and T.H. Pedersen. 2017. Chloride channels take center stage in acute regulation of excitability in

skeletal muscle: implications for fatigue. *Physiology (Bethesda)*. 32: 425–434. https://doi.org/10.1152/physiol.00006.2015

Baenziger, J.E., J.A. Domville, and J.P.D. Therien. 2017. The role of cholesterol in the activation of nicotinic acetylcholine receptors. *Curr. Top. Membr.* 80:95–137. https://doi.org/10.1016/bs.ctm.2017.05.002

Banfi, S., G. D'Antona, C. Ruocco, M. Meregalli, M. Belicchi, P. Bella, S. Erratico, E. Donato, F. Rossi, F. Bifari, et al. 2018. Supplementation with a selective amino acid formula ameliorates muscular dystrophy in mdx mice. *Sci. Rep.* 8:14659. https://doi.org/10.1038/s41598-018-32613-w

Barrantes, F.J., V. Bermudez, M.V. Borroni, S.S. Antollini, M.F. Pediconi, J.C. Baier, I. Bonini, C. Gallegos, A.M. Roccamo, A.S. Valles, et al. 2010. Boundary lipids in the nicotinic acetylcholine receptor microenvironment. *J. Mol. Neurosci.* 40:87–90. https://doi.org/10.1007/s12031-009-9262-z

Barthélémy, F., A. Defour, N. Lévy, M. Krahn, and M. Bartoli. 2018. Muscle cells fix breaches by orchestrating a membrane repair ballet. *J. Neuromuscul. Dis.* 5:21–28. https://doi.org/10.3233/JND-170251

Baumann, C.W., G.L. Warren, and D.A. Lowe. 2020. Plasmalemma function is rapidly restored in *mdx* muscle after eccentric contractions. *Med. Sci. Sports Exerc.* 52:354–361. https://doi.org/10.1249/MSS.0000000000002126

Bishop, C.A., V. Ricotti, C.D.J. Sinclair, M.R.B. Evans, J.W. Butler, J.M. Morrow, M.G. Hanna, P.M. Matthews, T.A. Yousry, F. Muntoni, et al. 2018. Semi-automated analysis of diaphragmatic motion with dynamic magnetic resonance imaging in healthy controls and non-ambulant subjects with Duchenne Muscular Dystrophy. *Front. Neurol.* 9:9. https://doi.org/10.3389/fneur.2018.00009

Bollensdorff, C., A. Knopp, C. Biskup, T. Zimmer, and K. Benndorf. 2004. Na(+) current through KATP channels: consequences for Na(+) and K(+) fluxes during early myocardial ischemia. *Am. J. Physiol. Heart Circ. Physiol.* 286:H283–H295. https://doi.org/10.1152/ajpheart.00232.2003

Bosco, J., Z. Zhou, S. Gabriëls, M. Verma, N. Liu, B.K. Miller, S. Gu, D.M. Lundberg, Y. Huang, E. Brown, et al. 2021. VEGFR-1/Flt-1 inhibition increases angiogenesis and improves muscle function in a mouse model of Duchenne muscular dystrophy. *Mol. Ther. Methods Clin. Dev.* 21: 369–381. https://doi.org/10.1016/j.omtm.2021.03.013

Boucher, P.A., B. Joós, and C.E. Morris. 2012. Coupled left-shift of Nav channels: modeling the Na^+-loading and dysfunctional excitability of damaged axons. *J. Comput. Neurosci.* 33:301–319. https://doi.org/10.1007/s10827-012-0387-7

Breitenbach, S., F. Lehmann-Horn, and K. Jurkat-Rott. 2016. Eplerenone repolarizes muscle membrane through Na,K-ATPase activation by Tyr10 dephosphorylation. *Acta Myol.* 35:86–89.

Burden, D.L., D. Kim, W. Cheng, E. Chandler Lawler, D.R. Dreyer, and L.M. Keranen Burden. 2018. Mechanically enhancing planar lipid bilayers with a minimal actin cortex. *Langmuir*. 34:10847–10855. https://doi.org/10.1021/acs.langmuir.8b01847

Burr, A.R., and J.D. Molkentin. 2015. Genetic evidence in the mouse solidifies the calcium hypothesis of myofiber death in muscular dystrophy. *Cell Death Differ.* 22:1402–1412. https://doi.org/10.1038/cdd.2015.65

Burr, A.R., D.P. Millay, S.A. Goonasekera, K.H. Park, M.A. Sargent, J. Collins, F. Altamirano, K.D. Philipson, P.D. Allen, J. Ma, et al. 2014. Na^+ dysregulation coupled with Ca^{2+} entry through NCX1 promotes muscular dystrophy in mice. *Mol. Cell. Biol.* 34:1991–2002. https://doi.org/10.1128/MCB.00339-14

Call, J.A., and A.S. Nichenko. 2020. Autophagy: an essential but limited cellular process for timely skeletal muscle recovery from injury. *Autophagy*. 16:1344–1347. https://doi.org/10.1080/15548627.2020.1753000

Call, J.A., G.L. Warren, M. Verma, and D.A. Lowe. 2013. Acute failure of action potential conduction in mdx muscle reveals new mechanism of contraction-induced force loss. *J. Physiol.* 591:3765–3776. https://doi.org/10.1113/jphysiol.2013.254656

Campbell, K.P., and S.D. Kahl. 1989. Association of dystrophin and an integral membrane glycoprotein. *Nature*. 338:259–262. https://doi.org/10.1038/338259a0

Cannon, S.C. 2017. Sodium channelopathies of skeletal muscle. *In* Voltage-gated Sodium Channels: Structure, Function and Channelopathies. Vol. 246. M. Chahine, editor. Springer, Cham. 309–330https://doi.org/10.1007/164_2017_52

Capitanio, D., M. Moriggi, E. Torretta, P. Barbacini, S. De Palma, A. Viganò, H. Lochmüller, F. Muntoni, A. Ferlini, M. Mora, and C. Gelfi. 2020. Comparative proteomic analyses of Duchenne muscular dystrophy and Becker muscular dystrophy muscles: changes contributing to preserve muscle function in Becker muscular dystrophy patients. *J. Cachexia Sarcopenia Muscle.* 11:547–563. https://doi.org/10.1002/jcsm.12527

Carlson, C.G., and T. Officer. 1996. Single channel evidence for a cytoskeletal defect involving acetylcholine receptors and calcium influx in cultured dystrophic (mdx) myotubes. *Muscle Nerve*. 19:1116–1126. https://doi.org/10.1002/(SICI)1097-4598(199609)19:9<1116::AID-MUS6>3.0.CO;2-2

Carroll, K., E.M. Yiu, M.M. Ryan, R.A. Kennedy, and K. de Valle. 2020. The effects of calf massage in boys with Duchenne muscular dystrophy: a prospective interventional study. *Disabil. Rehabil.* 1:1–7. https://doi.org/10.1080/09638288.2020.1753829

Carter, G.T., K.J. Longley, and R.K. Entrikin. 1992. Electromyographic and nerve conduction studies in the mdx mouse. *Am. J. Phys. Med. Rehabil.* 71:2–5. https://doi.org/10.1097/00002060-199202000-00002

Casane, D., and P. Laurenti. 2013. Why coelacanths are not 'living fossils': a review of molecular and morphological data. *BioEssays*. 35:332–338. https://doi.org/10.1002/bies.201200145

Cha, C.Y., and A. Noma. 2012. Steady-state solutions of cell volume in a cardiac myocyte model elaborated for membrane excitation, ion homeostasis and Ca2+ dynamics. *J. Theor. Biol.* 307:70–81. https://doi.org/10.1016/j.jtbi.2012.04.025

Chemello, F., R. Bassel-Duby, and E.N. Olson. 2020. Correction of muscular dystrophies by CRISPR gene editing. *J. Clin. Invest.* 130:2766–2776. https://doi.org/10.1172/JCI136873

Claflin, D.R., and S.V. Brooks. 2008. Direct observation of failing fibers in muscles of dystrophic mice provides mechanistic insight into muscular dystrophy. *Am. J. Physiol. Cell Physiol.* 294:C651–C658. https://doi.org/10.1152/ajpcell.00244.2007

Clausen, T. 2013. Quantification of Na^+,K^+ pumps and their transport rate in skeletal muscle: functional significance. *J. Gen. Physiol.* 142:327–345. https://doi.org/10.1085/jgp.201310980

Clausen, T. 2015. Excitation of skeletal muscle is a self-limiting process, due to run-down of Na+, K+ gradients, recoverable by stimulation of the Na+, K+ pumps. *Physiol. Rep.* 3:e12373. https://doi.org/10.14814/phy2.12373

Clausen, T., and J.A. Flatman. 1977. The effect of catecholamines on Na-K transport and membrane potential in rat soleus muscle. *J. Physiol.* 270:383–414. https://doi.org/10.1113/jphysiol.1977.sp011958

Cochet-Bissuel, M., P. Lory, and A. Monteil. 2014. The sodium leak channel, NALCN, in health and disease. *Front. Cell. Neurosci.* 8:132. https://doi.org/10.3389/fncel.2014.00132

Coles, C.A., L. Gordon, L.C. Hunt, T. Webster, A.T. Piers, C. Kintakas, K. Woodman, S.L. Touslon, G.M. Smythe, J.D. White, and S.R. Lamandé. 2019. Expression profiling in exercised mdx suggests a role for extracellular proteins in the dystrophic muscle immune response. *Hum. Mol. Genet.* 29:353–368. https://doi.org/10.1093/hmg/ddz266

Conklin, L.S., J.M. Damsker, E.P. Hoffman, W.J. Jusko, P.D. Mavroudis, B.D. Schwartz, L.J. Mengle-Gaw, E.C. Smith, J.K. Mah, M. Guglieri, et al. 2018. Phase IIa trial in Duchenne muscular dystrophy shows vamorolone is a first-in-class dissociative steroidal anti-inflammatory drug. *Pharmacol. Res.* 136:140–150. https://doi.org/10.1016/j.phrs.2018.09.007

Constantin, B. 2014. Dystrophin complex functions as a scaffold for signalling proteins. *Biochim. Biophys. Acta.* 1838:635–642. https://doi.org/10.1016/j.bbamem.2013.08.023

Cornelius, F., M. Habeck, R. Kanai, C. Toyoshima, and S.J. Karlish. 2015. General and specific lipid-protein interactions in Na,K-ATPase. *Biochim. Biophys. Acta.* 1848:1729–1743. https://doi.org/10.1016/j.bbamem.2015.03.012

Corrotte, M., P.E. Almeida, C. Tam, T. Castro-Gomes, M.C. Fernandes, B.A. Millis, M. Cortez, H. Miller, W. Song, T.K. Maugel, and N.W. Andrews. 2013. Caveolae internalization repairs wounded cells and muscle fibers. *eLife*. 2:e00926. https://doi.org/10.7554/eLife.00926

Cozzoli, A., A. Liantonio, E. Conte, M. Cannone, A.M. Massari, A. Giustino, A. Scaramuzzi, S. Pierno, P. Mantuano, R.F. Capogrosso, et al. 2014. Angiotensin II modulates mouse skeletal muscle resting conductance to chloride and potassium ions and calcium homeostasis via the AT1 receptor and NADPH oxidase. *Am. J. Physiol. Cell Physiol.* 307:C634–C647. https://doi.org/10.1152/ajpcell.00372.2013

Dabaj, I., J. Ferey, F. Marguet, V. Gilard, C. Basset, Y. Bahri, A.C. Brehin, C. Vanhulle, F. Leturcq, S. Marret, et al. 2021. Muscle metabolic remodelling patterns in Duchenne muscular dystrophy revealed by ultra-high-resolution mass spectrometry imaging. *Sci. Rep.* 11:1906. https://doi.org/10.1038/s41598-021-81090-1

Dahlmann, A., C. Kopp, P. Linz, A. Cavallaro, H. Seuss, K.U. Eckardt, F.C. Luft, J. Titze, M. Uder, and M. Hammon. 2016. Quantitative assessment of muscle injury by (^{23})Na magnetic resonance imaging. *Springerplus*. 5: 661. https://doi.org/10.1186/s40064-016-2193-6

Datta, N., and P.S. Ghosh. 2020. Update on muscular dystrophies with focus on novel treatments and biomarkers. *Curr. Neurol. Neurosci. Rep.* 20:14. https://doi.org/10.1007/s11910-020-01034-6

Deshmukh, A.S., D.E. Steenberg, M. Hostrup, J.B. Birk, J.K. Larsen, A. Santos, R. Kjøbsted, J.R. Hingst, C.C. Schéele, M. Murgia, et al. 2021. Deep muscle-proteomic analysis of freeze-dried human muscle biopsies reveals fiber type-specific adaptations to exercise training. *Nat. Commun.* 12:304. https://doi.org/10.1038/s41467-020-20556-8

Dietz, A.R., A. Connolly, A. Dori, and C.M. Zaidman. 2020. Intramuscular blood flow in Duchenne and Becker Muscular Dystrophy: Quantitative power Doppler sonography relates to disease severity. *Clin. Neurophysiol.* 131:1–5. https://doi.org/10.1016/j.clinph.2019.09.023

DiFranco, M., C. Yu, M. Quiñonez, and J.L. Vergara. 2015. Inward rectifier potassium currents in mammalian skeletal muscle fibres. *J. Physiol.* 593: 1213–1238. https://doi.org/10.1113/jphysiol.2014.283648

DiFranco, M., M. Quinonez, R.M. Dziedzic, A.M. Spokoyny, and S.C. Cannon. 2019. A highly-selective chloride microelectrode based on a mercuracarborand anion carrier. *Sci. Rep.* 9:18860. https://doi.org/10.1038/s41598-019-54885-6

Dijkstra, K., J. Hofmeijer, S.A. van Gils, and M.J. van Putten. 2016. A biophysical model for cytotoxic cell swelling. *J. Neurosci.* 36:11881–11890. https://doi.org/10.1523/JNEUROSCI.1934-16.2016

Dmitriev, A.V., A.A. Dmitriev, and R.A. Linsenmeier. 2019. The logic of ionic homeostasis: Cations are for voltage, but not for volume. *PLOS Comput. Biol.* 15:e1006894. https://doi.org/10.1371/journal.pcbi.1006894

Donohoe, P.H., T.G. West, and R.G. Boutilier. 2000. Factors affecting membrane permeability and ionic homeostasis in the cold-submerged frog. *J. Exp. Biol.* 203:405–414. https://doi.org/10.1242/jeb.203.2.405

Dooley, J.M., and E.K. Chiasson. 2014. Compartment syndrome in Duchenne muscular dystrophy. *J. Pediatr. Neurol.* 12:203–205. https://doi.org/10.3233/JPN-140663

Dos Santos Morais, R., O. Delalande, J. Pérez, D. Mias-Lucquin, M. Lagarrigue, A. Martel, A.E. Molza, A. Chéron, C. Raguénès-Nicol, T. Chenuel, et al. 2018. Human dystrophin structural changes upon binding to anionic membrane lipids. *Biophys. J.* 115:1231–1239. https://doi.org/10.1016/j.bpj.2018.07.039

Dowling, P., S. Gargan, S. Murphy, M. Zweyer, H. Sabir, D. Swandulla, and K. Ohlendieck. 2021. The dystrophin node as integrator of cytoskeletal organization, lateral force transmission, fiber stability and cellular signaling in skeletal muscle. *Proteomes.* 9:9. https://doi.org/10.3390/proteomes9010009

Dreier, J.P., C.L. Lemale, V. Kola, A. Friedman, and K. Schoknecht. 2018. Spreading depolarization is not an epiphenomenon but the principal mechanism of the cytotoxic edema in various gray matter structures of the brain during stroke. *Neuropharmacology.* 134(Pt B):189–207. https://doi.org/10.1016/j.neuropharm.2017.09.027

Duan, D., N. Goemans, S. Takeda, E. Mercuri, and A. Aartsma-Rus. 2021. Duchenne muscular dystrophy. *Nat. Rev. Dis. Primers.* 7:13. https://doi.org/10.1038/s41572-021-00248-3

Dubinin, M.V., E.Y. Talanov, K.S. Tenkov, V.S. Starinets, I.B. Mikheeva, M.G. Sharapov, and K.N. Belosludtsev. 2020. Duchenne muscular dystrophy is associated with the inhibition of calcium uniport in mitochondria and an increased sensitivity of the organelles to the calcium-induced permeability transition. *Biochim. Biophys. Acta Mol. Basis Dis.* 1866:165674. https://doi.org/10.1016/j.bbadis.2020.165674

Dudley, R.W., G. Danialou, K. Govindaraju, L. Lands, D.E. Eidelman, and B.J. Petrof. 2006. Sarcolemmal damage in dystrophin deficiency is modulated by synergistic interactions between mechanical and oxidative/nitrosative stresses. *Am. J. Pathol.* 168:1276–1287, quiz:1404–1405. https://doi.org/10.2353/ajpath.2006.050683

Dumont, N.A., Y.X. Wang, J. von Maltzahn, A. Pasut, C.F. Bentzinger, C.E. Brun, and M.A. Rudnicki. 2015. Dystrophin expression in muscle stem cells regulates their polarity and asymmetric division. *Nat. Med.* 21: 1455–1463. https://doi.org/10.1038/nm.3990

Dunn, J.F., N. Bannister, G.J. Kemp, and S.J. Publicover. 1993. Sodium is elevated in *mdx* muscles: ionic interactions in dystrophic cells. *J. Neurol. Sci.* 114:76–80. https://doi.org/10.1016/0022-510X(93)90052-Z

Dunn, J.F., K.A. Burton, and M.J. Dauncey. 1995. Ouabain sensitive Na^+/K^+-ATPase content is elevated in *mdx* mice: implications for the regulation of ions in dystrophic muscle. *J. Neurol. Sci.* 133:11–15. https://doi.org/10.1016/0022-510X(95)00167-Z

Düsterwald, K.M., C.B. Currin, R.J. Burman, C.J. Akerman, A.R. Kay, and J.V. Raimondo. 2018. Biophysical models reveal the relative importance of transporter proteins and impermeant anions in chloride homeostasis. *eLife.* 7:e39575. https://doi.org/10.7554/eLife.39575

Dutel, H., M. Galland, P. Tafforeau, J.A. Long, M.J. Fagan, P. Janvier, A. Herrel, M.D. Santin, G. Clément, and M. Herbin. 2019. Neurocranial development of the coelacanth and the evolution of the sarcopterygian head. *Nature.* 569:556–559. https://doi.org/10.1038/s41586-019-1117-3

Ehlen, J.C., A.J. Brager, J. Baggs, L. Pinckney, C.L. Gray, J.P. DeBruyne, K.A. Esser, J.S. Takahashi, and K.N. Paul. 2017. *Bmal1* function in skeletal muscle regulates sleep. *eLife.* 6:e26557. https://doi.org/10.7554/eLife.26557

Else, P.L. 2020. Postnatal development in the rat: Changes in Na^+ flux, sodium pump molecular activity and membrane lipid composition. *Mech. Dev.* 162:103610. https://doi.org/10.1016/j.mod.2020.103610

Emeryk-Szajewska, B., and J. Kopeć. 2008. Electromyographic pattern in Duchenne and Becker muscular dystrophy. Part II. Electromyographic pattern in Becker muscular dystrophy in comparison with Duchenne muscular dystrophy. *Electromyogr. Clin. Neurophysiol.* 48:279–284.

Farini, A., C. Sitzia, C. Villa, B. Cassani, L. Tripodi, M. Legato, M. Belicchi, P. Bella, C. Lonati, S. Gatti, et al. 2021. Defective dystrophic thymus determines degenerative changes in skeletal muscle. *Nat. Commun.* 12: 2099. https://doi.org/10.1038/s41467-021-22305-x

Filatov, G.N., M.J. Pinter, and M.M. Rich. 2005. Resting potential-dependent regulation of the voltage sensitivity of sodium channel gating in rat skeletal muscle in vivo. *J. Gen. Physiol.* 126:161–172. https://doi.org/10.1085/jgp.200509337

Filippelli, R.L., and N.C. Chang. 2021. Empowering muscle stem cells for the treatment of Duchenne muscular dystrophy. *Cells Tissues Organs.* 28: 1–14. https://doi.org/10.1159/000514305

Forbes, S.C., H. Arora, R.J. Willcocks, W.T. Triplett, W.D. Rooney, A.M. Barnard, U. Alabasi, D.J. Wang, D.J. Lott, C.R. Senesac, et al. 2020. Upper and lower extremities in Duchenne muscular dystrophy evaluated with quantitative MRI and proton MR spectroscopy in a multicenter cohort. *Radiology.* 295:616–625. https://doi.org/10.1148/radiol.2020192210

Franco, A. Jr., and J.B. Lansman. 1990. Calcium entry through stretch-inactivated ion channels in *mdx* myotubes. *Nature.* 344:670–673. https://doi.org/10.1038/344670a0

Fraser, J.A., and C.L. Huang. 2004. A quantitative analysis of cell volume and resting potential determination and regulation in excitable cells. *J. Physiol.* 559:459–478. https://doi.org/10.1113/jphysiol.2004.065706

Fraser, J.A., and C.L. Huang. 2007. Quantitative techniques for steady-state calculation and dynamic integrated modelling of membrane potential and intracellular ion concentrations. *Prog. Biophys. Mol. Biol.* 94:336–372. https://doi.org/10.1016/j.pbiomolbio.2006.10.001

Fraser, J.A., C.L. Huang, and T.H. Pedersen. 2011. Relationships between resting conductances, excitability, and t-system ionic homeostasis in skeletal muscle. *J. Gen. Physiol.* 138:95–116. https://doi.org/10.1085/jgp.201110617

Fu, Y., A. Struyk, V. Markin, and S. Cannon. 2011. Gating behaviour of sodium currents in adult mouse muscle recorded with an improved two-electrode voltage clamp. *J. Physiol.* 589:525–546. https://doi.org/10.1113/jphysiol.2010.199430

Fucile, S. 2004. Ca2+ permeability of nicotinic acetylcholine receptors. *Cell Calcium.* 35:1–8. https://doi.org/10.1016/j.ceca.2003.08.006

García-Pelagio, K.P., R.J. Bloch, A. Ortega, and H. González-Serratos. 2011. Biomechanics of the sarcolemma and costameres in single skeletal muscle fibers from normal and dystrophin-null mice. *J. Muscle Res. Cell Motil.* 31:323–336. https://doi.org/10.1007/s10974-011-9238-9

Gee, S.H., R. Madhavan, S.R. Levinson, J.H. Caldwell, R. Sealock, and S.C. Froehner. 1998. Interaction of muscle and brain sodium channels with multiple members of the syntrophin family of dystrophin-associated proteins. *J. Neurosci.* 18:128–137. https://doi.org/10.1523/JNEUROSCI.18-01-00128.1998

Gerhalter, T., P.G. Carlier, and B. Marty. 2017. Acute changes in extracellular volume fraction in skeletal muscle monitored by ^{23}Na NMR spectroscopy. *Physiol. Rep.* 5:e13380. https://doi.org/10.14814/phy2.13380

Gerhalter, T., L.V. Gast, B. Marty, J. Martin, R. Trollmann, S. Schüssler, F. Roemer, F.B. Laun, M. Uder, R. Schröder, et al. 2019. ^{23} Na MRI depicts early changes in ion homeostasis in skeletal muscle tissue of patients with duchenne muscular dystrophy. *J. Magn. Reson. Imaging.* 50: 1103–1113. https://doi.org/10.1002/jmri.26681

Glemser, P.A., H. Jaeger, A.M. Nagel, A.E. Ziegler, D. Simons, H.P. Schlemmer, F. Lehmann-Horn, K. Jurkat-Rott, and M.A. Weber. 2017. ^{23}Na MRI and myometry to compare eplerenone vs. glucocorticoid treatment in Duchenne dystrophy. *Acta Myol.* 36:2–13.

Gnanasambandam, R., C. Ghatak, A. Yasmann, K. Nishizawa, F. Sachs, A.S. Ladokhin, S.I. Sukharev, and T.M. Suchyna. 2017. GsMTx4: mechanism of inhibiting mechanosensitive ion channels. *Biophys. J.* 112:31–45. https://doi.org/10.1016/j.bpj.2016.11.013

Habeck, M., E. Kapri-Pardes, M. Sharon, and S.J. Karlish. 2017. Specific phospholipid binding to Na,K-ATPase at two distinct sites. *Proc. Natl. Acad. Sci. USA.* 114:2904–2909. https://doi.org/10.1073/pnas.1620799114

Hagberg, H. 1985. Intracellular pH during ischemia in skeletal muscle: relationship to membrane potential, extracellular pH, tissue lactic acid and ATP. *Pflugers Arch.* 404:342–347. https://doi.org/10.1007/BF00585346

Hakimjavadi, H., C.A. Stiner, T.L. Radzyukevich, J.B. Lingrel, N. Norman, J.A. Landero Figueroa, and J.A. Heiny. 2018. K^+ and Rb^+ Affinities of the Na,K-ATPase α_1 and α_2 Isozymes: An application of ICP-MS for quantification of Na^+ pump kinetics in myofibers. *Int. J. Mol. Sci.* 19:E2725. https://doi.org/10.3390/ijms19092725

Hamada, K., H. Matsuura, M. Sanada, F. Toyoda, M. Omatsu-Kanbe, A. Kashiwagi, and H. Yasuda. 2003. Properties of the Na+/K+ pump current in small neurons from adult rat dorsal root ganglia. *Br. J. Pharmacol.* 138: 1517–1527. https://doi.org/10.1038/sj.bjp.0705170

Hammon, M., S. Grossmann, P. Linz, C. Kopp, A. Dahlmann, R. Janka, A. Cavallaro, M. Uder, and J. Titze. 2015. 3 Tesla (23)Na magnetic resonance imaging during aerobic and anaerobic exercise. *Acad. Radiol.* 22: 1181–1190. https://doi.org/10.1016/j.acra.2015.06.005

Han, J.J., G.T. Carter, J.J. Ra, R.T. Abresch, J.S. Chamberlain, and L.R. Robinson. 2006. Electromyographic studies in mdx and wild-type C57 mice. *Muscle Nerve.* 33:208–214. https://doi.org/10.1002/mus.20455

Harfmann, B.D., E.A. Schroder, and K.A. Esser. 2015. Circadian rhythms, the molecular clock, and skeletal muscle. *J. Biol. Rhythms.* 30:84–94. https://doi.org/10.1177/0748730414561638

Hartman, A.G., L. Terhorst, N. Little, and R.M. Bendixen. 2020. Uncovering sleep in young males with Duchenne muscular dystrophy. *Eur. J. Paediatr. Neurol.* 26:20–28. https://doi.org/10.1016/j.ejpn.2020.02.012

Heiny, J.A., V.V. Kravtsova, F. Mandel, T.L. Radzyukevich, B. Benziane, A.V. Prokofiev, S.E. Pedersen, A.V. Chibalin, and I.I. Krivoi. 2010. The nicotinic acetylcholine receptor and the Na,K-ATPase alpha2 isoform interact to regulate membrane electrogenesis in skeletal muscle. *J. Biol. Chem.* 285:28614–28626. https://doi.org/10.1074/jbc.M110.150961

Heiny, J.A., S.C. Cannon, and M. DiFranco. 2019. A four-electrode method to study dynamics of ion activity and transport in skeletal muscle fibers. *J. Gen. Physiol.* 151:1146–1155. https://doi.org/10.1085/jgp.201912398

Helfman, G., B. Collette, and D.E. Facey. 2009. The Diversity of Fishes: Biology, Evolution and Ecology. Second edition. Blackwell Science, Malden, MA. 48–49.

Hernández-Ochoa, E.O., S.J.P. Pratt, K.P. Garcia-Pelagio, M.F. Schneider, and R.M. Lovering. 2015. Disruption of action potential and calcium signaling properties in malformed myofibers from dystrophin-deficient mice. *Physiol. Rep.* 3:e12366. https://doi.org/10.14814/phy2.12366

Hille, B. 2001. Ion Channels of Excitable Membranes. Third edition. Sinauer Associates, Sunderland, MA.

Hirn, C., G. Shapovalov, O. Petermann, E. Roulet, and U.T. Ruegg. 2008. Nav1.4 deregulation in dystrophic skeletal muscle leads to Na+ overload and enhanced cell death. *J. Gen. Physiol.* 132:199–208. https://doi.org/10.1085/jgp.200810024

Hoffman, E.P., R.H. Brown Jr., and L.M. Kunkel. 1987. Dystrophin: the protein product of the Duchenne muscular dystrophy locus. *Cell.* 51:919–928. https://doi.org/10.1016/0092-8674(87)90579-4

Horvath, B., L. Berg, D.J. Cummings, and G.M. Shy. 1955. Muscular dystrophy: cation concentrations in residual muscle. *J. Appl. Physiol.* 8:22–30. https://doi.org/10.1152/jappl.1955.8.1.22

Hossain, K.R., and R.J. Clarke. 2019. General and specific interactions of the phospholipid bilayer with P-type ATPases. *Biophys. Rev.* 11:353–364. https://doi.org/10.1007/s12551-019-00533-2

Houang, E.M., Y.Y. Sham, F.S. Bates, and J.M. Metzger. 2018. Muscle membrane integrity in Duchenne muscular dystrophy: recent advances in copolymer-based muscle membrane stabilizers. *Skelet. Muscle.* 8:31. https://doi.org/10.1186/s13395-018-0177-7

Hübel, N., E. Schöll, and M.A. Dahlem. 2014. Bistable dynamics underlying excitability of ion homeostasis in neuron models. *PLOS Comput. Biol.* 10: e1003551. https://doi.org/10.1371/journal.pcbi.1003551

Ibraghimov-Beskrovnaya, O., J.M. Ervasti, C.J. Leveille, C.A. Slaughter, S.W. Sernett, and K.P. Campbell. 1992. Primary structure of dystrophin-associated glycoproteins linking dystrophin to the extracellular matrix. *Nature.* 355:696–702. https://doi.org/10.1038/355696a0

Imbrici, P., C. Altamura, M. Pessia, R. Mantegazza, J.F. Desaphy, and D.C. Camerino. 2015. ClC-1 chloride channels: state-of-the-art research and future challenges. *Front. Cell. Neurosci.* 9:156. https://doi.org/10.3389/fncel.2015.00156

Ishpekova, B., I. Milanov, L.G. Christova, and A.S. Alexandrov. 1999. Comparative analysis between Duchenne and Becker types muscular dystrophy. *Electromyogr. Clin. Neurophysiol.* 39:315–318.

Iwata, Y., Y. Katanosaka, T. Hisamitsu, and S. Wakabayashi. 2007. Enhanced Na+/H+ exchange activity contributes to the pathogenesis of muscular dystrophy via involvement of P2 receptors. *Am. J. Pathol.* 171:1576–1587. https://doi.org/10.2353/ajpath.2007.070452

Jackson, D.C. 2002. Hibernating without oxygen: physiological adaptations of the painted turtle. *J. Physiol.* 543:731–737. https://doi.org/10.1113/jphysiol.2002.024729

Jackson, M.B., K. Imoto, M. Mishina, T. Konno, S. Numa, and B. Sakmann. 1990. Spontaneous and agonist-induced openings of an acetylcholine receptor channel composed of bovine muscle alpha-, beta- and delta-subunits. *Pflugers Arch.* 417:129–135. https://doi.org/10.1007/BF00370689

Janssen, I., S.B. Heymsfield, Z.M. Wang, and R. Ross. 2000. Skeletal muscle mass and distribution in 468 men and women aged 18-88 yr. *J Appl Physiol (1985).* 89:81–88. https://doi.org/10.1152/jappl.2000.89.1.81

Jeng, C.J., S.J. Fu, C.Y. You, Y.J. Peng, C.T. Hsiao, T.Y. Chen, and C.Y. Tang. 2020. Defective gating and proteostasis of human ClC-1 chloride channel: molecular pathophysiology of myotonia congenita. *Front. Neurol.* 11:76. https://doi.org/10.3389/fneur.2020.00076

Jentsch, T.J., and M. Pusch. 2018. ClC chloride channels and transporters: structure, function, physiology, and disease. *Physiol. Rev.* 98:1493–1590. https://doi.org/10.1152/physrev.00047.2017

Johnston, I.A., N.I. Bower, and D.J. Macqueen. 2011. Growth and the regulation of myotomal muscle mass in teleost fish. *J. Exp. Biol.* 214:1617–1628. https://doi.org/10.1242/jeb.038620

Johnstone, A.J., and D. Ball. 2019. Determining ischaemic thresholds through our understanding of cellular metabolism. *In* Compartment Syndrome: A Guide to Diagnosis and Management. C. Mauffrey, D.J. Hak, and M.P. Martin III, editors. SpringerOpen. https://doi.org/10.1007/978-3-030-22331-1_4

Joos, B., B.M. Barlow, and C.E. Morris. 2017. Calculating the consequences of left-shifted Nav channel activity in sick excitable cells. In: Chahine M. (eds) Voltage-gated Sodium Channels: Structure, Function and Channelopathies. *In* Handbook of Experimental Pharmacology. Vol. 246. Springer, Cham. 401–422. doi: . https://doi.org/10.1007/164_2017_63

Kager, H., W.J. Wadman, and G.G. Somjen. 2000. Simulated seizures and spreading depression in a neuron model incorporating interstitial space and ion concentrations. *J. Neurophysiol.* 84:495–512. https://doi.org/10.1152/jn.2000.84.1.495

Kang, Y., J.X. Wu, and L. Chen. 2020. Structure of voltage-modulated sodium-selective NALCN-FAM155A channel complex. *Nat. Commun.* 11:6199. https://doi.org/10.1038/s41467-020-20002-9

Kay, A.R. 2017. How cells can control their size by pumping ions. *Front. Cell Dev. Biol.* 5:41. https://doi.org/10.3389/fcell.2017.00041

Khairallah, R.J., G. Shi, F. Sbrana, B.L. Prosser, C. Borroto, M.J. Mazaitis, E.P. Hoffman, A. Mahurkar, F. Sachs, Y. Sun, et al. 2012. Microtubules underlie dysfunction in duchenne muscular dystrophy. *Sci. Signal.* 5:ra56. https://doi.org/10.1126/scisignal.2002829

Kiss, T., I. Battonyai, and Z. Pirger. 2014. Down regulation of sodium channels in the central nervous system of hibernating snails. *Physiol. Behav.* 131: 93–98. https://doi.org/10.1016/j.physbeh.2014.04.026

Kravtsova, V.V., A.M. Petrov, V.V. Matchkov, E.V. Bouzinova, A.N. Vasiliev, B. Benziane, A.L. Zefirov, A.V. Chibalin, J.A. Heiny, and I.I. Krivoi. 2016. Distinct α2 Na,K-ATPase membrane pools are differently involved in early skeletal muscle remodeling during disuse. *J. Gen. Physiol.* 147: 175–188. https://doi.org/10.1085/jgp.201511494

Kravtsova, V.V., E.V. Bouzinova, A.V. Chibalin, V.V. Matchkov, and I.I. Krivoi. 2020. Isoform-specific Na,K-ATPase and membrane cholesterol remodeling in motor endplates in distinct mouse models of myodystrophy. *Am. J. Physiol. Cell Physiol.* 318:C1030–C1041. https://doi.org/10.1152/ajpcell.00453.2019

Kristensen, M., and C. Juel. 2010. Potassium-transporting proteins in skeletal muscle: cellular location and fibre-type differences. *Acta Physiol. (Oxf.).* 198:105–123. https://doi.org/10.1111/j.1748-1716.2009.02043.x

Landfeldt, E., R. Thompson, T. Sejersen, H.J. McMillan, J. Kirschner, and H. Lochmüller. 2020. Life expectancy at birth in Duchenne muscular dystrophy: a systematic review and meta-analysis. *Eur. J. Epidemiol.* 35: 643–653. https://doi.org/10.1007/s10654-020-00613-8

Lansman, J.B. 2015. Utrophin suppresses low frequency oscillations and coupled gating of mechanosensitive ion channels in dystrophic skeletal muscle. *Channels (Austin).* 9:145–160. https://doi.org/10.1080/19336950.2015.1040211

Le, S., M. Yu, L. Hovan, Z. Zhao, J. Ervasti, and J. Yan. 2018. Dystrophin as a molecular shock absorber. *ACS Nano.* 12:12140–12148. https://doi.org/10.1021/acsnano.8b05721

Leermakers, P.A., K.L.T. Dybdahl, K.S. Husted, A. Riisager, F.V. de Paoli, T. Pinós, J. Vissing, T.O.B. Krag, and T.H. Pedersen. 2020. Depletion of

ATP limits membrane excitability of skeletal muscle by increasing both ClC1-open probability and membrane conductance. *Front. Neurol.* 11:541. https://doi.org/10.3389/fneur.2020.00541

Lehmann-Horn, F., M.A. Weber, A.M. Nagel, H.M. Meinck, S. Breitenbach, J. Scharrer, and K. Jurkat-Rott. 2012. Rationale for treating oedema in Duchenne muscular dystrophy with eplerenone. *Acta Myol.* 31:31–39.

Li, R.W., Y. Deng, H.N. Pham, S. Weiss, M. Chen, and P.N. Smith. 2020. Riluzole protects against skeletal muscle ischaemia-reperfusion injury in a porcine model. *Injury.* 51:178–184. https://doi.org/10.1016/j.injury.2019.12.030

Lindinger, M.I., M. Leung, K.E. Trajcevski, and T.J. Hawke. 2011. Volume regulation in mammalian skeletal muscle: the role of sodium-potassium-chloride cotransporters during exposure to hypertonic solutions. *J. Physiol.* 589:2887–2899. https://doi.org/10.1113/jphysiol.2011.206730

Lorusso, S., D. Kline, A. Bartlett, M. Freimer, J. Agriesti, A.A. Hawash, M.M. Rich, J.T. Kissel, and W. David Arnold. 2019. Open-label trial of ranolazine for the treatment of paramyotonia congenita. *Muscle Nerve.* 59: 240–243. https://doi.org/10.1002/mus.26372

Lu, B., Y. Su, S. Das, J. Liu, J. Xia, and D. Ren. 2007. The neuronal channel NALCN contributes resting sodium permeability and is required for normal respiratory rhythm. *Cell.* 129:371–383. https://doi.org/10.1016/j.cell.2007.02.041

Lukacs, P., M.C. Földi, L. Valánszki, E. Casanova, B. Biri-Kovács, L. Nyitray, A. Málnási-Csizmadia, and A. Mike. 2018. Non-blocking modulation contributes to sodium channel inhibition by a covalently attached photoreactive riluzole analog. *Sci. Rep.* 8:8110. https://doi.org/10.1038/s41598-018-26444-y

Lundbaek, J.A., R.E. Koeppe II, and O.S. Andersen. 2010. Amphiphile regulation of ion channel function by changes in the bilayer spring constant. *Proc. Natl. Acad. Sci. USA.* 107:15427–15430. https://doi.org/10.1073/pnas.1007455107

Lutas, A., C. Lahmann, M. Soumillon, and G. Yellen. 2016. The leak channel NALCN controls tonic firing and glycolytic sensitivity of substantia nigra pars reticulata neurons. *eLife.* 5:e15271. https://doi.org/10.7554/eLife.15271

MacDonald, D.R.W., D.W. Neilly, K.E. Elliott, and A.J. Johnstone. 2021. Real time measurement of intramuscular pH during routine knee arthroscopy using a tourniquet: a preliminary study. *Bone Joint Res.* 10:363–369. https://doi.org/10.1302/2046-3758.106.BJR-2020-0469.R1

MacKintosh, E.W., M.L. Chen, and J.O. Benditt. 2020. Lifetime care of Duchenne muscular dystrophy. *Sleep Med. Clin.* 15:485–495. https://doi.org/10.1016/j.jsmc.2020.08.011

Mankodi, A., N. Azzabou, T. Bulea, H. Reyngoudt, H. Shimellis, Y. Ren, E. Kim, K.H. Fischbeck, and P.G. Carlier. 2017. Skeletal muscle water T_2 as a biomarker of disease status and exercise effects in patients with Duchenne muscular dystrophy. *Neuromuscul. Disord.* 27:705–714. https://doi.org/10.1016/j.nmd.2017.04.008

Mantilla, C.B., R.V. Sill, B. Aravamudan, W.Z. Zhan, and G.C. Sieck. 2008. Developmental effects on myonuclear domain size of rat diaphragm fibers. *J Appl Physiol (1985).* 104:787–794. https://doi.org/10.1152/japplphysiol.00347.2007

Mareedu, S., E.D. Million, D. Duan, and G.J. Babu. 2021. Abnormal calcium handling in Duchenne muscular dystrophy: mechanisms and potential therapies. *Front. Physiol.* 12:647010. https://doi.org/10.3389/fphys.2021.647010

Mathes, C., F. Bezanilla, and R.E. Weiss. 1991. Sodium current and membrane potential in EDL muscle fibers from normal and dystrophic (*mdx*) mice. *Am. J. Physiol.* 261:C718–C725. https://doi.org/10.1152/ajpcell.1991.261.4.C718

McBride, T.A., B.W. Stockert, F.A. Gorin, and R.C. Carlsen. 2000. Stretch-activated ion channels contribute to membrane depolarization after eccentric contractions. *J Appl Physiol (1985).* 88:91–101. https://doi.org/10.1152/jappl.2000.88.1.91

McNeil, P.L., and R.A. Steinhardt. 2003. Plasma membrane disruption: repair, prevention, adaptation. *Annu. Rev. Cell Dev. Biol.* 19:697–731. https://doi.org/10.1146/annurev.cellbio.19.111301.140101

Mehta, A.R., C.L. Huang, J.N. Skepper, and J.A. Fraser. 2008. Extracellular charge adsorption influences intracellular electrochemical homeostasis in amphibian skeletal muscle. *Biophys. J.* 94:4549–4560. https://doi.org/10.1529/biophysj.107.128587

Meng, J., N.P. Sweeney, B. Doreste, F. Muntoni, M. McClure, and J. Morgan. 2020. Restoration of functional full-length dystrophin after intramuscular transplantation of foamy virus-transduced myoblasts. *Hum. Gene Ther.* 31:241–252. https://doi.org/10.1089/hum.2019.224

Menke, A., and H. Jockusch. 1991. Decreased osmotic stability of dystrophin-less muscle cells from the *mdx* mouse. *Nature.* 349:69–71. https://doi.org/10.1038/349069a0

Menke, A., and H. Jockusch. 1995. Extent of shock-induced membrane leakage in human and mouse myotubes depends on dystrophin. *J. Cell Sci.* 108:727–733. https://doi.org/10.1242/jcs.108.2.727

Methfessel, C., V. Witzemann, T. Takahashi, M. Mishina, S. Numa, and B. Sakmann. 1986. Patch clamp measurements on Xenopus laevis oocytes: currents through endogenous channels and implanted acetylcholine receptor and sodium channels. *Pflugers Arch.* 407:577–588. https://doi.org/10.1007/BF00582635

Metzger, S., C. Dupont, A.A. Voss, and M.M. Rich. 2020. Central role of subthreshold currents in myotonia. *Ann. Neurol.* 87:175–183. https://doi.org/10.1002/ana.25646

Miles, M.T., E. Cottey, A. Cottey, C. Stefanski, and C.G. Carlson. 2011. Reduced resting potentials in dystrophic (mdx) muscle fibers are secondary to NF-κB-dependent negative modulation of ouabain sensitive Na+-K+ pump activity. *J. Neurol. Sci.* 303:53–60. https://doi.org/10.1016/j.jns.2011.01.015

Mink, J.W., R.J. Blumenschine, and D.B. Adams. 1981. Ratio of central nervous system to body metabolism in vertebrates: its constancy and functional basis. *Am. J. Physiol.* 241:R203–R212. https://doi.org/10.1152/ajpregu.1981.241.3.R203

Moore, T.M., A.J. Lin, A.R. Strumwasser, K. Cory, K. Whitney, T. Ho, T. Ho, J.L. Lee, D.H. Rucker, C.Q. Nguyen, et al. 2020. Mitochondrial Dysfunction is an early consequence of partial or complete dystrophin loss in mdx mice. *Front. Physiol.* 11:690. https://doi.org/10.3389/fphys.2020.00690

Morris, C.E. 2012. Why are so many channels mechanosensitive? *In* Cell Physiology Source Book. Fourth edition. N. Sperelakis, editor. Elsevier, Amsterdam. 493–505. https://doi.org/10.1016/B978-0-12-387738-3.00027-5

Morris, C.E. 2018. Cytotoxic swelling of sick excitable cells - impaired ion homeostasis and membrane tension homeostasis in muscle and neuron. *Curr. Top. Membr.* 81:457–496. https://doi.org/10.1016/bs.ctm.2018.06.001

Morris, C.E., and R. Horn. 1991. Failure to elicit neuronal macroscopic mechanosensitive currents anticipated by single-channel studies. *Science.* 251:1246–1249. https://doi.org/10.1126/science.1706535

Morris, C.E., and B. Joos. 2016. Nav channels in damaged membranes. *Curr. Top. Membr.* 78:561–597. https://doi.org/10.1016/bs.ctm.2016.06.001

Morris, C.E., P.F. Juranka, W. Lin, T.J. Morris, and U. Laitko. 2006. Studying the mechanosensitivity of voltage-gated channels using oocyte patches. *Methods Mol. Biol.* 322:315–329. https://doi.org/10.1007/978-1-59745-000-3_22

Morris, C.E., P.A. Boucher, and B. Joós. 2012a. Left-shifted nav channels in injured bilayer: primary targets for neuroprotective nav antagonists? *Front. Pharmacol.* 3:19. https://doi.org/10.3389/fphar.2012.00019

Morris, C.E., P.F. Juranka, and B. Joós. 2012b. Perturbed voltage-gated channel activity in perturbed bilayers: implications for ectopic arrhythmias arising from damaged membrane. *Prog. Biophys. Mol. Biol.* 110:245–256. https://doi.org/10.1016/j.pbiomolbio.2012.07.003

Murphy, S., M. Zweyer, M. Henry, P. Meleady, R.R. Mundegar, D. Swandulla, and K. Ohlendieck. 2019. Proteomic analysis of the sarcolemma-enriched fraction from dystrophic mdx-4cv skeletal muscle. *J. Proteomics.* 191:212–227. https://doi.org/10.1016/j.jprot.2018.01.015

Nielsen, O.B., and T. Clausen. 1997. Regulation of Na(+)-K+ pump activity in contracting rat muscle. *J. Physiol.* 503:571–581. https://doi.org/10.1111/j.1469-7793.1997.571bg.x

Nojszewska, M., M. Gawel, E. Szmidt-Salkowska, A. Kostera-Pruszczyk, A. Potulska-Chromik, A. Lusakowska, B. Kierdaszuk, M. Lipowska, A. Macias, D. Gawel, et al. 2017. Abnormal spontaneous activity in primary myopathic disorders. *Muscle Nerve.* 56:427–432. https://doi.org/10.1002/mus.25521

Novak, K.R., J. Norman, J.R. Mitchell, M.J. Pinter, and M.M. Rich. 2015. Sodium channel slow inactivation as a therapeutic target for myotonia congenita. *Ann. Neurol.* 77:320–332. https://doi.org/10.1002/ana.24331

Nozoe, K.T., G.A. Moreira, J.R. Tolino, M. Pradella-Hallinan, S. Tufik, and M.L. Andersen. 2015. The sleep characteristics in symptomatic patients with Duchenne muscular dystrophy. *Sleep Breath.* 19:1051–1056. https://doi.org/10.1007/s11325-014-1103-9

Pan, N.C., J.J. Ma, and H.B. Peng. 2012. Mechanosensitivity of nicotinic receptors. *Pflugers Arch.* 464:193–203. https://doi.org/10.1007/s00424-012-1132-9

Patel, A., J. Zhao, Y. Yue, K. Zhang, D. Duan, and Y. Lai. 2018. Dystrophin R16/17-syntrophin PDZ fusion protein restores sarcolemmal nNOSμ. *Skelet. Muscle.* 8:36. https://doi.org/10.1186/s13395-018-0182-x

Pedersen, T.H., F.V. de Paoli, J.A. Flatman, and O.B. Nielsen. 2009. Regulation of ClC-1 and KATP channels in action potential-firing fast-twitch

muscle fibers. *J. Gen. Physiol.* 134:309–322. https://doi.org/10.1085/jgp.200910290

Pedersen, T.H., A. Riisager, F.V. de Paoli, T.Y. Chen, and O.B. Nielsen. 2016. Role of physiological ClC-1 Cl- ion channel regulation for the excitability and function of working skeletal muscle. *J. Gen. Physiol.* 147:291–308. https://doi.org/10.1085/jgp.201611582

Pennati, F., F. Arrigoni, A. LoMauro, S. Gandossini, A. Russo, M.G. D'Angelo, and A. Aliverti. 2020. Diaphragm involvement in Duchenne muscular dystrophy (DMD): an MRI study. *J. Magn. Reson. Imaging.* 51:461–471. https://doi.org/10.1002/jmri.26864

Petrof, B.J., J.B. Shrager, H.H. Stedman, A.M. Kelly, and H.L. Sweeney. 1993. Dystrophin protects the sarcolemma from stresses developed during muscle contraction. *Proc. Natl. Acad. Sci. USA.* 90:3710–3714. https://doi.org/10.1073/pnas.90.8.3710

Petrov, A.M., V.V. Kravtsova, V.V. Matchkov, A.N. Vasiliev, A.L. Zefirov, A.V. Chibalin, J.A. Heiny, and I.I. Krivoi. 2017. Membrane lipid rafts are disturbed in the response of rat skeletal muscle to short-term disuse. *Am. J. Physiol. Cell Physiol.* 312:C627–C637. https://doi.org/10.1152/ajpcell.00365.2016

Philippart, F., and Z.M. Khaliq. 2018. $G_{i/o}$ protein-coupled receptors in dopamine neurons inhibit the sodium leak channel NALCN. *eLife.* 7: e40984. https://doi.org/10.7554/eLife.40984

Podkalicka, P., O. Mucha, J. Dulak, and A. Loboda. 2019. Targeting angiogenesis in Duchenne muscular dystrophy. *Cell. Mol. Life Sci.* 76: 1507–1528. https://doi.org/10.1007/s00018-019-03006-7

Pratt, S.J.P., S.B. Shah, C.W. Ward, J.P. Kerr, J.P. Stains, and R.M. Lovering. 2015. Recovery of altered neuromuscular junction morphology and muscle function in mdx mice after injury. *Cell. Mol. Life Sci.* 72:153–164. https://doi.org/10.1007/s00018-014-1663-7

Raman, S.V., K.N. Hor, W. Mazur, X. He, J.T. Kissel, S. Smart, B. McCarthy, S.L. Roble, and L.H. Cripe. 2017. Eplerenone for early cardiomyopathy in Duchenne muscular dystrophy: results of a two-year open-label extension trial. *Orphanet J. Rare Dis.* 12:39. https://doi.org/10.1186/s13023-017-0590-8

Ramos, S.V., M.C. Hughes, L.J. Delfinis, C.A. Bellissimo, and C.G.R. Perry. 2020. Mitochondrial bioenergetic dysfunction in the D2.mdx model of Duchenne muscular dystrophy is associated with microtubule disorganization in skeletal muscle. *PLoS One.* 15:e0237138. https://doi.org/10.1371/journal.pone.0237138

Rebolledo, D.L., M.J. Kim, N.P. Whitehead, M.E. Adams, and S.C. Froehner. 2016. Sarcolemmal targeting of nNOSμ improves contractile function of *mdx* muscle. *Hum. Mol. Genet.* 25:158–166. https://doi.org/10.1093/hmg/ddv466

Reinl, E.L., P. Zhao, W. Wu, X. Ma, C. Amazu, R. Bok, K.J. Hurt, Y. Wang, and S.K. England. 2018. Na^+-Leak Channel, Non-Selective (NALCN) regulates myometrial excitability and facilitates successful parturition. *Cell. Physiol. Biochem.* 48:503–515. https://doi.org/10.1159/000491805

Ribaux, P., F. Bleicher, M.L. Couble, J. Amsellem, S.A. Cohen, C. Berthier, and S. Blaineau. 2001. Voltage-gated sodium channel (SkM1) content in dystrophin-deficient muscle. *Pflugers Arch.* 441:746–755. https://doi.org/10.1007/s004240000483

Rolfe, D.F., and G.C. Brown. 1997. Cellular energy utilization and molecular origin of standard metabolic rate in mammals. *Physiol. Rev.* 77:731–758. https://doi.org/10.1152/physrev.1997.77.3.731

Rongen, G.A., J.P. van Dijk, E.E. van Ginneken, D.F. Stegeman, P. Smits, and M.J. Zwarts. 2002. Repeated ischaemic isometric exercise increases muscle fibre conduction velocity in humans: involvement of Na(+)-K(+)-ATPase. *J. Physiol.* 540:1071–1078. https://doi.org/10.1113/jphysiol.2001.014290

Rudman, D., S.B. Chyatte, J.H. Patterson, G.G. Gerron, I. O'Beirne, J. Barlow, A. Jordan, and J.S. Shavin. 1972. Metabolic effects of human growth hormone and of estrogens in boys with Duchenne muscular dystrophy. *J. Clin. Invest.* 51:1118–1124. https://doi.org/10.1172/JCI106904

Ruff, R.L. 2011. Endplate contributions to the safety factor for neuromuscular transmission. *Muscle Nerve.* 44:854–861. https://doi.org/10.1002/mus.22177

Rungta, R.L., H.B. Choi, J.R. Tyson, A. Malik, L. Dissing-Olesen, P.J.C. Lin, S.M. Cain, P.R. Cullis, T.P. Snutch, and B.A. MacVicar. 2015. The cellular mechanisms of neuronal swelling underlying cytotoxic edema. *Cell.* 161: 610–621. https://doi.org/10.1016/j.cell.2015.03.029

Ryder-Cook, A.S., P. Sicinski, K. Thomas, K.E. Davies, R.G. Worton, E.A. Barnard, M.G. Darlison, and P.J. Barnard. 1988. Localization of the *mdx* mutation within the mouse dystrophin gene. *EMBO J.* 7:3017–3021. https://doi.org/10.1002/j.1460-2075.1988.tb03165.x

Sander, M., B. Chavoshan, S.A. Harris, S.T. Iannaccone, J.T. Stull, G.D. Thomas, and R.G. Victor. 2000. Functional muscle ischemia in neuronal nitric oxide synthase-deficient skeletal muscle of children with Duchenne muscular dystrophy. *Proc. Natl. Acad. Sci. USA.* 97:13818–13823. https://doi.org/10.1073/pnas.250379497

Saxena, A., M. St Louis, and M. Fournier. 2013. Vibration and pressure wave therapy for calf strains: a proposed treatment. *Muscles Ligaments Tendons J.* 3:60–62. https://doi.org/10.32098/mltj.02.2013.02

Schmucker, R.W., S.D. Mendenhall, J.D. Reichensperger, M. Yang, and M.W. Neumeister. 2015. Defining the salvage time window for the use of ischemic postconditioning in skeletal muscle ischemia reperfusion injury. *J. Reconstr. Microsurg.* 31:597–606. https://doi.org/10.1055/s-0035-1556066

Scott, K., M. Benkhalti, N.D. Calvert, M. Paquette, L. Zhen, M.E. Harper, O.Y. Al-Dirbashi, and J.M. Renaud. 2016. KATP channel deficiency in mouse FDB causes an impairment of energy metabolism during fatigue. *Am. J. Physiol. Cell Physiol.* 311:C559–C571. https://doi.org/10.1152/ajpcell.00137.2015

Sejersted, O.M., and G. Sjøgaard. 2000. Dynamics and consequences of potassium shifts in skeletal muscle and heart during exercise. *Physiol. Rev.* 80:1411–1481. https://doi.org/10.1152/physrev.2000.80.4.1411

Sheetz, M.P., J.E. Sable, and H.G. Döbereiner. 2006. Continuous membrane-cytoskeleton adhesion requires continuous accommodation to lipid and cytoskeleton dynamics. *Annu. Rev. Biophys. Biomol. Struct.* 35:417–434. https://doi.org/10.1146/annurev.biophys.35.040405.102017

Sherlock, S.P., Y. Zhang, M. Binks, and S. Marraffino. 2021. Quantitative muscle MRI biomarkers in Duchenne muscular dystrophy: cross-sectional correlations with age and functional tests. *Biomarkers Med.* 15:761–773. https://doi.org/10.2217/bmm-2020-0801

Shibuya, S., H. Hara, Y. Wakayama, M. Inoue, T. Jimi, and Y. Matsuzaki. 2008. Aquaporin 4 mRNA levels in neuromuscular tissues of wild-type and dystrophin-deficient mice. *Tohoku J. Exp. Med.* 215:313–319. https://doi.org/10.1620/tjem.215.313

Siegel, I.M. 1992. Compartmental syndrome in Duchenne muscular dystrophy: early evaluation of an epiphenomenon leading to wasting, weakness and contracture. *Med. Hypotheses.* 38:339–345. https://doi.org/10.1016/0306-9877(92)90029-C

Sim, J., and J.A. Fraser. 2014. The determinants of transverse tubular volume in resting skeletal muscle. *J. Physiol.* 592:5477–5492. https://doi.org/10.1113/jphysiol.2014.281170

Sinha, B., D. Köster, R. Ruez, P. Gonnord, M. Bastiani, D. Abankwa, R.V. Stan, G. Butler-Browne, B. Vedie, L. Johannes, et al. 2011. Cells respond to mechanical stress by rapid disassembly of caveolae. *Cell.* 144:402–413. https://doi.org/10.1016/j.cell.2010.12.031

Sjøgaard, G., R.P. Adams, and B. Saltin. 1985. Water and ion shifts in skeletal muscle of humans with intense dynamic knee extension. *Am. J. Physiol.* 248:R190–R196. https://doi.org/10.1152/ajpregu.1985.248.2.R190

Skov, M., F.V. de Paoli, O.B. Nielsen, and T.H. Pedersen. 2017. The anticonvulsants lacosamide, lamotrigine, and rufinamide reduce myotonia in isolated human and rat skeletal muscle. *Muscle Nerve.* 56:136–142. https://doi.org/10.1002/mus.25452

Sperelakis, N. 2012. Origin of resting membrane potentials. *In* Cell Physiology Source Book. Fourth edition. N. Sperelakis, editor. Elsevier, Amsterdam. 121–145. https://doi.org/10.1016/B978-0-12-387738-3.00009-3

Sreetama, S.C., G. Chandra, J.H. Van der Meulen, M.M. Ahmad, P. Suzuki, S. Bhuvanendran, K. Nagaraju, E.P. Hoffman, and J.K. Jaiswal. 2018. Membrane stabilization by modified steroid offers a potential therapy for muscular dystrophy due to dysferlin deficit. *Mol. Ther.* 26: 2231–2242. https://doi.org/10.1016/j.ymthe.2018.07.021

Stoughton, W.B., J. Li, C. Balog-Alvarez, and J.N. Kornegay. 2018. Impaired autophagy correlates with golden retriever muscular dystrophy phenotype. *Muscle Nerve.* 58:418–426. https://doi.org/10.1002/mus.26121

Tatman, L.M., W.J. Upchurch, N. Scholz, E. Wagstrom, L.L. Smith, J.E. Bechtold, A.H. Schmidt, and P.A. Iaizzo. 2020. Compartment Syndrome: evaluation of skeletal muscle ischemia and physiologic biomarkers in controlled conditions within ex vivo Isolated muscle bundles. *J. Orthop. Trauma.* 34:518–523. https://doi.org/10.1097/BOT.0000000000001799

Thomas, G.D. 2013. Functional muscle ischemia in Duchenne and Becker muscular dystrophy. *Front. Physiol.* 4:381. https://doi.org/10.3389/fphys.2013.00381

Thomassen, M., M. Hostrup, R.M. Murphy, B.A. Cromer, C. Skovgaard, T.P. Gunnarsson, P.M. Christensen, and J. Bangsbo. 2018. Abundance of ClC-1 chloride channel in human skeletal muscle: fiber type specific differences and effect of training. *J Appl Physiol (1985).* 125:470–478. https://doi.org/10.1152/japplphysiol.01042.2017

Timpani, C.A., A. Hayes, and E. Rybalka. 2015. Revisiting the dystrophin-ATP connection: How half a century of research still implicates

mitochondrial dysfunction in Duchenne Muscular Dystrophy aetiology. *Med. Hypotheses.* 85:1021–1033. https://doi.org/10.1016/j.mehy.2015.08.015

Trontelj, J., and E. Stålberg. 1983. Bizarre repetitive discharges recorded with single fibre EMG. *J. Neurol. Neurosurg. Psychiatry.* 46:310–316. https://doi.org/10.1136/jnnp.46.4.310

Usher-Smith, J.A., C.L. Huang, and J.A. Fraser. 2009. Control of cell volume in skeletal muscle. *Biol. Rev. Camb. Philos. Soc.* 84:143–159. https://doi.org/10.1111/j.1469-185X.2008.00066.x

van Moorsel, D., J. Hansen, B. Havekes, F.A.J.L. Scheer, J.A. Jörgensen, J. Hoeks, V.B. Schrauwen-Hinderling, H. Duez, P. Lefebvre, N.C. Schaper, et al. 2016. Demonstration of a day-night rhythm in human skeletal muscle oxidative capacity. *Mol. Metab.* 5:635–645. https://doi.org/10.1016/j.molmet.2016.06.012

Verhaart, I.E.C., and A. Aartsma-Rus. 2019. Therapeutic developments for Duchenne muscular dystrophy. *Nat. Rev. Neurol.* 15:373–386. https://doi.org/10.1038/s41582-019-0203-3

Verma, M., Y. Shimizu-Motohashi, Y. Asakura, J.P. Ennen, J. Bosco, Z. Zhou, G.H. Fong, S. Josiah, D. Keefe, and A. Asakura. 2019. Inhibition of FLT1 ameliorates muscular dystrophy phenotype by increased vasculature in a mouse model of Duchenne muscular dystrophy. *PLoS Genet.* 15: e1008468. https://doi.org/10.1371/journal.pgen.1008468

Wagner, K.R., N.L. Kuntz, E. Koenig, L. East, S. Upadhyay, B. Han, and P.B. Shieh. 2021. Safety, tolerability, and pharmacokinetics of casimersen in patients with Duchenne muscular dystrophy amenable to exon 45 skipping: A randomized, double-blind, placebo-controlled, dose-titration trial. *Muscle Nerve.* 64:285–292. https://doi.org/10.1002/mus.27347

Wallinga, W., S.L. Meijer, M.J. Alberink, M. Vliek, E.D. Wienk, and D.L. Ypey. 1999. Modelling action potentials and membrane currents of mammalian skeletal muscle fibres in coherence with potassium concentration changes in the T-tubular system. *Eur. Biophys. J.* 28:317–329. https://doi.org/10.1007/s002490050214

Wan, X., P. Juranka, and C.E. Morris. 1999. Activation of mechanosensitive currents in traumatized membrane. *Am. J. Physiol.* 276:C318–C327. https://doi.org/10.1152/ajpcell.1999.276.2.C318

Wang, X., K.L. Engisch, Y. Li, M.J. Pinter, T.C. Cope, and M.M. Rich. 2004. Decreased synaptic activity shifts the calcium dependence of release at the mammalian neuromuscular junction in vivo. *J. Neurosci.* 24: 10687–10692. https://doi.org/10.1523/JNEUROSCI.2755-04.2004

Wang, J.A., W. Lin, T. Morris, U. Banderali, P.F. Juranka, and C.E. Morris. 2009. Membrane trauma and Na+ leak from Nav1.6 channels. *Am. J. Physiol. Cell Physiol.* 297:C823–C834. https://doi.org/10.1152/ajpcell.00505.2008

Ward, C.W., F. Sachs, E.D. Bush, and T.M. Suchyna. 2018. GsMTx4-D provides protection to the D2.*mdx* mouse. *Neuromuscul. Disord.* 28:868–877. https://doi.org/10.1016/j.nmd.2018.07.005

Webb, J., F.F. Wu, and S.C. Cannon. 2009. Slow inactivation of the NaV1.4 sodium channel in mammalian cells is impeded by co-expression of the beta1 subunit. *Pflugers Arch.* 457:1253–1263. https://doi.org/10.1007/s00424-008-0600-8

Weber, M.A., A.M. Nagel, K. Jurkat-Rott, and F. Lehmann-Horn. 2011. Sodium (^{23}Na) MRI detects elevated muscular sodium concentration in Duchenne muscular dystrophy. *Neurology.* 77:2017–2024. https://doi.org/10.1212/WNL.0b013e31823b9c78

Weber, M.A., A.M. Nagel, M.B. Wolf, K. Jurkat-Rott, H.U. Kauczor, W. Semmler, and F. Lehmann-Horn. 2012. Permanent muscular sodium overload and persistent muscle edema in Duchenne muscular dystrophy: a possible contributor of progressive muscle degeneration. *J. Neurol.* 259:2385–2392. https://doi.org/10.1007/s00415-012-6512-8

White, Z., C.H. Hakim, M. Theret, N.N. Yang, F. Rossi, D. Cox, G.A. Francis, V. Straub, K. Selby, C. Panagiotopoulos, et al. 2020. High prevalence of plasma lipid abnormalities in human and canine Duchenne and Becker muscular dystrophies depicts a new type of primary genetic dyslipidemia. *J. Clin. Lipidol.* 14:459–469.e0. https://doi.org/10.1016/j.jacl.2020.05.098

Whitehead, N.P., E.W. Yeung, S.C. Froehner, and D.G. Allen. 2010. Skeletal muscle NADPH oxidase is increased and triggers stretch-induced damage in the *mdx* mouse. *PLoS One.* 5:e15354. https://doi.org/10.1371/journal.pone.0015354

Williams, M.W., and R.J. Bloch. 1999. Extensive but coordinated reorganization of the membrane skeleton in myofibers of dystrophic (mdx) mice. *J. Cell Biol.* 144:1259–1270. https://doi.org/10.1083/jcb.144.6.1259

Yeung, E.W., H.J. Ballard, J.P. Bourreau, and D.G. Allen. 2003. Intracellular sodium in mammalian muscle fibers after eccentric contractions. *J Appl Physiol (1985).* 94:2475–2482. https://doi.org/10.1152/japplphysiol.01128.2002

Yeung, E.W., N.P. Whitehead, T.M. Suchyna, P.A. Gottlieb, F. Sachs, and D.G. Allen. 2005. Effects of stretch-activated channel blockers on $[Ca^{2+}]_i$ and muscle damage in the mdx mouse. *J. Physiol.* 562:367–380. https://doi.org/10.1113/jphysiol.2004.075275

Yu, N., C.E. Morris, B. Joós, and A. Longtin. 2012. Spontaneous excitation patterns computed for axons with injury-like impairments of sodium channels and Na/K pumps. *PLOS Comput. Biol.* 8:e1002664. https://doi.org/10.1371/journal.pcbi.1002664

Zhang, B., C. Wang, H. Wang, H. Kong, F. Gao, M. Yang, and J. Zhang. 2020. Feasibility of MRI based oxygenation imaging for the assessment of acute limb ischemia. *Ann. Transl. Med.* 8:315. https://doi.org/10.21037/atm.2020.02.139

Zubrzycka-Gaarn, E.E., D.E. Bulman, G. Karpati, A.H. Burghes, B. Belfall, H.J. Klamut, J. Talbot, R.S. Hodges, P.N. Ray, and R.G. Worton. 1988. The Duchenne muscular dystrophy gene product is localized in sarcolemma of human skeletal muscle. *Nature.* 333:466–469. https://doi.org/10.1038/333466a0

Supplemental material

Shortcomings of SM-CD as is, simplifying choices, and upgrades

Flux models

In SM-CD, fluxes via P_K, P_{Na}, and P_{Cl} are given solely as GHK electrodiffusion (see I-V plots at left, Fig. 14 and Fig. 4 C) through always-open (i.e., non-gated) channels. In reality, the P_K of SMF combines strongly and weakly inwardly rectifying K^+ channels (Fig. 14 B) plus Ca^+-activated K^+ channels and possibly others (Wallinga et al., 1999; Pedersen et al., 2009; Kristensen and Juel, 2010; DiFranco et al., 2015). DiFranco et al. (2015) emphasize that in t-tubules (Fig. 14 G), strong inward rectifiers are ideally suited for rapidly recapturing potassium ions from the tubule lumen in connection with repetitive stimulation under physiological conditions. However, even though this (i.e., propagating APs and K^+ accumulation in excitable t-tubules) is precisely the issue addressed by Fraser et al. (2011) (a CD-modeling plus experiments paper), they use non-gated electrodiffusion to depict P_K in their model. Nor do they furnish P_{Cl} with ClC-1 gating features (e.g., Fig. 14 E). Fraser et al. (2011) do not discuss these points, but good agreement is achieved agreement between their (surface-measured) and computed APs (influenced by the modeled t-tubular K^+ accumulation and ion homeostatic recovery). Even in that demanding context (tiny extracellular volume, repetitive firing), the combined flux/gating characteristics of SMFs' K^+ and Cl^- permeabilities seem to be mimicked acceptably well by simple GHK fluxes. The same is true for subsequent work (Sim and Fraser, 2014) addressing the determinants of t-tubular volume (over minutes to hours) as parameter values are varied.

ATP, P_{H2O}, Donnan effectors (impermeant anions)

SM-CD assumes (see Fraser and Huang, 2004; Fraser et al., 2011; Dijkstra et al., 2016) that cytoplasmic ATP is available ad libitum; ↓ATP supply would be represented as ↓pump strength. Also like those other models, SM-CD has a large P_{H2O} that makes osmotic equilibration instantaneously track net $[Cl^- + Na^+]$ flux (starting at any net Na^+ influx, as shown at the H_2O blips in Fig. S1). Note how, late during the Fig. 8 SM*-CD trajectory (where E_{Na} has reached 0 mV), it becomes net Cl^- influx through [big P_{Cl}] that sets the (slow) swelling rate. SMFs express aquaporin 4; in *mdx* SMFs, aquaporin 4 mRNA is at abnormally low levels (Shibuya et al., 2008). Whether P_{H2O} falls enough to be rate limiting during osmotic Na^+ loading is, however, unknown. In SM-CD, the impermeant anion quantity (N_{Ai}) and their average valence is invariant; this is not plausible in vivo, but how (and how tightly) SMFs regulate their N_{Ai} and its average valence is unknown. Fraser and Huang (2004) address some consequences of having these values vary in, say, working or growing fibers.

External milieu

SM-CD's external milieu is fixed (mimicking a large experimental bath volume, a finite volume over short time, or a finite volume continually replenished by vascular exchanges). Thus, SM-CD experiences no K^+-accumulation–induced depolarization, and its $3Na^+/2K^+$-ATPase is not stimulated via the external K^+ binding site. A small finite extracellular volume would be required to computationally examine the suggestion (Hille, 2001) that SMF K^+ fluxes through inwardly rectifying K^+ channels serve to stanch the electrogenic pump's hyperpolarization at high $[Na^+]_i$ (e.g., as in Fig. 7 A, iii). The concentration and average valence are of external milieu Donnan effectors is fixed here, but CD modeling (Mehta et al., 2008) shows how, when it does change, it affects cytoplasmic ion homeostasis.

Regarding variations in extracellular $[K^+]$ that could occur in vivo, we quote one of our reviewers: "…if intracellular [K] were to decrease by more than just a few mM then unless the kidneys were able to rapidly excrete K into urine then a lethal extracellular [K] would quickly develop…the accompanying changes of extracellular [K], [Na], [Cl] would have a major impact on intracellular [ion] homeostasis that would differ substantially from the simulation results." A grim case-in-point would be the compartment syndrome–like situation of Fig. 6. There, the fixed external milieu implies a continually flushed external milieu, which is not the case with blood seriously constricted. Depolarizing extracellular accumulation of K^+ would modify that scenario.

The fixed milieu is inappropriate, too, for channels and secondary active transporters (not represented in SM-CD) and whose activities modify and depend on both internal and external milieu ions.

Secondary active transport

SMFs intermittently activate various gradient-dissipating transport systems. Unlike in neurons, though, none are considered fundamental to the resting state (the contribution of CN-CD's constitutively active K/Cl co-transporter is evident via the CN-CD/MN-CD comparison, Table 2). As seen in Fig. 14 E (inset box), Fraser and Huang (2004) demonstrated how Na-K-2Cl co-transporters alter steady state in their SMF model (comparable to SM*-CM, i.e., nonexcitable SM-CD). V_{rest} depolarizes by 40 mV; this much activation would be pathological. The electroneutral secondary active-Cl^- transporter increases $[Cl^-]_i$ by stoichiometrically depleting cellular Na^+ and K^+ gradients, thereby swelling and depolarizing the cell. Pathological overactivity of Na-K-2Cl would cause osmotic-

Na^+ overload (in contrast to the nonosmotic-Na^+ overload reported for DMD patients by Gerhalter et al. [2019]). Pedersen et al. (2016) emphasize that, given what they call the shortcircuiting effect of ClC-1 ([big P_{Cl}]), any (secondary) active transport of Cl^- is hard to detect in SMFs. What evidence is available, they say, suggests that its physiological role (including for regulatory volume increase) is limited (Sejersted and Sjøgaard, 2000; Usher-Smith et al., 2009; Lindinger et al., 2011). In minimal P-L/D systems, V_{rest} coincides with E_{Cl}; Leermakers et al. (2020) reiterate that SMF V_{rest} stays within a few mV of E_{Cl}. Experiments using newly developed Cl-selective microelectrodes (DiFranco et al., 2019) will likely clarify the value of V_{rest}-E_{Cl} in resting SMFs, and help study the transporters involved. While it is technically possible to add a collection of flux models, a caveat, especially for excitable-cell CD models, is that they grow intractable. The Cha and Noma (2012) cardiac CD-approach model, for example, appears to be thoroughly rigorous, but it has seen little uptake.

T-tubules

Like the Fraser and Huang (2004) SMF model, SM-CD is 0-D and so does not depict SMFs' t-tubular geometry. That geometry (and thus lumenal electrodiffusion) is made explicit in Fraser et al. (2011), where t-tubule SA is four times the SA of the sarcolemma and total lumenal volume is ∼0.3% of fiber volume. After trains of t-tubular APs, ion homeostatic recovery takes only several seconds (Fraser et al., 2011). If, for SM-CD, the 2,000 μm² of membrane (or C_m equivalent) encircled a cylindrical slice of 8 μm radius (see Fig. 3 C), it would have approximately three times excess SA rather than four times. Making the simplifying assumption of identical flux mechanisms in sarcolemmal and t-tubular membrane, SM-CD's steady-state values (for steady state, access resistance is irrelevant) can be regarded as arising from a hybrid of the two regions.

SMF-specific pumps

SM-CD as is simply copies the CN-CD pump model (Eq. 10). For systems at or near a healthy steady state, pump-model specifics matter little (Fraser and Huang, 2004; Düsterwald et al., 2018) provided they generate an appropriate resting $[Na^+]_i$. Table 1 shows that resting $[Na^+]_i$ is lower in mice than humans; SM-CD as is generates a resting $[Na^+]_i$ near the mouse range. Fig. S2 E shows in principle how (all else held constant) steady-state $[Na^+]_i$ changes if the pump model's Na^+-binding characteristics are changed. In the present context, the inflection region and steepness of the low–pump-strength danger zone (Fig. 9) would change with changed pump-model kinetics. This matters; diaphragm and postural muscle fibers differ in their pump isozyme profiles and in their susceptibility to DMD damage (Kravtsova et al., 2020). To render future SM-CD iterations fiber-type–specific (Deshmukh et al., 2021), a first requirement will therefore be appropriate isozyme profiles (relative densities and appropriate kinetics; Hakimjavadi et al., 2018). Fig. S2 E illustrates an entirely hypothetical case in which (via Eq. 10) the relative density of two isozymes is held constant but the Na^+_i binding affinities for both are doubled.

SMF-specific V-gated channels

The present generic H-H description of excitability could be replaced with Nav1.4 gating, including its slow-gated states (Webb et al., 2009; Fu et al., 2011; Cannon, 2017). That way, SMF-specific subthreshold Nav activity (e.g., Filatov et al., 2005) would shape the danger zone, and contributions of slow-inactivated states to fiber longevity (e.g., during post-injury cyto-remodeling) could be probed. Nav1.4 slow-state kinetics are important for conformation-state–dependent inhibition by agents in clinical use for SMFs (e.g., Skov et al., 2017; Lukacs et al., 2018) and whose free-running impacts could be probed in an appropriately fitted P-L/D model. To model the ion homeostatic impact of, say, Nav/Nav-reagent interactions (e.g., as per Lukacs et al., 2018) or of Nav channelopathies (Cannon, 2017), a Markov chain Nav channel (with the necessary states and transitions) would need to replace the H-H Nav channel. Kv gating would then need to be tuned to yield acceptable APs.

P-L/D modeling of myotonia congenita: SMFs with a [small P_{Cl}][small I_{Naleak}] steady state

Though ClC-1 channels underlie ∼80% of P_{Cl} in SMFs, ClC-1–minus mice (a myotonia congenita model) are viable, their SMF V_{rest} is the same as for wild type, and fibers are hyperexcitable (Pedersen et al., 2009; Novak et al., 2015; Imbrici et al., 2015; Pedersen et al., 2016; Jeng et al., 2020). WD-CD, the [small P_{Cl}] counterfactual analog of SM-CD with the same P_K:P_{Na} and thence, same V_{rest}, is not, however, a P-L/D model for myotonia congenita. WD-CD's input impedance is on par with SM-CD's due to ↑ absolute P_K and P_{Na} values (thus WD-CD's elevated ATP consumption and fast rundown; Fig. S2, C and D).

SM-CD with 0.1 × P_{Cl} (all else equal) is a hyperexcitable system, with V_{rest} and ATP consumption unchanged, but with anoxic rundown time almost unchanged. This [small P_{Cl}][small I_{Naleak}] system would more closely approximate the mytonia congenita situation, where, as Metzger et al. (2020) emphasize, any ↑operational P_{Na} is problematic. For healthy SMFs, a small-valued P_{Na} is a necessary but not a sufficient steady-state element; an SMF needs a [big P_{Cl}][small I_{Naleak}] (Donnan dominated) steady state.

P-L/D modeling of SM injury, tourniquets, compartment syndrome

Qualitatively, SM-CD's response to a sudden step to low pump strengths provides insight into, e.g., the Na^+ loading in SMFs that, until an abrupt tissue injury, were healthy (e.g., Dahlmann et al., 2016). Impeded blood flow that lowers pump strength also impedes external milieu replenishment. To model such scenarios well, a computationally finite extracellular milieu is required. ^{23}Na-proton-MRI measurements during experimental application/release of tourniquets are feasible, and could be repeated, in animal

models, with ouabain. Given an appropriately upgraded SM-CD model, the measured versus modeled rapidity and extent of Na^+ and H_2O loading and recovery speeds could be assessed for these and many other interventions.

Questions and answers

Question and answer 1: Question: WD-CD performs well after AP; could a Pump-Leak dominated excitable cell not just forgo Cl^- channels and use pure Pump-Leak homeostasis? Answer: That could work only if all AP-related Na^+ and K^+ fluxes and the Na^+ and K^+ driving forces were precisely adjusted to ensure zero excess Na^+ entry (AP-induced H_2O blips would reverse fully) and if pumps were electroneutral (electrogenic pump polarization of V_m would alter any perfectly tuned driving forces). Any $P_{Cl} = 0$ ion homeostatic system would have zero physiological latitude. Question and answer 2: Question: WD-CD has a very small Donnan bounce; is that not preferable to SM-CD? Answer: Inside a cranium, any $\uparrow Vol_{cell}$ is problematic; not so for SMFs. Physiologically speaking, the SM-CD Vol_{cell} excursion (even from stress-test AP trains; Fig. 5) would be almost unnoticeable. For SMFs, WD-CD's large resting ATP consumption, small pump reserve, and several-fold faster anoxic rundown would all be physiologically intolerable.

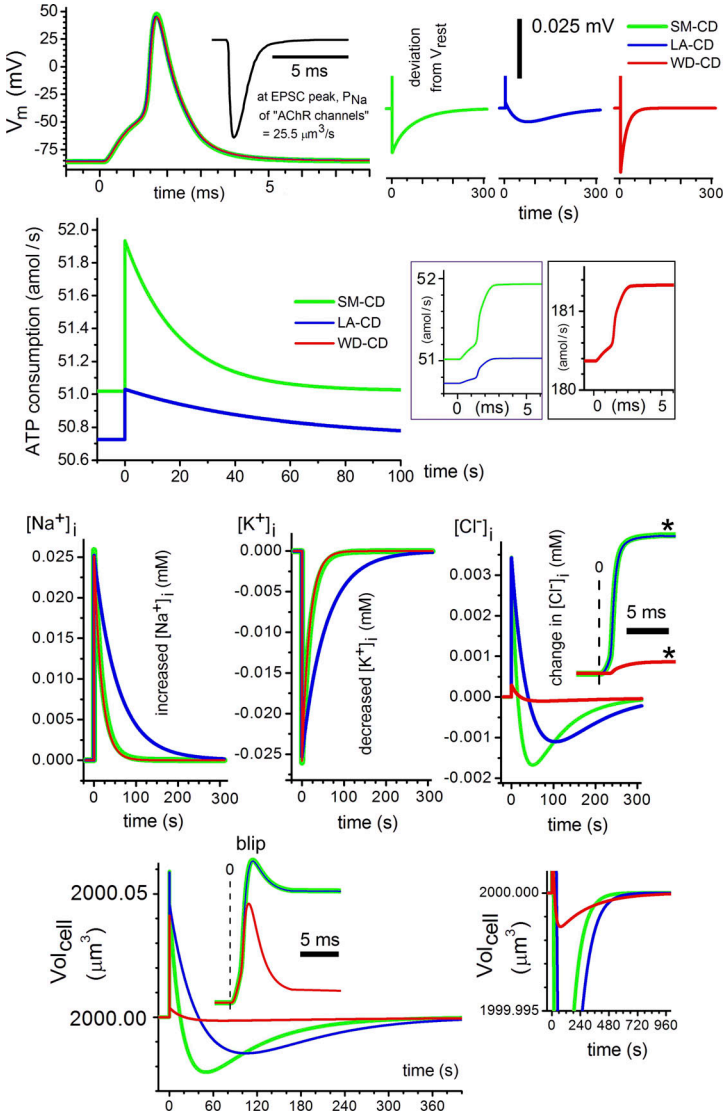

Figure S1. **Single EPSC-triggered APs (SM-CD, LA-CD, and WD-CD).** The canonical P-L/D task for SMFs: restore steady state after a cholinergic AP. The process is shown at high resolution (note scale variations) here for single EPSC-triggered APs in SM-CD, LA-CD, and WD-CD; $V_m(t)$ traces almost completely overlap (in stress tests [Fig. 5, Fig. 12, and Fig. S2 D], these APs are triggered at 120 Hz). Osmo-balancing is almost instantaneous (P_{H2O} is very large), so the initial AP-induced P-L/D response is a H_2O blip (abrupt ↑Vol_{cell}, millisecond traces) whose height reflects the excess Na^+ entry (i.e., Na^+ entry not countered by simultaneous K^+ exit). SM-CD and LA-CD blips (see overlapping traces) are slightly bigger than for WD-CD (whose larger P_K accounts for the slightly smaller H_2O blip). This fast ↑Vol_{cell} then partially reverses, to an extent dependent on how much electroneutralization of excess Na^+ entry is achieved by Cl^- entry (most of it for [big P_{Cl}] SM-CD and LA-CD; very little of it for [small P_{Cl}] WD-CD; see ↑$[Cl^-]_i(t)$ at asterisks). Millisecond AP-related ion fluxes stimulate ion homeostatic feedback fluxes that take minutes. The restoration pace is set by sensor/effector pumping (Fig. 2 A) as it extrudes Na^+ and reacquires K^+ (= hyperpolarizing $I_{NaKpump}$), its rate proportional to $[Na^+]_i$. Passive Donnan–effector–centered sensor/effector feedbacks, meanwhile, move Cl^- and H_2O as required to keep H_2O activity inside/outside balanced and the cytoplasm electroneutral. Low pump strength slows recovery (see LA-CD, $\Delta[ion]_i(t)$ trajectories). After its fast double jump (responses to ↑$[Na^+]_i$ from EPSC then AP), ATP consumption decays monotonically to steady state, at almost the same speed for SM-CD and WD-CD (WD-CD lies offscale; note y axes, double jump insets). $\Delta Na^+(t)$ and $\Delta K^+(t)$ overlap, therefore, for SM-CD and WD-CD, while low–pump strength LA-CD lags. The $\Delta V_m(t)$ traces (top right) show the consequence of (post-AP) hyperpolarizing $I_{NaKpump}(t)$. $[Cl^-]_i(t)$ and $Vol_{cell}(t)$ trajectories are not monotonic (nor is $[A^-]_i(t)$, which changes inversely with $Vol_{cell}(t)$ and $[Cl^-]_i$, not shown). The single oscillation (= Donnan bounce) reflects the interplay of P-L/D systems' two sensor/effector processes. The Donnan bounce amplitude of WD-CD (see vertically amplified traces) is <0.1 that for Donnan-dominated SM-CD. Donnan bounces are bigger when P_{Cl} is bigger and slower when pump strength is weaker. Why the bounce? AChR channels support mostly Na^+ entry. Then Nav channels open before Kv channels. So, Na^+ + H_2O enter (→blip), and then Kv activates (some K^+ and H_2O exit→partial reversal of blip) and (as needed for electroneutrality) Cl^- enters. Meanwhile, $[Na^+]_i$-stimulated $I_{NaKpump}$ extrudes 3Na^+ per 2K^+ imported, slightly hyperpolarizing V_m (top right). Ongoing Na^+ extrusion makes the (previously swollen) cells transiently shrink because (with 3Na^+ extruded per 2K^+ imported) neutralizing Cl^- plus osmo-balancing H_2O exit the cell to accompany the net (extruded) Na^+. $[Cl^-]_i$ and Vol_{cell} resume steady-state levels as $[Na^+]_i$ finishes its monotonic return. As $I_{NaKpump}$ and I_{Naleak} equalize, steady state is reestablished. See Question and answers in the supplemental text for further information.

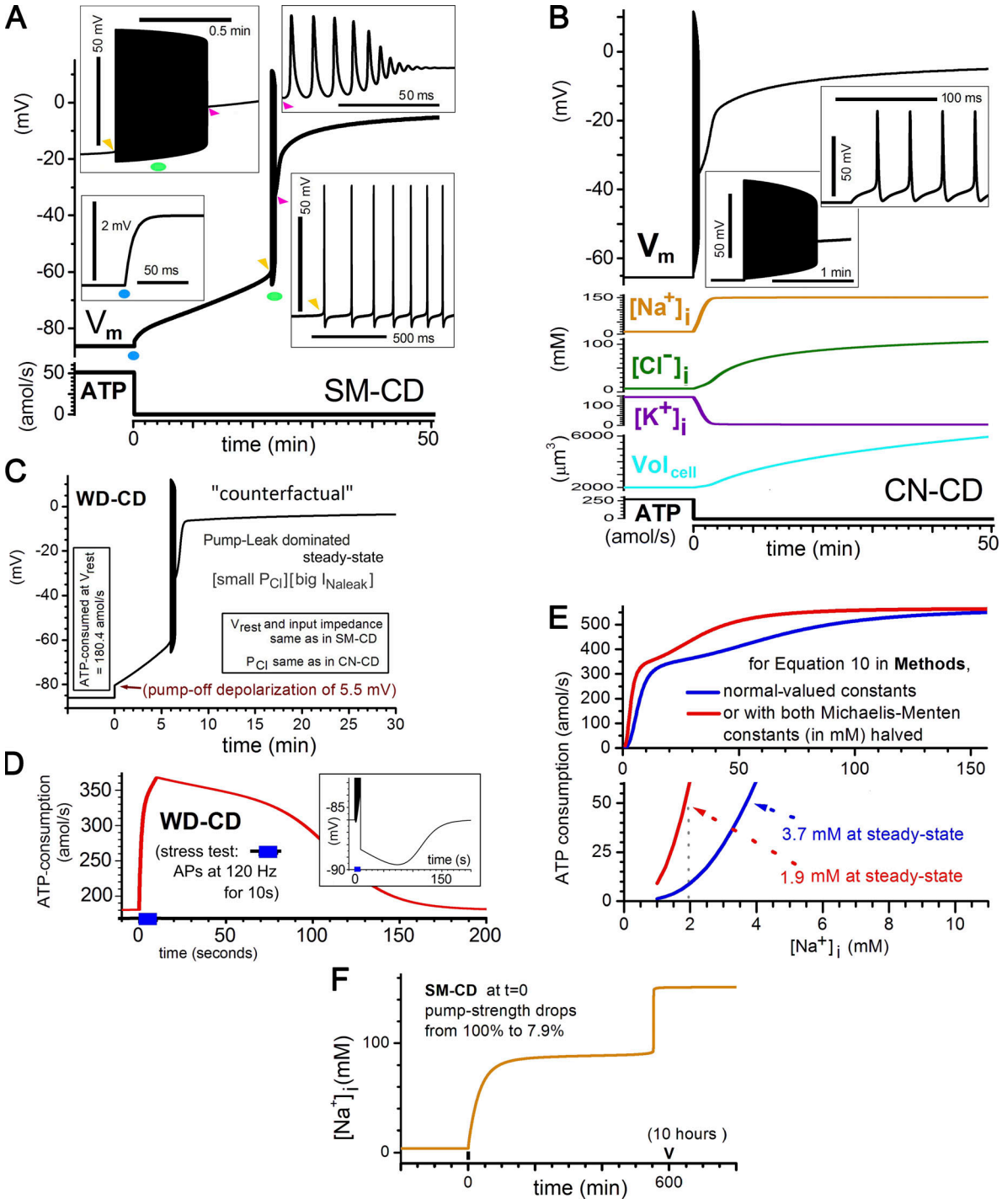

Figure S2. **Anoxic rundown details, stress testing WD-CD, and other computations. (A)** SM-CD anoxic rundown. $V_m(t)$ with spontaneous firing expanded; note various colored locators. The t = 0 blue dot highlights the ~2 mV pump off resistive-capacitive (RC) depolarization (from step turn off of hyperpolarizing $I_{NaKpump}$). 50 mV scale, lower right inset, applies also to upper right inset. **(B)** CN-CD anoxic rundown. The pump off depolarization triggers spontaneous APs almost immediately (the large $I_{NaKpump}$-off depolarization is more self-evident in Fig. 8, for inexcitable CN*-CD) and continues for ~1 min. Ion gradients dissipate precipitously, a dire situation accelerated by the (pathological) opening, at approximately −20 mV, of a depolarization-activated Cl^- pathway (Rungta et al., 2015; Dijkstra et al., 2016). **(C)** WD-CD anoxic rundown: $V_m(t)$ and ATP consumption for the counterfactual Pump-Leak dominated SM-CD analog. **(D)** WD-CD stress tested: ATP consumption(t) and $V_m(t)$ (boxed inset; same stress test as for SM-CD in Fig. 5). The WD-CD saddle node (the bifurcation analysis is not shown) occurs at 26.5% pump strength (versus 7.9% for SM-CD). **(E)** Shows how a post–stress-test $[Na^+]_i$ undershoot in SMFs could occur if the mechanism for excitation activation involved modifying the pumps' Michaelis–Menten kinetics as labeled in (V_{rest} −86.0→ −86.4 mV; E_{Na} 99→118 mV; ATP consumption 51.0→51.2 amol/s). **(F)** The $[Na^+]_i(t)$ trajectory corresponding to the $V_m(t)$ trajectory of Fig 6.

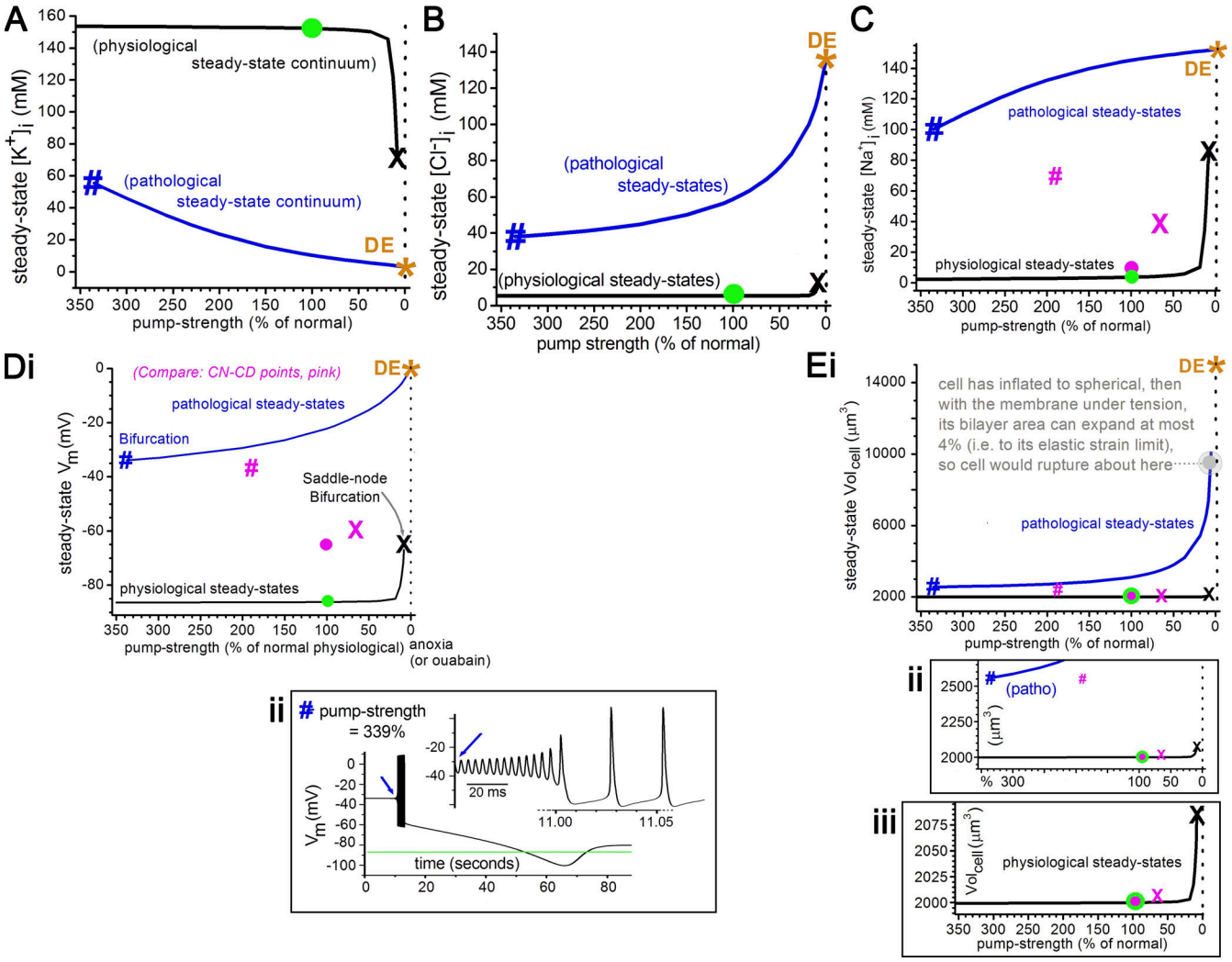

Figure S3. **Full SM-CD bifurcation analysis for five P-L/D parameters.** Analysis is partially shown in Fig. 9. Shown are (A) $[K^+]_i$, (B) $[Cl^-]_i$, (C) $[Na^+]_i$, (D, i and ii) V_m, and (E, i–iii) Vol_{cell}. Bifurcation plots show the physiological and pathological continua, with X, the saddle node on the physiological steady-state continua, and #, the unstable threshold on the pathological steady-state continua (Dijkstra et al. [2016] designate the CN-CD # a Hopf bifurcation point). In D, ii, at t = 0, SM-CD (on the pathological continuum at 338% pump strength) is stepped →339% pump strength, which destabilizes the pathological system. SM-CD's spontaneous $V_m(t)$ recovery trajectory is plotted (D, ii) with expanded section at blue arrow. The Vol_{cell} bifurcation plot (E) is expanded twice. For comparison, CN-CD's unstable points are added in some plots; SM-CD's greater Nav density is a factor in the greater pump strength needed (#399% versus #181% for CN-CD) for return to the physiological continuum. DE values are notional since, as indicated (E, i), DE could not be achieved given C_m and N_{Ai} (membrane rupture would occur near the indicated Vol_{cell}). In Dijkstra et al. (2016), cross-sectional area for CN-CD is plotted, not Vol_{cell}, so CN-CD threshold points are recalculated here. Saddle nodes (X) in E, iii, show that until CN-CD destabilizes (<65% pump strength), it swells negligibly, and that until SM-CD destabilizes (<8% pump strength), it swells more, but still by only a few percent.

One table is provided as a separate file online. Table S1 shows data regarding skeletal muscle and brains in ancient and modern vertebrates..